JP0150896

JAERI TANDEM ANNUAL REPORT 2000

April 1, 2000 - March 31, 2001

November 2001

Department of Materials Science

日 本 原 子 力 研 究 所
Japan Atomic Energy Research Institute

JAERI TANDEM Annual Report 2000
April 1, 2000 – March 31, 2001

Department of Materials Science[※]

Tokai Research Establishment
Japan Atomic Energy Research Institute
Tokai-mura, Naka-gun, Ibaraki-ken

This annual report describes research activities which have been performed with the JAERI tandem accelerator and the Van de Graaff accelerator from April 1, 2000 to March 31, 2001. Summary reports of 46 papers, and lists of publication, personnel and cooperative research with universities are contained.

原研タンデム加速器
２０００年度年次報告

日本原子力研究所東海研究所
物質科学研究部※

（２００１年１０月１日受理）

　本年次報告書は、東海研究所の原研タンデム及びバンデグラフ加速器で、２０００年４月１日から２００１年３月３１日までの間に行われた研究活動をとりまとめたものである。
　(1) 加速器の運転と開発研究　(2)原子核構造　(3)原子核反応　(4)核化学 (5)核理論 (6)原子分子物理及び固体物理 (7)材料の照射効果の７部門にまたがる４６編の研究報告、公表された文献、関与した職員及び大学等との協力研究のリストを収録している。

東海研究所：〒319-1195　茨城県那珂郡東海村白方白根２－４
※（編集者）竹内末広・池添　博・千葉　敏・永目諭一郎・左高正雄
　　　　　　岩本　昭

Preface

This report covers research and development activities using the tandem accelerator and its superconducting booster at JAERI, Tokai, for the period of April 1, 2000 to March 31, 2001. During this period, the tandem accelerator was operated over 4,750 hours or 212 days to deliver ion beams to the experiments in the fields of nuclear structure, nuclear reactions, atomic physics, solid state physics and radiation effects in materials. The superconducting booster was utilized over 56 days for 16 experimental subjects. Twenty-two research programs have been carried out in collaboration with about a hundred researchers from universities and research institutes.

The fruits of studies and special topics in FY2000 are the following: The in-terminal ECR ion source system was improved to supply stable beams of ^{1}H, ^{14}N, ^{16}O, ^{84}Kr, ^{136}Xe for experiments. A new complete spectroscopy based on multiple Coulomb excitation of projectiles was successfully applied to ^{76}Ge, ^{78}Se and ^{84}Kr nuclei to get their electro-magnetic properties. The radioactive nuclide ^{129}I in the environment was quantified with high selectivity by an activation analysis coupled with multiple gamma-ray detection.
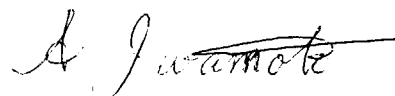
The recoil mass separator (JAERI-RMS) was utilized for a preliminary experiment to produce a radioactive nuclear beam(RNB) from reaction products, as well as operating for the measurement of evaporation residues in heavy-ion fusion reactions near Coulomb barrier.

Three neutron-rich lanthanide isotopes ^{159}Pm, ^{162}Sm and ^{16}Gd produced in the proton-induced fission of ^{238}U were identified for the first time with the gas-jet coupled JAERI-ISOL.

With respect to theoretical studies, systematic calculations on the potential energy surfaces of actinide nuclei were performed and a thorough understanding of the fission mass division mechanism was obtained, which result was published as an article in Nature. A new molecular dynamics method with imaginary time was proposed to simulate the tunneling multi-fragmentation phenomena, and the soft-rotator-model based coupled-channels approach was applied successfully to nucleon-nucleus interaction at medium mass nuclei. A massively parallel PC cluster "Helios" was installed in the tandem accelerator building to support theoretical studies.

A spinel ($MgAl_2O_4$) sample irradiated with energetic ^{127}I ions at the ambient temperature changed in phase from poly-crystalline to amorphous at lower thresholds of both electronic excitation density and integrated dose, compared to α-Al_2O_3. The oxides are likely to be more susceptive to the amorphization with increasing complexity.

A project of an RNB accelerator facility in collaboration with KEK-IPNS (Institute of Particle and Nuclear Studies) was studied further and the layout plan was finally settled. We plan to produce neutron-rich RNB from proton-induced fission products. An ion source with uranium-carbide, an ISOL and a charge breeder will be used to produce RNB. One expects the RNB intensity to the order of 10^7 particle/s. The project will start from FY2001 by building a utility building for accelerator power supplies and cooling systems, followed by the re-construction for the RNB accelerator room to place KEK's RNB linacs. We expect the first experiment with RNB in FY 2004.

Akira Iwamoto

Director

Department of Materials Science

Contents

This is a blank page.

目次

This is a blank page.

1. Accelerator Operation and Development

This is a blank page.

1.1 TANDEM ACCELERATOR AND BOOSTER OPERATION

TANDEM ACCELERATOR GROUP

Tandem Accelerator and Booster: There were three scheduled machine times in this fiscal year and the operations of the tandem accelerator and booster for experiments were performed as scheduled. The operation time of the tandem accelerator was 4753 hours in 212 days. The super-conducting booster was operated steadily for 56 days for 16 experimental subjects. During these times, the helium refrigeration systems for the tandem booster were in operation for 129 days from March 27 in 1999, 145 days from September 11 in 2000. The summary of the operation from April 1, 2000 to March 31, 2001 is as follows.

1) Time distribution in terms of terminal voltages (Tandem accelerator)

>16 MV	4 days	1.9 %
15-16	86	41.7
14-15	52	25.2
13-14	6	2.9
12-13	7	3.4
11-12	6	2.9
10-11	27	13.1
9-10	8	3.9
8-9	0	0
<8	10	4.9

Booster operation for research program

^{58,60}Ni	~400 MeV	7 days
^{76}Ge	~635	4
^{76,78,82}Se	~420	26
^{84}Kr	~250	4
^{90}Zr	~382	10
^{136}Xe	~663	5

The tandem accelerator had 2 scheduled maintenance times. During these periods, the yearly government inspection of the gas handling system and the helium refrigeration system is scheduled and a self-inspection is required in advance. We performed the self-inspection by the low for these systems on early August, and passed the government inspections in September and the end of the FY 2000.

1.2 UTILIZATION OF TANDEM ACCELERATOR AND BOOSTER

T. YOSHIDA and S. KANDA

The utilization of the tandem accelerator facility was carried out for 212 days for various experiments in three scheduled machine times in the FY 2000. Collaboration research proposals for the FY 2000 were examined at late November in 1999, and 22 subjects were accepted by the program committee. These programs accounted for approximately 61% of the whole machine time. Twenty three ion species were utilized in the 3 experimental periods as follows. The vacuum system for the terminal ion source system were improved for the inert gas evacuation. After improved this system, the terminal ion source system(ECR ion source) is working very steadily. We are able to accelerate 4 kinds of inert gas ions and also low energy, high current ion beams like H,N,O ions by the support gas for the ion source operation.

1) Time distribution in terms of projectiles

^{1}H	17 days	^{74}Ge	4 days
^{6,7}Li	9	^{79}Br	2
^{12,13}C	14	^{82}Se	27
^{14}N	8	^{90}Zr	6
^{16,18}O	7	^{107}Ag	1
^{19}F	11	^{127}I	8
^{32,33}S	25	^{136}Xe	9
^{35,37}Cl	7	^{197}Au	12
^{58,60}Ni	28		

The experimental terms allotted in the three periods were 106 days in April 10 to July 30, 109 days in September 14 to January 30 and 17 days in March 15 to end of March in 2001. The last term continued to the 1st machine time period in FY 2001. The summary of allotted days to various experimental subjects are as follows.

Research field	allotted days	total number of subjects
Nuclear physics	88	27
Atomic and Solidstate physics	57	52
Nuclear chemistry	45	22
Material research	10	10
Accelerator development	13	10

1.3   JAERI-KEK JOINT RNB PROJECT

S.TAKEUCHI and H. MIYATAKE[1]

JAERI-Tokai and KEK-IPNS(Institute of Particle and Nuclear Studies) have been planing to move and use the radioactive-nuclear-beam(RNB) linac which was developed at KEK-Tanashi, for acceleration of RNB and stable nuclear beams(SNB) at this tandem accelerator lab. For producing RNB, proton beams of 3 μA from the tandem accelerator are to be used as the drive beams. A prospective RNB production target is uranium-carbide which emits a number of neutron-rich fission products(FP). An existing ISOL system will be utilized for isotope separation. A charge breeder will be used to strip electrons of the RNB +1 ions from the ion source to inject high charge state ions to the RNB linac. An ECR ion source is also planned to be implemented as an injector for intense SNB. The first acceleration unit is a Split-Coaxial RFQ linac of 26MHz with acceleration energy of 0.17 MeV/u and the second unit is an IH(interdigital-H type) linac of 52 MHz with exit beam energy of 1 MeV/u[1,2]. Another linac with exit beam energy of 2 MeV/u needs to be built in future to inject the beams into the booster(of which freqency is 130 MHz) in order to get the beam energy beyond the Coulomb barrier energy for most of the beams and targets).

One expects the RNB of FP to be obtained with an intensity of 10^5 to 10^7 particle/s and to be used for studies on nuclear structure of unstable nuclei, formation processes of nulear spieces in astro-physics, material science with RNB implantation and so on. For SNB from the ECR ion source and accelerated by linacs, there is a big prospect to multiply the present intensities from the tandem or booster by orders of 10 to 1000, or to the order of 1 pμA. The SNB with high intensity are useful for the study of nuclear synthesis to approach superheavy nuclei, chemical structures of actinoids from the point of relativistic effect on electrons and for other experiments which have been carried out with rare events or have wanted a high beam fluence.

A part of the project has proceeded toward an approval in FY 2001, which constitutes an 1 MeV/u RNB facility without further acceleration of RNB and SNB into the booster. In FY2000, layout plans, building re-construction plans and various practical problems were studied by working groups which involved users and staff members of the tandem accelerator lab and KEK staff members of nuclear physics and accelerator sections. The layout plan is shown in Fig. 1. The existing SCRFQ and 1 MeV/u IH linacs and experimental apparatus are going to be placed in the old neutron target room with some expansion. KEK started to develop an ECR type charge breeder in FY2000. In FY2001, a utility building for accelerator power supplies and cooling systems will be built. In FY2002, the old target room will be reconstructed into the accelerator room.To begin with the reconstruction, it requires time consuming work of obtaining authorization for the use of nuclear fuel materials and radio-active isotopes and for the nuclear radiation safety. In FY2003, the linacs will be installed. The first beam is expected in FY 2004.

---

[1] Institute of Particle and Nuclear Studies, KEK
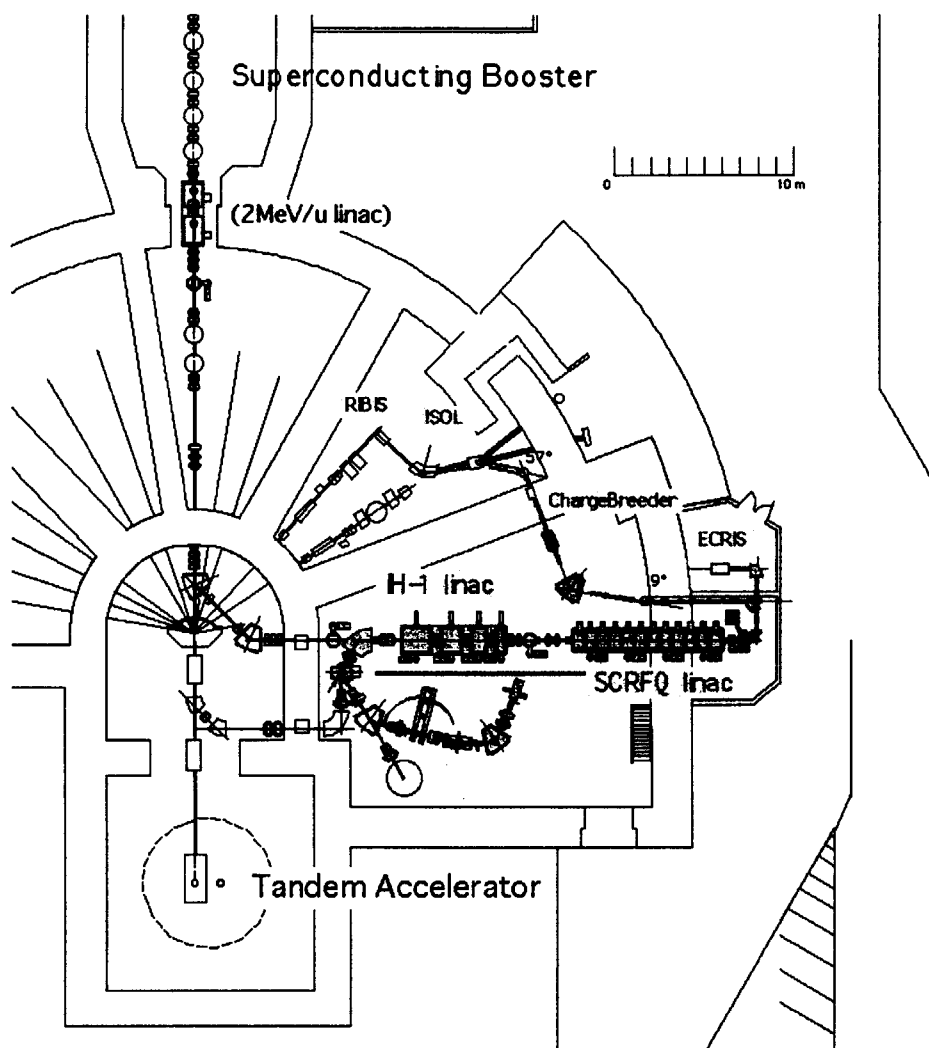
Fig. 1. Layout plan of the JAERI-KEK's RNB project.
(The first three year plan does not include the transport line and additional injector linac to the superconducting booster.)

References
[1] S. Arai et al, Nucl. Instr. and Methods **A390**(1997)9-24.
[2] M. Tomizawa et al, Proc. of the Heavy Ion Accelerator Technology:Eighth International Conference, AIP 1-56396-806-1/99, pp451-465

1.4 STATUS REPORT OF IN-TERMINAL ECR ION SOURCE

M. MATSUDA, Y.FUJII*, S. TAKEUCHI

The in-terminal ECR ion source (TECRIS) project started in 1997. A small permanent magnet ECR ion source which works at 10 GHz and RF power up to 200 W was installed in the high voltage terminal of the JAERI tandem accelerator for the purpose of increasing the beam intensity, beam energy and ion species. In the early time, it was difficult to operate stably TECRIS, because some troubles were occurred such as vacuum troubles and control device failures due to high pressure SF_6 gas and electric surges from occasional high voltage sparks. In FY2000, stable operation of TECRIS was realized after frequent improvements in maintenance periods.

The results of accelerated ions are presented in Table 1. Comparisons of the beam energies and the intensities between a conventional negative ion source with foil stripping process and the TECRIS were shown in Fig. 1. The beam intensities of accelerated ions from the TECRIS were about ten times as large as those of nearby ions from the negative ion source. The beam energy of xenon ions from the TECRIS was about one and a half times as much as that of iodine ions (neighboring mass number) from the negative ion source with foil stripping method.
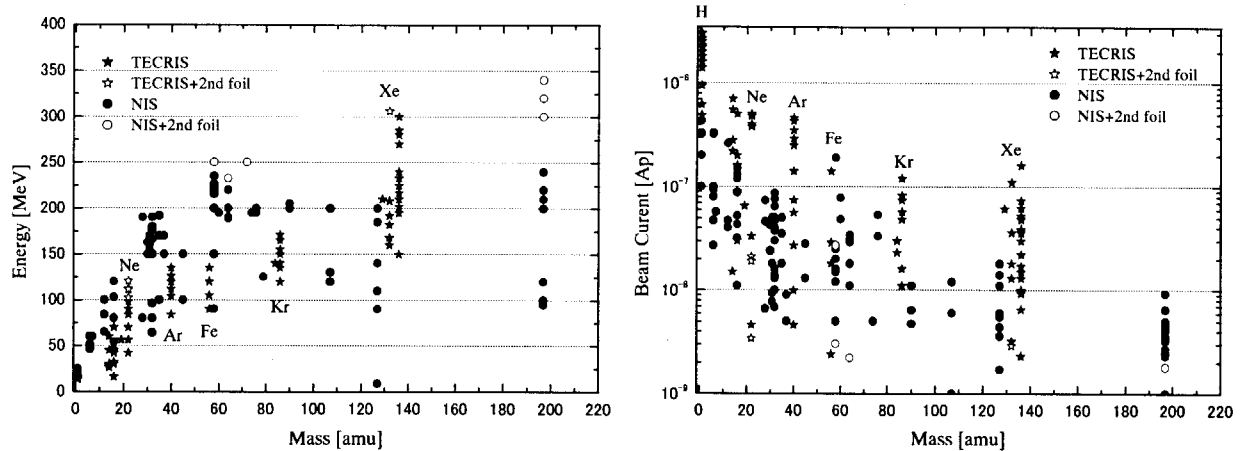
Figure 1. Comparisons of the beam energies (left) and the beam intensities (right) between a conventional negative ion source (NIS) with foil stripping process and TECRIS.

Some effective improvements are described as follows.

Installation of a turbo molecular pump; Since the previous vacuum system had only an ion pump, in case of generating krypton or xenon ion beam, ion pump instability appeared in several hours. The vacuum changed worse about one order and the beam from the TECRIS became unstable, because ion pumps do not absorb noble gases except argon gas. To settle the vacuum troubles, a magnetically suspended turbo molecular pump (TMP) of which pumping speed is 450 l/sec was installed in the vacuum system, and a rotary pump (RP) was used for the fore-line. The TMP was directly attached to the vacuum chamber without a gate valve. An electro-magnetic pipeline valve for the vacuum partition was located between the TMP and the RP. The RP was set in a vessel to keep it at atmospheric pressure and to accumulate the exhaust gas. The RP vessel is connected to a reservoir vessel which has the sufficient capacity to keep the pressure as close to atmospheric pressure as possible. The electric power to the RP, TMP and fore-line valve driver was provided from a 50 Hz inverter circuit. The TMP driver is set in an airtight vessel to keep atmospheric pressure in order to protect the complicated electric circuit from the electric discharge and the high pressure SF_6 insulating gas. When the TMP driver indicates a normal operation signal, the pipeline

---

* Nihon Advanced Technology. Co.

valve is opened, and if the TMP driver indicates a fail signal or an electric power failure, the pipeline valve closes at once. After setting TMP, instability of the ion pump disappeared during xenon beam operation.

Table 1. The intensities of the accelerated ions by TECRIS

Ion Species	T.V.* [MV]	Energy [MeV]	Current [μAe]	Ion Species	T.V.* [MV]	Energy [MeV]	Current [μAe]
$^1H^+$	15	15	3.0**	$^{56}Fe^{8+}$	15	120	0.14
$^{14}N^{2+}$	15	30	0.5**	$^{56}Fe^{9+}$	15	135	0.022
$^{14}N^{3+}$	15	45	0.83	$^{84}Kr^{10+}$	14	140	0.30
$^{14}N^{4+}$	15	60	0.060	$^{86}Kr^{8+}$	15	120	0.38
$^{16}O^{2+}$	8	16	1.0**	$^{86}Kr^{9+}$	15	135	0.67
$^{16}O^{3+}$	15	45	1.5**	$^{86}Kr^{10+}$	15	150	0.57
$^{16}O^{4+}$	8	32	0.62	$^{86}Kr^{11+}$	15	165	0.18
$^{16}O^{5+}$	15	75	0.15	$^{129}Xe^{14+}$	15	210	0.85
$^{22}Ne^{3+}$	14	42	1.5**	$^{132}Xe^{12+}$	16	192	0.30
$^{22}Ne^{4+}$	14	56	2.0**	$^{132}Xe^{13+}$	16	208	0.47
$^{22}Ne^{5+}$	14	70	1.9	$^{136}Xe^{14+}$	15	210	2.3
$^{22}Ne^{6+}$	14	84	2.9	$^{136}Xe^{15+}$	15	225	1.1
$^{22}Ne^{7+}$	14	98	0.23	$^{136}Xe^{16+}$	15	240	0.77
$^{22}Ne^{8+}$	14	114	0.037	$^{136}Xe^{18+}$	15	270	0.89
$^{40}Ar^{6+}$	14	84	2.1	$^{136}Xe^{19+}$	15	285	0.41
$^{40}Ar^{8+}$	14	112	3.7	$^{136}Xe^{20+}$	15	300	0.13
$^{40}Ar^{9+}$	15	135	0.5	$^{22}Ne^{6+,9+}$	14	111	0.17
$^{56}Fe^{6+}$	15	90	0.81	$^{22}Ne^{6+,10+}$	14	120	0.034
$^{56}Fe^{7+}$	15	105	0.20	$^{132}Xe^{12+,23+}$	16	306	0.067

* Terminal Voltage, ** Limited by a criterion of radiation safety

Source gas feeding system; The number of gas bottles in the source gas feeding system was increased from three to six in order to increase the beam species. The source gases were previously mixed with support gas. The mixed gas was fed through a capillary leak with a shut-off valve for simplified operation. However, the gas flow control is very important for generating high charge-state ions. One of gas lines was specially installed with a thermo-mechanical-leak (TML) valve connected to a motor driven slidac for gas flow control. In table 1, extractions of ions with high charge states over 16+ were realized for xenon by the TML valve.

Accelerating metal ions; For generation of metal ion beams from the TECRIS, the MIVOC (Metal Ions from VOlatile Compounds) method was chosen, because the MIVOC method works in a same manner as in the case of gaseous elements. In order to research the possibility of generating metal ions, the chamber including ferocene, $Fe(C_5H_5)_2$, was connected to the gas-feeding tube via a regulation valve to control the flow rate of the vapor of the compounds. Hydrogen support gas was fed during the experiments. Experimental results were shown in Table 1. The iron ions were readily generated, but the carbon ions strongly dominated. As a result at a test bench for several hundred hours, the ECRIS became unstable due to the degradations of ferocene in the plasma chamber. It was put off to utilize the MIVOC method, because organic compounds may cause electric discharges in the accelerating tube.

References
[1] M. Matsuda et al., JAERI TANDEM & V.d.G. Annual Report (1996) p.7.
[2] M. Matsuda et al., JAERI TANDEM & V.d.G. Annual Report (1997) p.10.
[3] M. Matsuda et al., JAERI TANDEM & V.d.G. Annual Report (1998) p.7.
[4] T. Nakagawa et al., Nucl. Instrum. Methods A396 (1997) 9.

1.5   ION SOURCE DEVELOPMENT FOR ON-LINE MASS SEPARATION OF FISSION PRODUCTS

A. OSA, M. MATSUDA, K. TSUKADA and S. ICHIKAWA

A new Radioactive Nuclear Beam Facility has been designed to provide neutron-rich radioactive ion beams having energy of 1 MeV/u for nuclear physics, material sciences and nuclear astrophysics researches. To produce these beams, proton ions from the 20 UR tandem accelerator will be input to a thick uranium-carbide target in an ion source of the isotope separator. The extracted radioactive ions after mass separation and charge breeding are then injected into a series of linacs. For this purpose, two types of integrated target ion sources were designed and manufactured according to the physical and chemical properties of elements. The one is a surface-ionization (SI) ion source for ionization of alkali, alkaline earth and lanthanide elements, and other is a FEBIAD (forced electron beam induced arc discharge) ion source for ionization of rare gasses, elements from Cu to Br and from Ag to I. With these ion sources, about 30 elements produced in the proton-induced fission of ^{238}U can be ionized.

The ion sources were designed to install about 1-g/cm^2 uranium as a carbide form. With 3-μA proton beam provided from the tandem accelerator, the intensity of ^{132}Sn ion beam is expected to be 10^6 pps based on the ionization efficiency measured by R. Krichner [1] by FEBIAD-type ion source. In addition, the particle intensity expected from the SI ion source will be at least one order of magnitude higher than that of the present gas-jet coupled ion source system for neutron-rich lanthanide region [2]. This will give opportunity to determine the half-lives, atomic masses and nuclear properties of many new nuclei. Fig. 1 shows the integrated target FEBIAD ion source.

It is important to production of radioactive nuclear beam that the ion source has high ionization
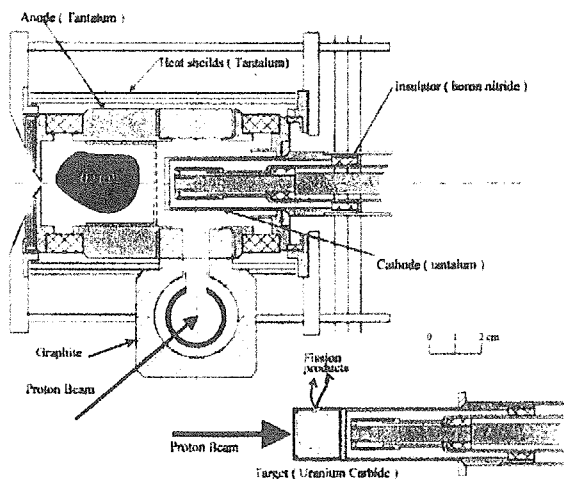
Fig. 1. Schematic view of FEBIAD ion source.

efficiency and selectivity to the element of interest. In the region of Z=50, selective ionization of indium isotopes is expected using a SI ion source, because the ionization potential is small only for indium (5.786 eV). Thus, selective mass separation of indium isotope produced in $^{93}Nb(^{19}F,pxn)$ reaction was performed. Fig. 2 shows a γ-ray spectrum observed at mass 106 fraction provided with the SI
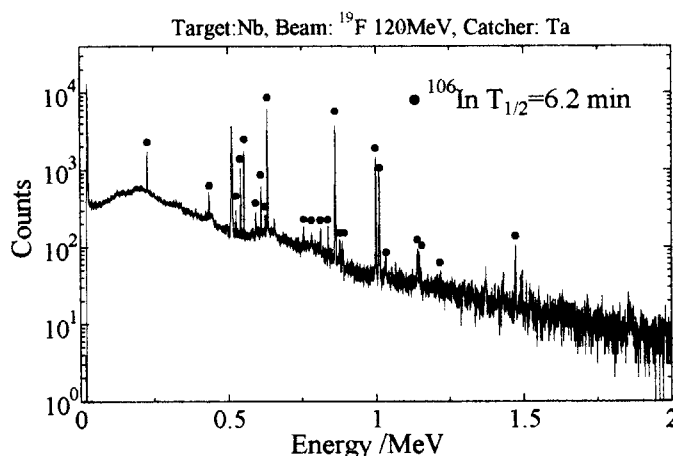
Fig. 2. Selective separation of In using the surface ionization source.

ion source. The γ-rays following the EC/β⁺-decay of ^{106}In are clearly observed and no γ-rays events observed following the EC/β⁺-decay of ^{106}Sn and ^{106}Cd produced in the reaction. However, the ionization efficiency was measured to be 0.3% that is about 1/10 of the calculated one based on the Langmuir equation at the ion source temperature of 2500 K. For the FEBIAD ion source, off-line experiments were performed and the ionization efficiencies ere measured to be 20 and 15% for Xe and Kr, respectively. To increase the ionization efficiency, improvement of vacuum around the exit-hole of the ion source, optimization of the structure of extraction electrode and conditioning of the ion source are required.

The integrated target-ion sources have various problems such as the improvement of the ion sources, the handling of the uranium target, the operation of the ion sources, and the safekeeping of the ion sources before and after irradiation. We plan to proceed with the development of the ion sources as follows.

1) Improvement of the ion source performance including diffusion of the reaction products in the target. This work uses the stable beams from the tandem accelerator and the fusion evaporation reaction products.

2) R&D with a small amount of uranium targets (~mg/cm²).

3) Study the operation and the safekeeping of ion sources with an uranium target of 1g/cm² scale.

References
[1] R. Kirchner, Nucl. Instr. Meth. B70(1992)186.
[2] S. Ichikawa et al., Nucl. Instr. Meth. A 374(1996)330.

2. Nuclear Structure

This is a blank page.

2.1 IDENTIFICATION OF ^{159}Pm, ^{162}Sm, and ^{166}Gd

M. ASAI, K. TSUKADA, S. ICHIKAWA, H. HABA, A. OSA, Y. NAGAME, S. GOTO[1],
M. SAKAMA[2], Y. KOJIMA[3], M. SHIBATA[4], K. AKIYAMA[5], A. TOYOSHIMA[6]

Experimental investigations for neutron-rich nuclei far from the β stability line provide various information on nuclear shell structure, deformation, stability, and also concerning the nucleosyntheses in astrophysical environments. We have been studying β^- decays of neutron-rich nuclei in $A \approx 160$–170 region produced in the proton-induced fission of ^{238}U using an on-line isotope separator (ISOL). Up to now, new isotopes ^{159}Pm, ^{161}Sm, ^{165}Gd, and ^{166,167,168}Tb have been identified [1–3]. Their β-decay half-lives were determined experimentally, and it was found that the half-lives calculated by the gross theory (GT2-1996) [4] agreed well with the experimental ones. For some nuclei, excited states in their daughter nuclei were established, and their deformation and nuclear structure were discussed. In this report, we present new results on the first identification of more neutron-rich nuclei ^{162}Sm and ^{166}Gd, and on remeasurements for the decay of ^{159}Pm and ^{166}Tb.

A stack of eight ^{238}U targets was bombarded with a 15.5 MeV proton beam of about 3 μA intensity from a terminal ECR ion source of the tandem accelerator. Each target was electrodeposited with a thickness of about 4 mg/cm^2 on an aluminum-foil backing. Fission products emitted from the targets were thermalized in He gas loaded with PbI$_2$ aerosols, and transported into an ion source of the ISOL with gas-jet stream. The transported products were ionized and mass-separated as monoxide ions. Details of the system are described in Ref. [5]. The mass-separated ions of interest were implanted into an aluminum-coated Mylar tape in a tape transport system, and periodically transported to a measuring position equipped with a sandwich-type plastic scintillator, a short coaxial Ge detector (ORTEC LOAX) and a 35% Ge detector (ORTEC GAMMA-X). β-γ and γ-γ coincidence measurements were performed.

In the mass $159 + 16$ fraction, 71.8, 261.3 keV γ rays, and Sm KX rays with $\sim$1.5 s half-lives were observed together with γ rays associated with the decay of ^{159}Sm with $T_{1/2} = 11.37$ s. The 71.8 and 261.3 keV γ rays were coincident weakly with Sm KX rays, and thus, assigned as the ones associated with the decay of ^{159}Pm. By taking a weighted average of deduced half-lives of 71.8 keV γ, 261.3 keV γ, Sm K$_\alpha$X, and K$_{\beta_1}$X rays, the half-life of ^{159}Pm was determined to be 1.47 ± 0.15 s. According to the systematics of $N = 97$ isotones, the configuration of the ground state of ^{159}Sm is expected to be $\nu 5/2^-[523]$, and the first excited $7/2^-$ state in the $5/2^-[523]$ band to lie at about 70 keV. The 71.8 keV γ ray assigned in this experiment is considered as the $7/2^- \rightarrow 5/2^-$ transition in the $5/2^-[523]$ band in ^{159}Sm.

In the mass $162 + 16$ fraction, 36.0, 736.6, and 741.1 keV γ rays with $\sim$2.4 s half-lives were observed in addition to Eu KX rays, attributable to the β^- decay of ^{162}Sm. The ^{162}Eu γ

[1]Department of Chemistry, Niigata University
[2]Department of Radiological Technology, University of Tokushima
[3]Graduate School of Engineering, Hiroshima University
[4]Facility for Nuclear Materials, Nagoya University
[5]Department of Chemistry, Tokyo Metropolitan University
[6]Department of Chemistry, Osaka University

rays observed in the spectra were relatively weak because Eu atoms were not ionized as monoxide ions. There are no γ transitions with the same energy in ^{162}Eu ($T_{1/2} = 10.6$ s) and in long-lived ^{162}Gd ($T_{1/2} = 8.2$ min). The half-life was determined to be 2.4 ± 0.5 s.

Gamma-ray spectra for the mass $166 + 16$ fraction were measured under two different conditions where intervals of tape transports, that is, the collection and measuring periods for each cycle, were set 10 s for short-lived ^{166}Gd and 60 s for ^{166}Tb. Six unknown γ transitions were observed in the former spectrum more intensely than in the latter. These γ rays were coincident with each other and with Tb KX rays, indicating that these transitions were attributed to the β^- decay of ^{166}Gd. On the basis of the coincidence relationships, a partial decay scheme of ^{166}Gd was established as shown in Fig. 1. The half-life of ^{166}Gd was determined to be 4.8 ± 1.0 s taking a weighted average of deduced half-lives for 40.0, 118.8, and 158.8 keV γ rays. The half-life of ^{166}Tb was also determined as 25.6 ± 2.2 s, which is more precise than the previous one of 21 ± 6 s [1].

In Table 1, theoretical half-lives for ^{159}Pm, ^{162}Sm, ^{166}Gd, and ^{166}Tb calculated by GT2-1996 [4] were compared with the present experimental ones. The deviations were within a factor of $\sim$2. This result confirmed again that the GT2-1996 could accurately predict β-decay half-lives of neutron-rich $A \approx 160$–170 nuclei.

Table 1. The present experimental half-lives for ^{159}Pm, ^{162}Sm, ^{166}Gd, and ^{166}Tb compared with theoretical ones calculated by GT2-1996 [4].

Nuclide	Experimental	GT2-1996
^{159}Pm	1.47±0.15 s	3.08 s
^{162}Sm	2.4±0.5 s	2.69 s
^{166}Gd	4.8±1.0 s	5.58 s
^{166}Tb	25.6±2.2 s	33.6 s
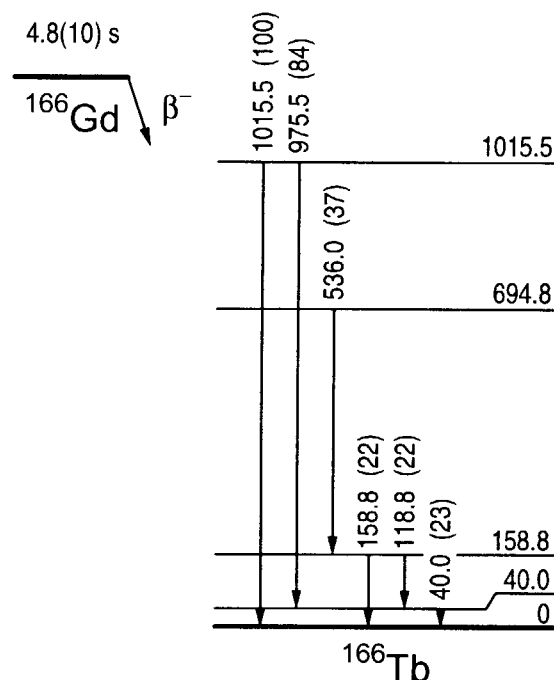
Fig. 1. A partial decay scheme of ^{166}Gd.

References

[1] M. Asai et al., J. Phys. Soc. Jpn. **65** (1996) 1135.

[2] S. Ichikawa et al., Phys. Rev. C **58** (1998) 1329.

[3] M. Asai et al., Phys. Rev. C **59** (1999) 3060.

[4] T. Tachibana and M. Yamada, ENAM 95 (Editions Frontières, Gif-sur-Yvette, 1995) p. 763; T. Horiguchi, T. Tachibana, and J. Katakura, Chart of the Nuclides 1996 (JAERI, Tokai, 1996).

[5] S. Ichikawa et al., Nucl. Instrum. Methods A **374** (1996) 330.

2.2 HIGH-SPIN STATES IN ^{183}Os

T. SHIZUMA, Y. TOH, T. HAYAKAWA, M. OSHIMA,
T. KOMATSUBARA[1] and K. FURUNO[1]

In the region of nuclei around $A \approx 180$, the proton and neutron Fermi surfaces are among orbitals with large angular momentum projections, Ω, on the nuclear symmetry axis. Therefore, high-$K (= \sum \Omega)$ multi-quasiparticle states can lie close to the yrast line. Since the K quantum number is approximately conserved, transitions involving changes in the K values are forbidden if the K change is greater than the transition multipolarity, i.e., $\Delta K > \lambda$, K-selection rule. As a result, high-K states are often observed as isomers with long half-lives. Mechanism of deexcitation of such high-K isomers has been extensively studied, e.g. Ref. [1]. In our previous experiment, we observed several new bands in ^{183}Os. The present experiment was intended for measurements of DCO ratios for the transitions.

High-spin states of ^{183}Os have been populated with the ^{170}Er(^{18}O,5n) reaction at a beam energy of 85 MeV. A 2.0 mg/cm^2 ^{170}Er target enriched to 95.88 % with a 10 mg/cm^2 lead backing was bombarded by an ^{18}O beam. Emitted γ rays were detected by the GEMINI Ge-detector array consisting of twelve Compton-suppressed HP-Ge detectors. A total of 1 $\times$ 10^8 γ-γ coincidence events were collected. Figure 1 shows a partial level scheme of ^{183}Os.

The spins and parities of the lower-lying states in the $K = 15/2$ band have been assigned by the DCO ratios for the inter-band transitions to the $9/2^+$[624] and $7/2^-$[503] 1-quasiparticle bands. The small value of $R_{\mathrm{DCO}} = 0.26(11)$ for the 114 keV transition indicates the negative sign of the mixing ratio, while the values obatained as $R_{\mathrm{DCO}} = 0.55 \sim 0.87$ at spins higher than $23/2 \, \hbar$ are consistent with the positive signs of the mixing ratios. The results are used for determintaion of the signs of $(g_K - g_R)$ values in configuration assignment. From comparison between the experimental and calculated g_K-factors shown in Fig. 2, the configuration of the $K = 15/2$ band can be assigned as $\nu\{9/2^+[624]\} \otimes \pi\{1/2^-[541] \, 5/2^+[402]\}$. Since the g_K-factors are known to have a form [2],

$$g_K^{\mathrm{eff}} - g_R = \frac{\sum_j (g_{K_j} - g_R)K_j}{K} - \frac{\sum_j (g_{K_j} - g_R)i_j}{\sqrt{I^2 - K^2}}$$

where g_{K_j} is the gyromagnetic factor of the jth quasiparticle, i_j the aligned angular momentum, K_j the angular momentum projection on the deformation axis, and $K = \sum_j K_j$. The second term includes the alignments of the constituent quasiparticles and has an opposite contribution to the first term. The change in the sign of the mixing ratios observed in the $K = 15/2$ band can, therefore, be understood by the alignment effect of the quasiparticles involved in the configuration.

---

[1]Tandem Accelerator Center, University of Tsukuba

$^{183}_{76}$Os$_{107}$
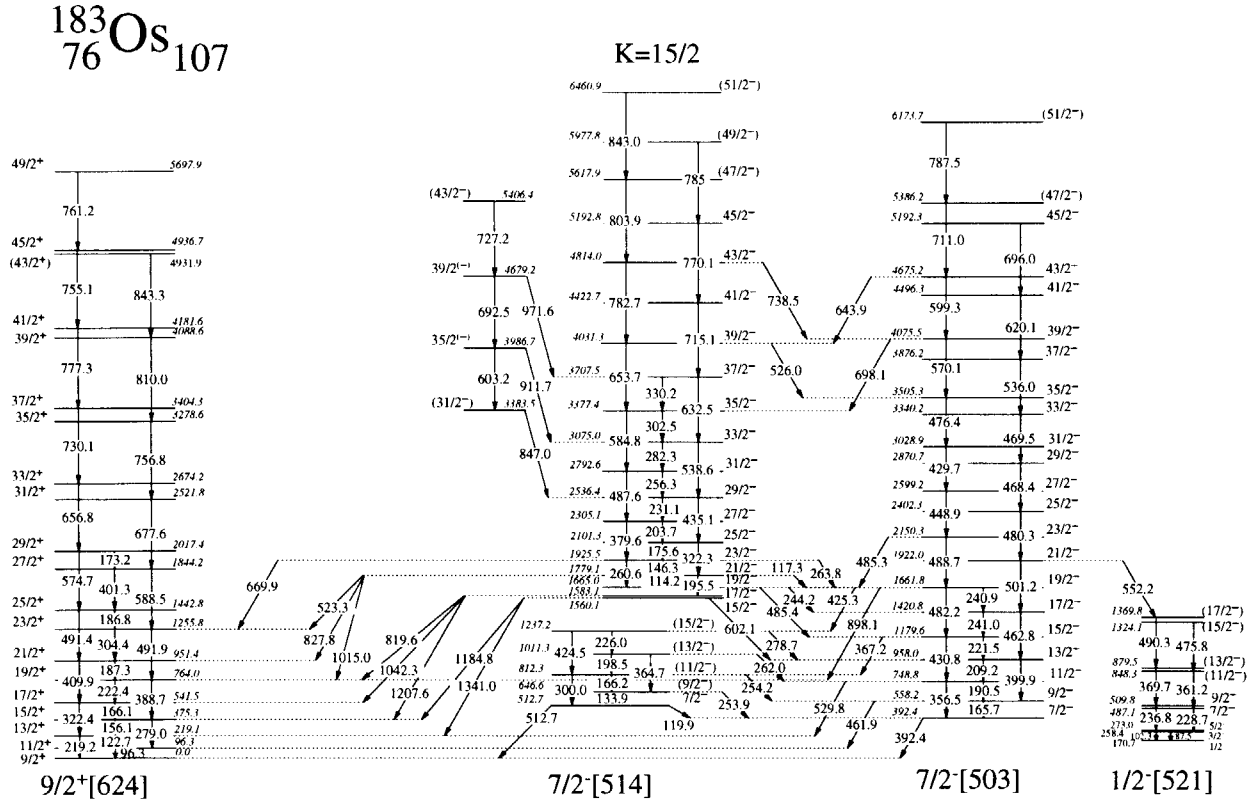
Fig. 1. A partial level scheme for ^{183}Os.
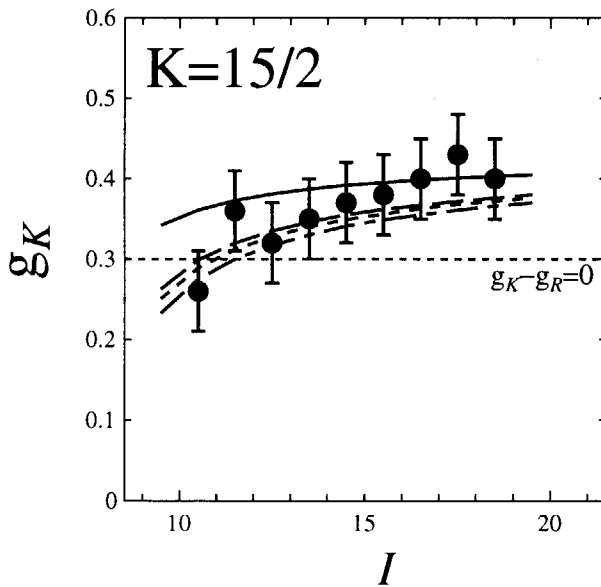
Fig. 2. Comparison of the experimental and calculated g_K-factors for the $K = 15/2$ band. The experimental values are plotted with filled circles, while the calculated values are drawn with solid lines for the proposed configuration. Long dashed, short dashed and Long-short dashed lines are calculated with $i = 0.5$ for $5/2^+[402]$, $i = 1.0$ for $9/2^+[624]$ and $i = 4.5$ for $1/2^-[541]$, respectively.

References

[1] K. Narimatsu, Y.R. Shimizu and T. Shizuma, Nucl. Phys. **A 601** (1996) 69.

[2] R.A. Bark *et al.*, Nucl. Phys. **A 591** (1995) 265.

2.3 SHAPE COEXISTENCE IN ^{76}Ge

Y. TOH, T. CZOSNYKA[1], M. OSHIMA, T. HAYAKAWA, Y. HATSUKAWA,
A. OSA, M. KOIZUMI J. KATAKURA, M. MATSUDA, N. SHINOHARA,
H. KUSAKARI[2], M. SUGAWARA[3]

Nuclei around N=40 exhibit similar low-lying level structures. These nuclei are located in a region of weak deformation, therefore thier excited states are often interpreted in terms of a phonon vibrational model. However, previous experimental studies reported that some of these nuclei exhibit the structure associated with the ground-state and γ bands[1-3].

In our previous work[4], E2 matrix elements related to five low-lying states in ^{74}Ge were extracted from the primary beam multiple Coulomb excitation. The low-lying states in this nucleus exhibit band structure. The centroids $<Q^2>$ of the ground-state and γ bands imply a weakly deformed band while the 0_2^+ state is more spherical, indicating shape coexistence.

The ^{76}Ge beam of 300MeV and 1pnA from the tandem accelerator bombarded on a self-supporting ^{nat}Pb target of 1.7mg/cm^2 thickness. The experimental setup, whose details are described elsewhere, consists of a gamma-ray detector array of 12 Ge detectors with BGO anti-Compton suppressors, GEMINI[5], and a newly developed position-sensitive particle detector system with 4 photomultiplier tubes in combination with 2 plastic and 2 Yap Ce scintillators[6]. The least-squares analysis code GOSIA [7] was used to extract the E2 matrix elements and the Q moments from the experimental data.

Fifteen E2 matrix elements of ^{76}Ge, including diagonal ones for seven low-lying states, were determined from the present Coulomb-excitation experiment. The large values of the matrix elements, $<2_2^+||E2||4_2^+>$ and $<2_1^+||E2||2_2^+>$, suggest that the 2_2^+ and 4_2^+ states are collective and may be interpreted as forming a rotational band based on the 2^+ band head (γ-band). The centroids $<Q^2>$ of the 0_2^+ state imply a spherical state.

References

[1] N. Yoshikawa *et al.*, Nucl. Phys. **A 327**(1979) 477.
[2] A.E. Kavka *et al.*, Nucl. Phys. **A 593**(1995) 177.
[3] B. Kotlinski *et al.*, Nucl. Phys. **A 519**(1990) 646.
[4] Y. Toh *et al.*, Eur. Phys. J. **A 9**(2000) 353.
[5] K. Furuno *et al.*, Nucl. Instrum. Methods Phys. Res. **A421**(1999) 211.
[6] Y. Toh *et al.*, Rev. Sci. Instrum. (submitted).
[7] T. Czosnyka *et al.*, Nucl. Phys. **A458**(1986) 123.

[1]SLCJ, University of Warsaw
[2]Faculty of Education, Chiba University
[3]Chiba Institute of Technology

2.4 EXCITED 0^+ BANDS IN ^{154}Sm

T. MORIKAWA[1], H. KUSAKARI[2], M. OSHIMA, Y. TOH,
T. HAYAKAWA, Y. HATSUKAWA, J. KATAKURA,
A. OSA, M. KOIZUMI, T. SHIZUMA,
M. SUGAWARA[3], M. SUGIE[2] and Y. SATO[2]

Low-lying excited 0^+ levels are systematically observed in rare-earth deformed nuclei. The lowest excited 0_2^+ states have been traditionally interpreted as collective β vibrational states. Recently, however, Casten and von Brentano proposed [1,2] a possibility of the interpretation for these states as phonon excitation of $K^\pi = 2^+$ γ vibrational states.

In ^{154}Sm nucleus [3], two excited 0^+ levels are known. The lowest excited 0_2^+ level at 1099 keV has been understood as the band head of β band. The 1202 keV 0_3^+ level is the lowest member of another 0^+ band lying slightly higher in energy. R. Krücken et al. investigated [4] recently these 0^+ levels by DSAM measurement following Coulomb excitation. They interpreted the 0_3^+ level as a spherical shape coexisting state, which is mixed with a spherical component in the ground state in ^{152}Sm, from its very weak population intensity as compared to the β vibrational 0_2^+ state. As pointed out in Ref. [4], this interpretation is consistent with the large ^{152}Sm(t,p) cross section [5] to the 0_3^+ level. However, for this 0_3^+ band, no direct information has been reported so far on the deformation of the band head and the collectivity of higher-spin members. To clarify the nature of these states, it is indispensable to directly determine the deformation and the collectivity in a model-independent way.

We performed a Coulomb excitation experiment of ^{154}Sm nucleus. Metallic foil of 1.47 mg/cm^2 mass density was bombarded by ^{90}Zr beam at 340 MeV and ^{136}Xe beam at 614 MeV delivered from the JAERI Tandem-Booster Accelerator. γ-rays and particles were measured by the GEMINI BGO-Ge array [6] and a compact position sensitive particle detector [7]. Fig. 1 shows a portion of Doppler corrected γ-ray spectrum of ^{154}Sm Coulex with ^{90}Zr beam. In Fig. 1, transitions deexciting the 0_3^+ band are marked, together with those from the 0_2^+ band. From the intensity ratios of these transitions, the population intensities of these levels were estimated as shown in Fig. 2.

It is interesting that the 2_3^+ state, which is 2^+ state built on the 0_3^+ band head, is populated with an intensity comparable to those of β vibrational band, while the population of the band head is very weak. This observation seems to contradict the fact that the 0_3^+ state is not collective [4]. It may need to take account of the contribution due to the band-mixing and/or the feedings from higher-lying states. Further analysis is in progress to clarify the nature of the 0_3^+ band as well as the 0_2^+ band.

---

[1] Faculty of Sciences, Kyushu University.
[2] Faculty of Education, Chiba University.
[3] Chiba Institute of Technology.
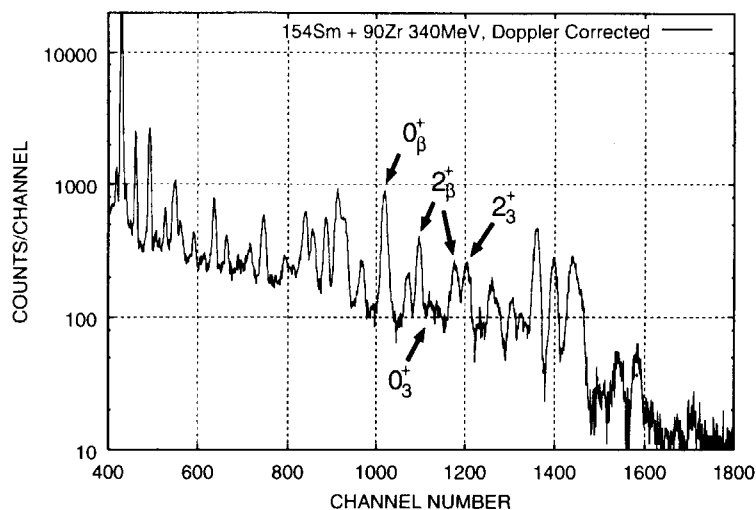
Fig. 1. A portion of Doppler corrected γ-ray spectrum of ^{154}Sm. Transitions from 0_2^+ and 0_3^+ bands are indicated.
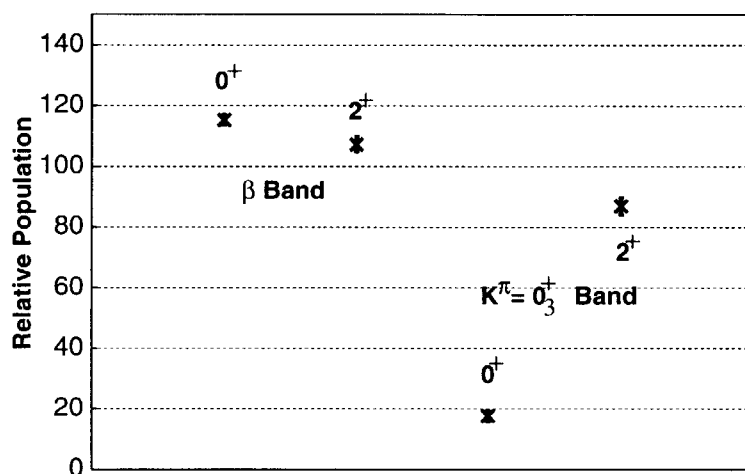
Fig. 2. Relative population intensities of 0^+ and 2^+ states in the 0_2^+ (β) band (*left*) and the 0_3^+ band (*right*).

References

[1] R. F. Casten and von Brentano, Phys. Rev. **C50** (1994) R1280.

[2] R. F. Casten and von Brentano, Phys. Rev. **C51** (1995) 3525.

[3] R. B. Firestone, Table of Isotopes 8th ed., (1996)

[4] R. Krücken et al., Phys. Lett. **B454** (1999) 15.

[5] J. H. Bjerregaard et al., Nucl. Phys. **86** (1966) 145.

[6] K. Furuno et al., Nucl. Instr. Meth. **A421** (1999) 211.

[7] Y. Toh et al., to be published.

2.5 COULOMB EXCITATION OF ^{78}Se

T. HAYAKAWA, Y. TOH, M. OSHIMA, A. OSA, M. KOIZUMI, Y. HATSUKAWA,
Y. UTSUNO, J. KATAKURA, M. MATSUDA, T. MORIKAWA[1], M. SUGAWARA[2],
H. KUSAKARI[3] T. CZOSNYKA[4]

Excited states of ^{78}Se nuclus have been studied via a multiple Coulomb excitation. A natural lead target was irradiated by the ^{78}Se beam and the γ-rays in coincidence with the scattered projectiles were detected. Resulting yields were used as an input for the least squares analysis code GOSIA. Four known excited states were observed and 11 matrix elements including 3 diagonal ones were derived from the analysis. The deformation of ^{78}Se is discussed in terms of the deformation parameters $\langle \cos 3\delta \rangle$ and $\langle Q^2 \rangle$. The 0^+ and 2^+ states in the ground-band were found to be triaxially deformed of $\delta \sim 14-24°$, being consistent with the one obtained from the asymmetric rotor model. The quadrupole moments of the 2_1^+ and 2_2^+ suggested that the both levels have the same intrinsic state. The asymmetric rotor model and the measured quadrupole moment of the second 0^+ level suggested that this level corresponds to the different intrinsic state from that of the ground state.
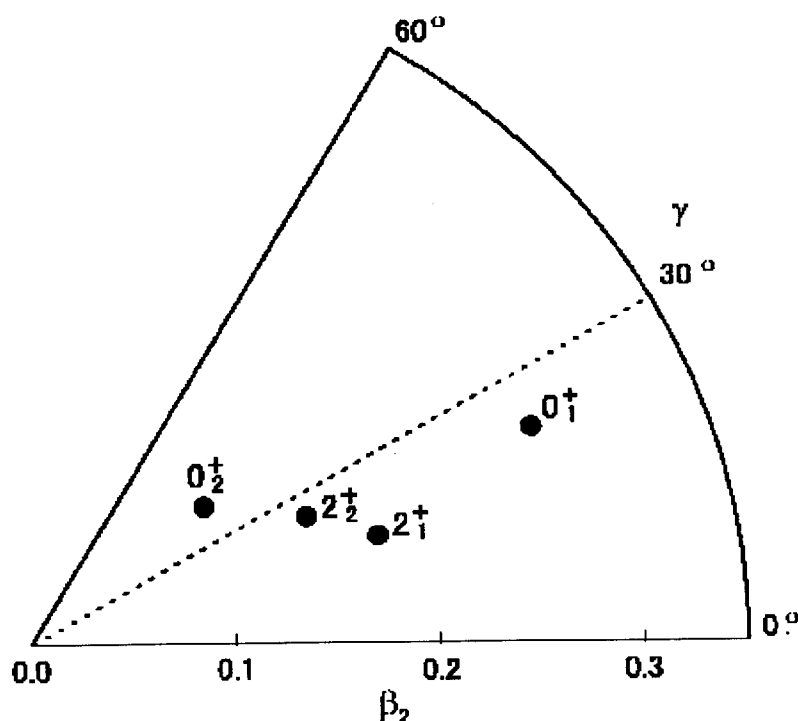
Fig. 1. Deformations of the states in ^{78}Se.

1 Kyushu University
2 Chiba Institute of Technology
3 Chiba University
4 Heavy Ion Laboratory, Warsaw University

2.6 LIFETIME MEASUREMENT IN ^{154}Sm

H. KUSAKARI[1], M. OSHIMA, Y. TOH, T. HAYAKAWA, T. MORIKAWA[2],

M. SUGAWARA[3], Y. HATSUKAWA, J. KATAKURA and Y. SATO[1]

The nucleus ^{154}Sm is a characteristic deformed nucleus. The band structures of this nucleus were investigated by the gamma-ray spectroscopic method using Coulomb excitation [1,2]. In the present experiment, lifetime measurement in ^{154}Sm was made by the recoil-distance method. The nucleus ^{154}Sm was excited and recoiled with 382 MeV ^{90}Zr beam from the JAERI tandem and booster accelerator. The target of ^{154}Sm was an enriched metallic foil, 1.47 mg/cm^2 in thickness. The plunger (stopper) was a Au foil of 10 μ m in thickness. The value of recoil velocity was about 0.05c. Present results are shown in Fig. 1. The preliminary present values of lifetimes are: $T_{1/2} = 23.8$ ps (6^+), 6.8 ps (8^+), and 2.3 ps (10^+). These values are consistent with the previous data [3,4]. Further analysis of the data in this experiment is in progress.
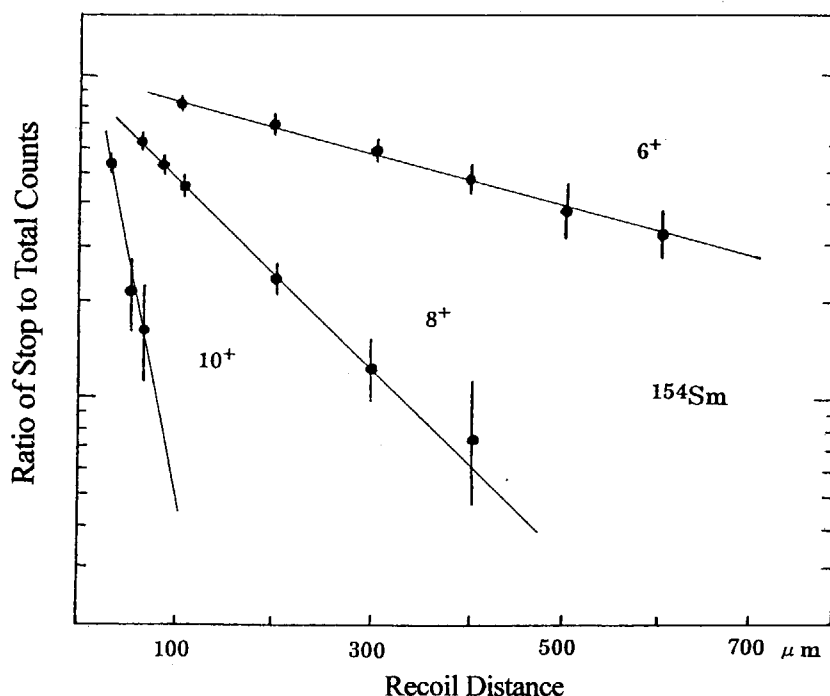
Fig. 1.　Ratios of stopped peak counts to total counts in RDM measurements for ^{154}Sm.

References

[1] T. Morikawa et al., Zeitschrift für Physik　A343 (1992) 373.

[2] H. Kusakari et al., JAERI-Review 2000-018　(Nov. 2000) 24.

[3] R. B. Firestone et al., Table of Isotopes 8th ed., Wiley-Interscience, (1996)

[4] C. W. Reich and R. G. Helmer, Nuclear Data Sheets 85 (1998) 171.

[1] Faculty of Education, Chiba University

[2] Faculty of Sciences, Kyushu University

[3] Chiba Institute of Technology

2.7 LIFETIME OF THE GROUND-STATE BAND IN ^{165}Ho

Y. SASAKI, [1], K. FURUNO[1], K. YAMADA[1], S. YOKOSE[1], M. OSHIMA,
T. HAYAKAWA, Y. HATSUKAWA, Y. TOH, T. SHIZUMA and M. MATSUDA

The nucleus ^{165}Ho is a stable nucles. The excited states of this nucleus are observed as rotational and vibrational sequences at low excitation energies. The ground state rotational sequence is known to be described by the rotational model in which a proton in the 7/2⁻[523] Nilsson orbital is coupled to a core having axially symmetric deformation. When the perturbation of the core due to the rotation is small enough, the E2 transition probability and the static Q momet are conneted to the intrinsic quadrpole moment Q_0 by simple kinematic factors. Similarly, the M1 transition probability and the static μ moment are related to the g_K and g_R factors. When the rotational perturbation or Coriolis mixing is appreciable, the above simple relations are no longer valid. In fact, Robinson *et al* have recently reported that E2 transitions are not sensitive to the mixing of the 1/2⁺[411] and 2/3⁺[411] band, while M1 transitions and g factors are affected by the mixing in the ground-state rotational band of ^{169}Tm[1]. Since the ^{165}Ho nucleus is neutron rich stable nucleus, the rotational or vibrational states have been investigated by means of Coulomb excitation[2-4]. The ground-state band is assigned up to the state of $I^\pi = 39/2^-$, but no lifetime measurement has been reported yet[5]. The present work aims at the measurement of lifetimes to investigate the electromagnetic property of the ground-state band in ^{165}Ho.

The levels of the ground-state rotational band of ^{165}Ho were populated through the Coulomb excitation with ^{58}Ni beam at a bombarding energy of 250 MeV. The beam was provided by the 20UR tandem accelerator at the Japan Atomic Energy Research Institute(JAERI). A compact plunger was installed in the center of GEMINI spectrometer. The target was a 2 mg/cm^2 thick Ho foil, while the stopper was a 50 μm lead foil. In the plunger system, the target was fixed, and the stopper was moved with a linear actuater driven in the shortest step of 1 μm. The target and the stopper were mounted in parallel by observing the reflection of a laser beam in air. The distance between the target and the stopper was monitored by capacitance method. To limit the direction of recoiled Ho nuclei, ^{58}Ni nuclei scattered in backward angles were observed with an annular plastic scintillation detector in coincidence with γ rays. The thickness and the diameter of the plastic scintillator were 0.2 and 26 mm, respectively. The particle window of the scintillator was covered with 2 μm aluminized mylar. The plastic scintillator was attached to a light guide which was coated with white paint for light reflection. A hole of 5 mm in diameter was prepared through both of the light guide and the plastic scintillator at its center. Two photomultipliers with an photo-sensitive area of 9.4 mm in diameter were mounted on the light guide. This annular plastic scintillation detector was placed at 15 mm upstream of the target. The angles of back-scattered ^{58}Ni nuclei were limited from 137 to 170.5°(lab). Gamma rays were observed with 12 Compton suppressed Ge detectors. They were placed two detector each at angles of 32°, 58°, 122° and 148°, and four detectors at 90°.

Figure 1 shows typical Doppler shift spectra for 328 keV γ ray emitted in the 17/2⁻ → 13/2⁻ E2 transition. An average recoil velocity was estimated to be $\beta = v/c = (3.1 \pm 0.2)$ % from energies of Doppler shift for all γ rays observed. The ratios of I_u/I_{tot} are plotted in Figure 2 as a function of the target-stopper distance. The symbol I_u denotes the number of counts for peaks without

[1]Institute of Physics and Tandem Accelerator Center, University of Tsukuba, Tsukuba, Ibaraki 305 JAPAN

Doppler shift, while I_{tot} is the sum of the counts of shifted and unshifted peaks. The solid lines in these figures are drawn for only guide to the eye. A problem occurred during in this experiment. The capacitance between the target and stopper appreciably changed at a certain reading of the distance on the plunger. It could be ascribed to the local distortion of the target and the stopper caused by the local heating due to beam irradiation. Large uncertainty was introduced into the calibration of the null target-stopper distance. A new experiment is necessary in a condition that the change in the target-stopper distance is minimized before the evaluation of lifetimes using the present data.
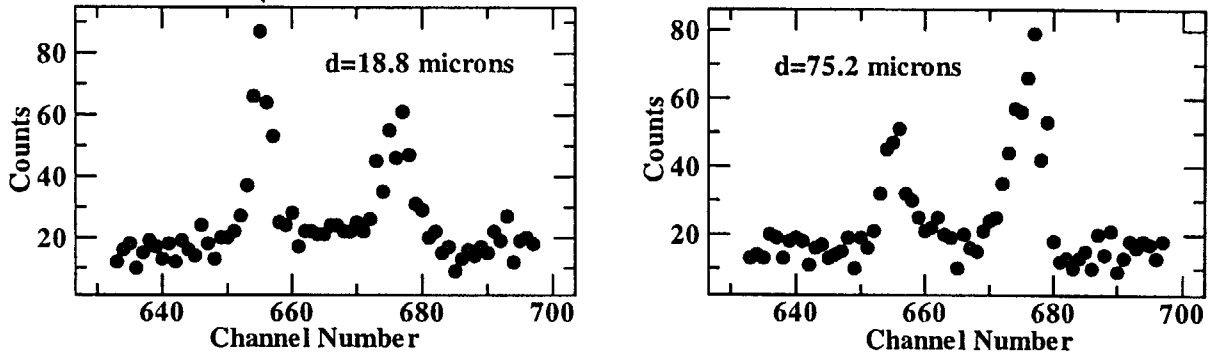
Fig. 1. Doppler shift spectra of 328 keV γ ray emitted from the $17/2^- \to 13/2^-$ E2 transition. The target-stopper distance d written in the graphs are not the actual distance but the readings of the plunger.
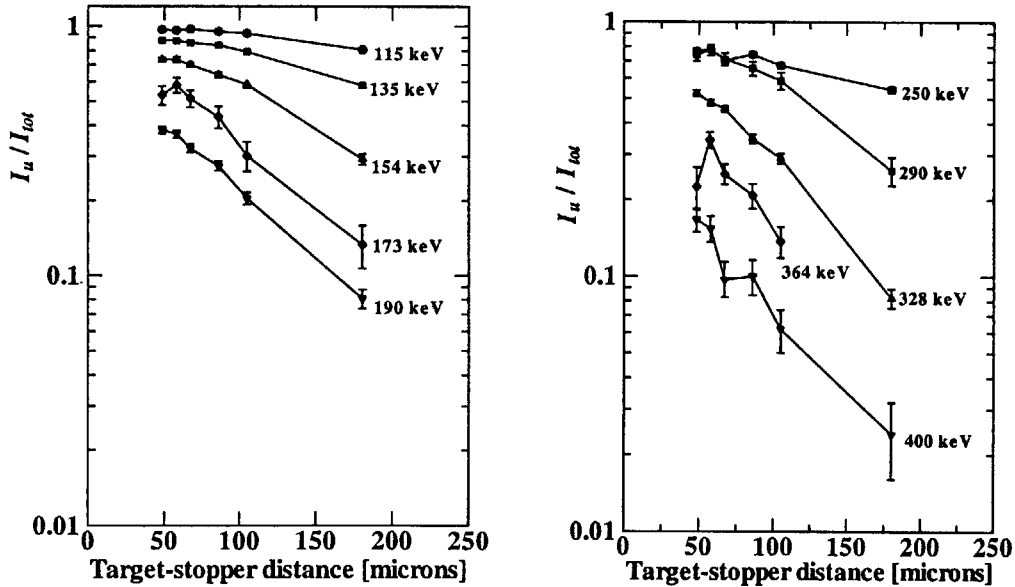
Fig. 2. The ratios of I_u/I_{tot} plotted as a function of the target-stopper distance. The groups of γ rays in M1 transitions are given in the left panel. The right figure is the ratio for E2 transitions.

References

[1] M.P. Robinson, A.E. Stuchbery, E. Bezakova, S.M. Mullins and H.H. Bolotin,
    Nucl. Phys. **A647**(1999)175.

[2] R.M. Diamond, B. Elbek and F.S. Stephens, Nucl. Phys. **43**(1963)560.

[3] G.G. Seaman, E.M. Bernstein and J.M. Palms, Phys. Rev. **161** No. 4 (1967)1223.

[4] K.P. Singh, D.C. Tayal, Gulzer Singh and H.S. Hans, Phys. Rev. **C31** No. 5 (1985)1276.

[5] G. Gervais, D.C. Radford, Y.R. Shimizu, M. Cromaz, J Degraaf, T.E. Drake, S. Flibotte,
    A Galindo-Uribarri, D.S. Haslip, V.P. Janzen, M. Matsuzaki, S.M. Mullins, J.M. Nieminen,
    C.E. Svensson, J.C. Waddington, D. Ward and J.N. Wilson, Nucl. Phys. **A624**(1997)257.

2.8 ROTATIONAL BANDS OF ^{159}Dy

M. SUGAWARA[1], S. MITARAI[2], H. KUSAKARI[3], M. OSHIMA,

T. HAYAKAWA, Y. TOH, Y. HATSUKAWA, J.KATAKURA,

H.IIMURA, Y. H. ZHANG[4], M. SUGIE[3] and Y. SATO[3]

For the N=93 rare-earth nuclei, substantial Nilsson orbits for neutrons near the fermi suface are [505]11/2(originating from $h_{11/2}$), [642]5/2($i_{13/2}$) and [521]3/2($h_{9/2}$), each of which responds differently to the rotational motion. For example in ^{157}Gd, the ground state is of [521]3/2 at first, however the [642]5/2 configuration lies lower to be yrast immediately after the rotational motion sets in. After that, these two rotational bands of opposite parity coexist along the yrast line over the relatively wide range of rotational frequency. Since it is well known that even-even nuclei in this region have the K=0⁻ or 1⁻ octupole band[1,2], this situation gives us a good opportunity to study the low energy E1 transitions in neutron-odd rare-earth nuclei caused by the octupole collectivity. In fact, several E1 transitions connecting the [521]3/2 and [642]5/2 bands have been observed in the Coulomb excitation experiment of ^{157}Gd with a ^{136}Xe beam[3]. Since ^{159}Dy is the isotone it is interesting to see if the analogous E1 transitions can be observed or not.

Before this experiment, the rotational bands based on the configurations of ν[521]3/2, ν[642]5/2 and ν[505]11/2 were known up to 21/2⁻, 45/2⁺ and 23/2⁻ states respectively[4]. Recently, Liang et al. extended the α=1/2 sequence of the ν [642]5/2 band up to 61/2⁺ state and observed the $i_{13/2}$ band crossing by using the EUROBALL IV array and the deep-inelastic reaction [5]. The ^{159}Dy nuclei were produced with the reaction ^{150}Nd(^{13}C, 4n) using a 65 MeV ^{13}C beam. The target was a self-supporting ^{150}Nd metallic foil enriched to 96.1 % with a thickness of 2 mg/cm^2. Gamma-rays from excited states of ^{159}Dy were observed as by-product in the course of the study of ^{156}Gd[6] with an array of 12 HPGe detectors with BGO Compton suppressors(GEMINI)[7]. Since the neutron emission channel was dominant in this experiment, the γ-rays in ^{159}Dy were also observed accidentally even under the trigger condition of particle-γ coincidence.

The level scheme for ^{159}Dy established in this experiment is shown in Fig.1. We could extend three rotational bands based on the configurations of ν[521]3/2, ν[642]5/2 and ν[505]11/2 up to 57/2⁻, 61/2⁺ and 29/2⁻ states respectively. Our result for the ν[642]5/2(α=1/2) sequence is consistent with the recent result by Liang et al. [5] except that the γ-ray energies of the highest two transitions differ only a few keV. Moreover several E1 transitions were observed between the ν[521]3/2 band and ν[642]5/2 band.

---

[1]Chiba Institute of Technology

[2]Faculty of Science, Kyushu University

[3]Faculty of Education, Chiba University

[4]Institute of Modern Physics, P. R. China
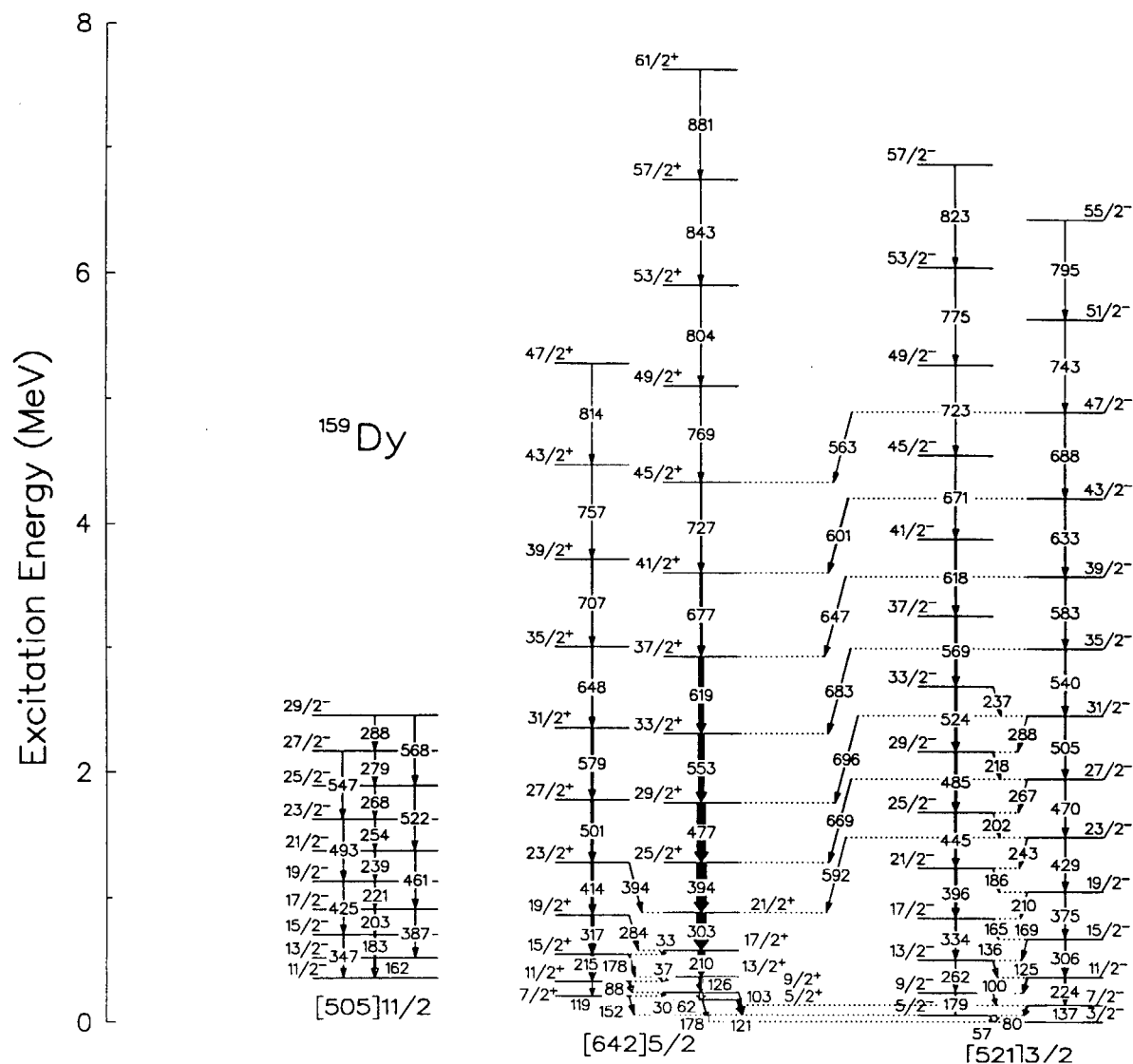
Fig. 1. The level scheme for ^{159}Dy established in this experiment. Corresponding configurations are indicated at the bottom of the respective sequences.

References

[1] F. K. McGowan et al., Phys. Rev. C 23(1981)1926.

[2] M. Sugawara et al., Nucl. Phys. A557(1993)653c.

[3] T. Hayakawa et. al. to be published.

[4] R. B. Firestone, V. S. Shirley, C. M. Baglin, S. Y. Flank Chu, and J. Zipkin, Table of Isotopes, Eighth Edition, Wiley Interscience, (1998)

[5] X. Liang et al., Eur. Phys. J. A10(2001)41.

[6] M. Sugawara et al., Nucl. Phys. A686(2001)29.

[7] K. Furuno et al., Nucl. Instrum. Methods A421(1999)211.

2.9 FABRICATION OF Si-ΔE DETECTORS FOR THE ISOMER-SCOPE

T. ISHII, M. ASAI, A. MAKISHIMA[1], M. OGAWA[2], M. MATSUDA, and S. ICHIKAWA

The isomer-scope is a useful tool to measure γ rays from isomers produced in deep-inelastic collisions [1]. In the isomer-scope, projectile-like fragments(PLFs) are detected by Si ΔE-E detectors and the atomic number of the PLF is determined by the energy loss in the Si-ΔE detector of about 20 μm in thickness. The energy resolution of the ΔE detector is essential to reduce background γ rays from neighboring nuclei with different atomic numbers. The energy resolution of such a thin Si detector is mainly determined by the uniformity of the thickness. We have made Si detectors from a Si wafer of 20 μm in thickness and 100 mm in diameter bought from Virginia Semiconductor Inc. After cutting the wafer to small pieces of 23mm in diameter, we selected wafers with good uniformity of thickness by measuring the α spectrum of ^{241}Am through the Si wafer. Then, surface-barrier Si detectors were fabricated.

The E-ΔE plots are shown in Fig. 1, which were obtained in ^{76}Ge(635 MeV)+ ^{198}Pt reaction. The most intense part in the right corner corresponds to elastic particles of $^{76}_{32}$Ge. The energy resolution of the hand-made detectors is roughly twice as good as the commercial ones. Using new ΔE detectors with good energy resolution and also larger Ge detectors, we are searching for isomers in ^{71,72}Ni.
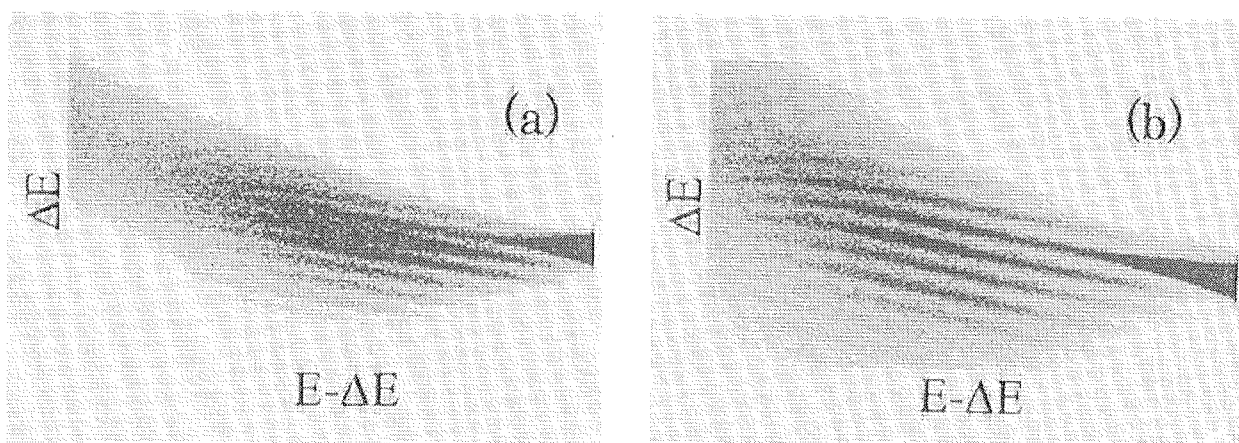
Fig. 1. E-ΔE plots measured by (a) a commercial Si-ΔE detector and by (b) a hand-made Si-ΔE detector. The stripe connecting to an elastic part (right corner) corresponds to Z=32.

Reference

[1] T. Ishii et al., Nucl. Instrum. Methods Phys. Res. A395 (1997) 210.

[1]Department of Liberal Arts and Sciences, National Defense Medical College
[2]Department of Energy Sciences, Tokyo Institute of Technology

2.10 HYPERFINE STRUCTURE AND ISOTOPE SHIFT MEASUREMENTS OF LONG-LIVED La ISOTOPES BY COLLINEAR LASER SPECTROSCOPY

H. IIMURA, Y. ISHIDA[1], M. KOIZUMI, T. SHIBATA, N. SHINOHARA,
T. HORIGUCHI[2] and H.A. SCHUESSLER[3]

The La isotopes (Z=57) are in a region of rapid transition from nuclei with nearly spherical shape (the singly magic ^{139}La) to nuclei that are soft towards deformation, presenting a good opportunity to test various nuclear models. There exist two naturally occurring La isotopes: the stable ^{139}La and the long-lived ^{138}La ($T_{1/2}$=1.05x10^{11}y). The natural abundance of ^{138}La is very low (0.090%). So far, there is no measurement of the hyperfine structure (HFS) and the isotope shift (IS) of ^{138}LaII. In order to extract changes in mean-square nuclear charge radii from IS data on LaII, a detailed knowledge of the ionic structure of La is essential. Therefore, for future measurements of short-lived isotopes, we have measured the HFS and IS of several transitions in ^{138,139}LaII with collinear laser ion-beam spectroscopy. In addition to these naturally occurring nuclides, measurements for accelerator produced ^{137}La (6x10^4 y) were also made.

The nuclide ^{137}La was produced by (p,n) or (p,2n) reactions. After the irradiation, La was chemically separated from Ba targets by an ion exchange technique. The sample of ^{137}La was then deposited in the surface ionization ion source of a mass separator. In case of the measurements of ^{138,139}La, samples of unenriched La were used. The La ions were accelerated to 40 keV and mass-separated by a magnet. The intensity of the beam was typically 3-30 nA for ^{139}La, and 10 pA for ^{137}La. The ions were excited by a counter propagating laser beam. Optical resonance was observed by detecting the fluorescence light by a photomultiplier tube. The signal from the photomultiplier tube was counted during the laser frequency scanning. Typical hyperfine spectra for ^{137,138}LaII from the metastable $6s^2$ $^1S_0$ level to the $5d6p$ $^3D_1$ level (λ=538.2 nm) are shown in Fig.1. The linewidth is approximately 120 MHz (FWHM). Peaks not labelled by F quantum numbers are those of ^{139}La, which remained at A=137 or 138 fractions even after mass separation because of their strong beam intensity.
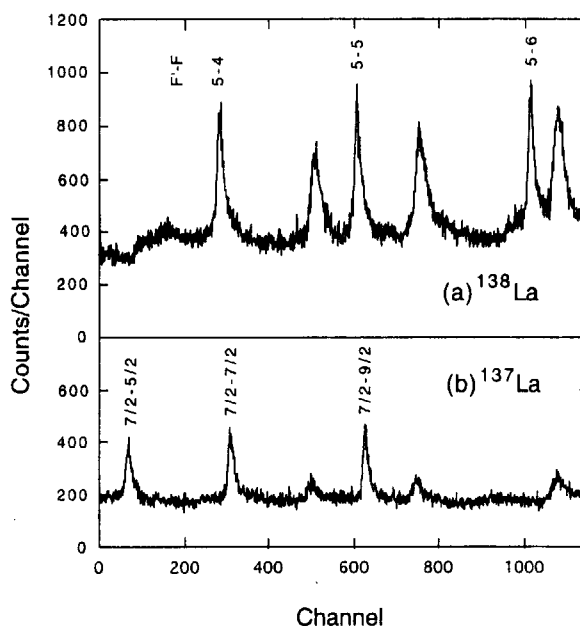
Fig. 1. Typical hyperfine spectra of the 538.2-nm transition of (a) ^{138}La and (b) ^{137}La. The unlabeled peaks are due to ^{139}La.

From the analysis of these spectra, the nuclear moments of ^{137}La were obtained. Our value of the magnetic moment is in good agreement with the value of Fisher et al. [1], which was obtained from a Fabry-Pérot interferometer measurement. However, our value of the electric quadrupole moment is considerably smaller than their value. The IS's of several transitions in ^{137,138}La were obtained from the observed shifts in the fluorescence signals. Further analysis to determine the changes in mean-square nuclear charge radii from the IS's is now in progress.

References

[1] W. Fischer, H. Hühnermann and K. Mandrek, Z. Phys. **254** (1972) 127.

[1]Institute of Physical and Chemical Research (RIKEN)
[2]Hiroshima International University
[3]Texas A&M University

This is a blank page.

— 29 —

3. Nuclear Reactions

This is a blank page.

3.1 STRONG ENHANCEMENT OF FOUR-NUCLEON TRANSFER IN THE ^{58}NI+^{58}NI REACTION AROUND THE COULOMB BARRIER

Y.SUGIYAMA, T.ISHI and A.YAMAZAKI[1]

Since a semi-classical theory of the nuclear Josephson effect was first suggested by Gol'danski and Larkin[1], there have been considerable theoretical and experimental efforts to clarify the nature of the current produced in a heavy-ion reaction between superfluid nuclei. Weiss pointed out from the semiclassical approach that multiple transfer of nucleon pair should be observed if Josephson currents could really exist[2]. In the collision of two nuclei around the Coulomb barrier, a differential cross section $\sigma_{tr}(\theta)$ of a transfer reaction is described well by the following semiclassical approach,

$$\sigma_{tr}(\theta) = <\sigma_{el}(\theta)> \times P_t(\theta) \times F(Q) \qquad (1)$$

where $<\sigma_{el}(\theta)>$ is elastic scattering cross section, $P_t(\theta)$ is transfer probability and $F(Q)$ is a correction factor due to Q-value effect. When we describe multinucleon transfer as a successive process, x-nucleon transfer probability of $P_x(\theta)$ can be approximated as

$$P_x(\theta) = (P_1(\theta))^x \qquad (2)$$

The enhancement of two-nucleon transfer probability $(P_2 > (P_1)^2)$ was observed in several systems. We could expect the enhancement of multiple-pair transfer e.g. $P_4 > (P_2)^2$ in four nucleon transfer if Josephson currents could exist. However there was no clear evidence of the enhanced four nucleon transfer.

So far we made systematic measurements of multinucleon transfer reactions between several Ni isotopes[3]. We measured the cross sections up to four nucleon transfer reactions in the ^{58}Ni+^{58}Ni system. The experiment of the ^{58}Ni+^{58}Ni system was carried out at $E_{c.m.}$=110MeV by using the JAERI tandem accelerator and the heavy-ion magnetic spectrograph "ENMA". In order to identify the mass number we measured a time-of-flight (TOF) of the outgoing particle. We measured also kinematic coincidences between the outgoing and recoiling particles with a position-sensitive surface-barrier detector in order to identify the charge states of the outgoing particles.

Figure 1 shows the transfer probability for energy-integrated cross sections ranging from one-nucleon P_1 to four-nucleon P_4 without the correction factor. The dashed and solid lines show the probability for the two- and four-nucleon transfer obtained from the relations of $(P_1)^2$and $(P_2)^2$, respectively. The probability for the two-nucleon transfer is enhanced with respect to the one-nucleon transfer probability. In addition, the probability for the four-nucleon transfer is enhanced with respect to the two-nucleon transfer probability.

The energy- and angle-integrated cross sections from one- to four-nucleon transfer reactions are plotted in Fig.2 as a function of the number of transferred nucleon. The cross sections falloff exponentially as the number of transferred nucleon.The solid line is a least-squares fit to the data which gives a reduction factor for the cross sections of 2.37±0.20 per each transferred nucleon. It is seen

---

[1]Physics Department, Tohoku University

that three-nucleon transfer is reduced while four-nucleon transfer is enhanced with respect to the solid line.

The reduction factor so far obtained in multi-neutron transfer reactions[4] was about 4-5, while the ratio between one- and two-proton transfer cross sections[5] was only about 2. The small reduction factor of 2 provided an evidence that the two-proton transfer process was enhanced with respect to one-proton transfer reaction by the pairing correlation[5]. The present data show small reduction factor of 2.37±0.20 up to four nucleon transfer cross sections. Therefore the energy- and angle-integrated cross sections support the result that not only the two-nucleon transfer cross section is enhanced with respect to the one-nucleon transfer cross section but also the four-nucleon transfer cross section is enhanced with respect to the two-nucleon transfer reaction.

References

[1] V.I.Gol'danskii and A.I.Lapkin, Th. Eksp.Theor. Fiz.**53**(1967)1032.
[2] H.Weiss, Phys. Rev. **C19** (1979) 834.
[3] Y.Sugiyama, S.Hamada, T.Ikuta and A.Yamazaki, J. Phys. **G 23** (1997) 1393.
[4] C.L.Jiang et al., Phys. Rev. **C57** (1998) 2393.
[5] K.E.Rehm et al., Phys.Rev.**C42**(1990) 2497.
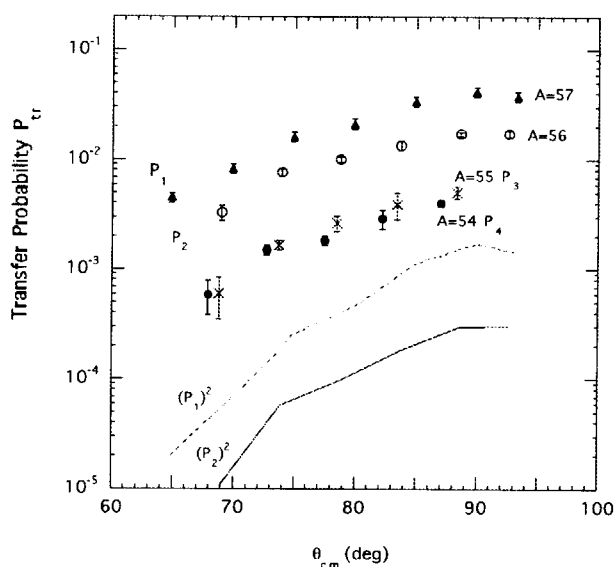
Fig.1. Transfer probabilities ranging from one-nucleon P_1 to four-nucleon P_4 obtained from the energy-integrated cross sections without the correction factor. The dashed and solid lines represent the square of one-nucleon P_1 and two-nucleon P_2 transfer probability, respectively.
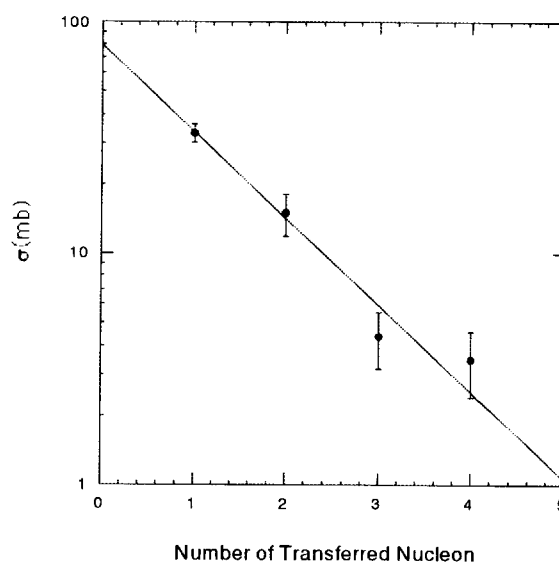
Fig.2. Angle- and energy-integrated cross sections as a function of the number of transferred nucleon. The solid line is a least-square fit to the data. The reduction factor for each transferred nucleon is 2.37±0.20.

3.2   MEASUREMENT OF THE (α, n) REACTION CROSS SECTIONS FOR THE ASTROPHYSICAL INTEREST

H. MIYATAKE[1], Y. FUCHI[1], T. FUKUDA[1], T. HASHIMOTO[2], S. ICHIKAWA, H. IKEZOE, T. ISHIKAWA[2], H. ISHIYAMA[1], S.C. JEONG[1], I. KATAYAMA[1], H. KAWAKAMI[1], T. KAWAMURA[2], M. MASTUDA, Y. MASTUYAMA[1], S. MITSUOKA, Y. MIZOI[3], K. NISHIO, T. NOMURA[1], M. TANAKA[1], Y. WATANABE[3], N. YOSHIKAWA[1],

In a recent progress of nuclear astrophysics, it is suggested the light-mass nuclei as well as heavy nuclei play important roles in the production of seed nuclei and r-process elements in supernovae [1]. Particularly, to clarify the possibility of the r-process in the light-mass nuclear region, it is important to measure the (α, n) and (n, γ) reaction rates of neutron-rich light nuclei. Hence, we proposed the direct measurements of the (α, n) reaction cross sections with low-energy neutron-rich nuclear beams, such as ^{8}Li, ^{10,11}Be and ^{12}B.

For this series of measurements, we newly constructed a multi-sampling and tracking proportional chamber (MSTPC); similar to the former model [2], and a neutron detector. The MSTPC determines the reaction points and reaction energies using the information from the trajectories and deposited energies of the injecting and outgoing charged particles. The neutron detector consists of 28 plastic scintillators, which covers 31.4% of 4π surrounding the MSTPC. It is noted that the detection efficiency of the MSTPC is high (80-90%), since He-gas filled in the MSTPC is also used as a target for the (α, n) reaction. Each final state of this reaction is clearly assigned with the help of the neutron time-of-flight measured by the neutron detector. Some additional devices, micro-channel plate detector and parallel plate avalanche counter, are also installed upstream the MSTPC as a time pick-up counter and as a beam on-line monitor, respectively.

The overall efficiency of this detection system was estimated on the basis of the reaction simulation for the ^{8}Li(α, n) case, which is a candidate for the first experiment [3]. Fig. 1 shows an expected efficiency with respect to individual neutron transitions feeding to 6 excitation levels in ^{11}B.

The light neutron-rich RNB is produced as a similar manner as ref. [4]. A different point is concerned to the beam separation method. We will separate neutron-rich RNB from the primary beam and other contaminants by means of their Eρ- and Bρ-values with using the JAERI recoil mass separator (RMS)[5], while the ref. [4] uses the momentum separation only.

Since the use of ^{7}Li-beam at the JAERI RMS course is under admission process, the ^{8}Li-beam production was tested with ^{14}N^{6+}-beam having with A/q=7/3' at E/A =2 MeV was used. The fig. 2 is measured suppression rate of the ^{14}N-elastic component to the primary beam intensity as a function of the injection angle of the RMS (θ_{RMS}). From this result, it can be found the suppression rate decreases to 1×10^{-8} at θ_{RMS}=4°, which corresponds to the ^{7}Li-beam suppression factor of 1×10^{-11} with taking accounts of the differences of the charge fraction and elastic scattering cross section between ^{14}N-beam and ^{7}Li-beam. The contamination of ^{7}Li in the ^{8}Li-beam is expected 0.14% and the ^{8}Li-beam intensity will be 1.4×10^4 pps for the 100 pnA ^{7}Li in our experimental set-up. This result together with the expected efficiency of our detection system satisfies the statistical condition to perform the measurement of the ^{8}Li(α, n) reaction and this experiment will be done whenever the ^{7}Li-beam is available.

1 Institute of Particle and Nuclear Studies, KEK
2 Science University of Tokyo
3 RIKEN
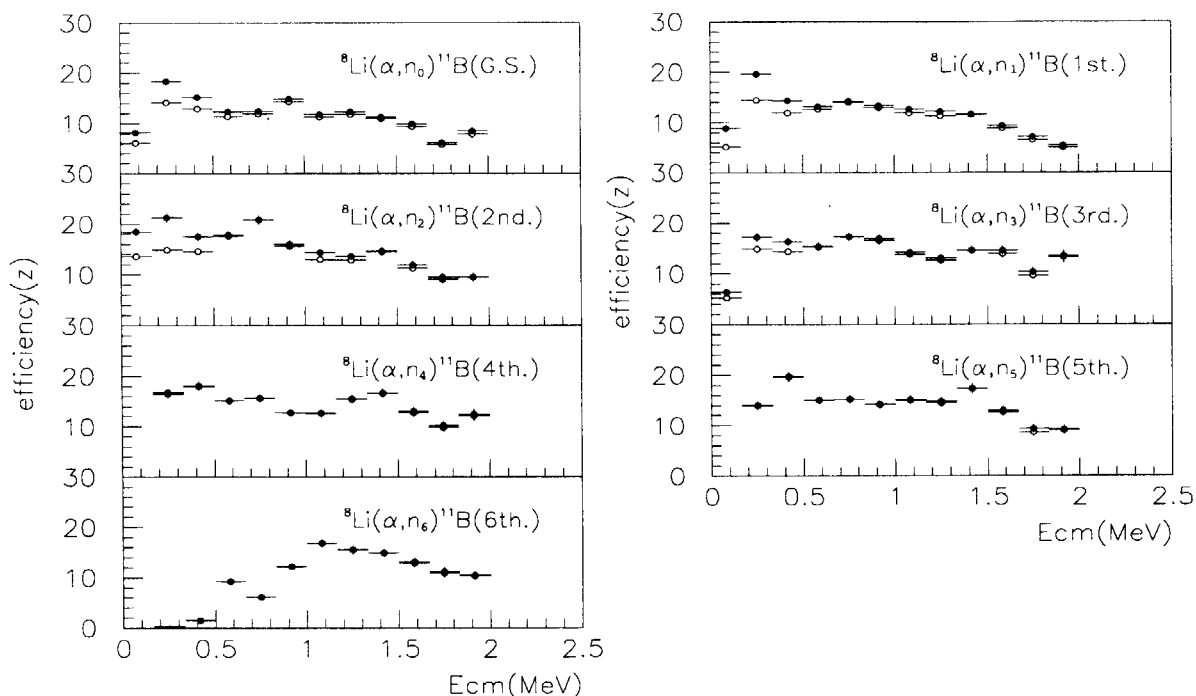
Fig. 1. Estimated detection efficiency of the measurement system. Estimation was based on the event-by-event reaction simulation of ^{8}Li and He. The black points indicate the efficiency taking the sudden changes of the energy-loss and the trajectory of ^{8}Li into account, while only the change of the energy-loss is considered for the white points. The details of this simulation are described in ref. [3].

RMS θ(deg)
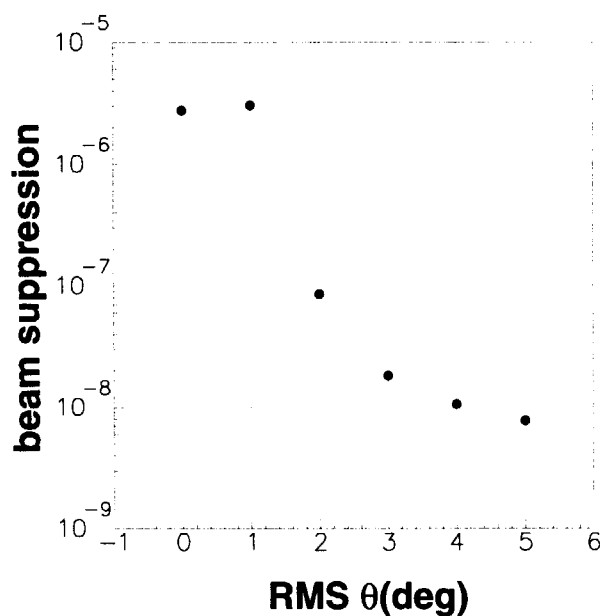
Fig. 2. The ^{14}N-beam suppression rate as a function of the θ_{RMS}. The RMS was set to A/q=8/3$^+$ and E/A=2 MeV. The Al-target (1 mg/cm^2) was used to simulate the ^{7}Li-elastic scattering. The angular acceptance of the RMS was $\Delta\theta=3°$ and $\Delta\phi=6°$.

References

[1] M. Terasawa et al, to be published in Astrophysical Journal.

[2] Y. Mizoi et al., Nucl. Instrum. And Methods A431(1999)112.

[3] T. Hashimoto, Master thesis, Science University of Tokyo(2000)

[4] F.D. Becchetti et al., Nucl. Instrum. And Methods B56/57(1991)554.

[5] H. Ikezoe et al., Nucl. Instrum and Methods, A376(1996)420.

3.3 SUB-BARRIER FUSION OF ^{60,64}Ni+^{154}Sm

S. MITSUOKA, H. IKEZOE, K. NISHIO, and K. SATOU

As a new approach to the superheavy-element production, the gentle fusion [1] and the hugging fusion [2] between well deformed nuclei have been theoretically proposed. It is predicted that the fusion cross section to form the compound nucleus may be significantly large when two deformed nuclei take the most compact touching configuration. In order to investigate this speculation experimentally and also to see the effect of neutron number of heavy projectile on the sub-barrier fusion, we have measured the evaporation residue cross sections in the reactions of ^{60}Ni and ^{64}Ni projectiles with deformed ^{154}Sm target at the energies around the Coulomb barrier.

^{60}Ni and ^{64}Ni beams (250 - 325 MeV) from the JAERI tandem accelerator were used to bombard a rotating ^{154}Sm target (350 μg/cm^2) made by sputtering on an Al foil (0.8 μm). The evaporation residues were separated in flight from the primary beam by the JAERI-RMS [3] and then implanted into a double-sided position sensitive detector. Their identification was achieved by the correlation analysis of the α-decay events.

The measured excitation functions of the evaporation residue cross sections for xn, pxn and α-xn channels ($x = 2 - 5$) were shown in our previous report [4] for ^{64}Ni + ^{154}Sm and in our paper [5] for ^{60}Ni + ^{154}Sm. Here, the statistics have gained 10 times in the present measurement for the ^{60}Ni-induced reaction at the $E_{cm} = 182$ MeV, because the previous measurements below this energy gave only the upper limit of a few nb. The evaporation residue cross sections in the ^{64}Ni-induced reaction were larger about 100 times than that in the ^{60}Ni-induced reaction. This is mainly due to the exit channel effect of the small neutron separation energy in the 4 more neutron-rich projectile system. To see the entrance channel effect in both the reaction systems, the fusion probability has been obtained with the aid of the calculated survival probability [6], which had been confirmed in the same compound nucleus system of ^{32}S + ^{182}W [5].

Figure 1 shows the fusion probability thus obtained as a function of E_{cm}/V_{Bass}. The two reaction systems show the similar trend, against the expectation that the neutron excess may effect on the enhancement of the fusion probability by some entrance channel effects like neck formation or something. The lines in the figure are results of the standard coupled channel calculations [7]. In the CCDEF calculation, the Coulomb barrier height depends on the colliding angle of the projectile with respect to the orientation of the symmetric axis of the deformed ^{154}Sm target [4,5]. The fusion probabilities at the energies corresponding to the collisions with the tips of the deformed target were significantly smaller than the standard coupled channel calculations by 3 orders of magnitude, whereas no hindrance was observed above the barrier. This is consistent with our previous conclusion [4,5] that the near tip collision needs some extra kinetic energy of about 20 MeV to fuse each other, while the side collision leads complete fusion without such extra energy. This supports the original idea of the hugging fusion that the compact touching configuration leads to form the compound nucleus more easily than an elongated configuration.
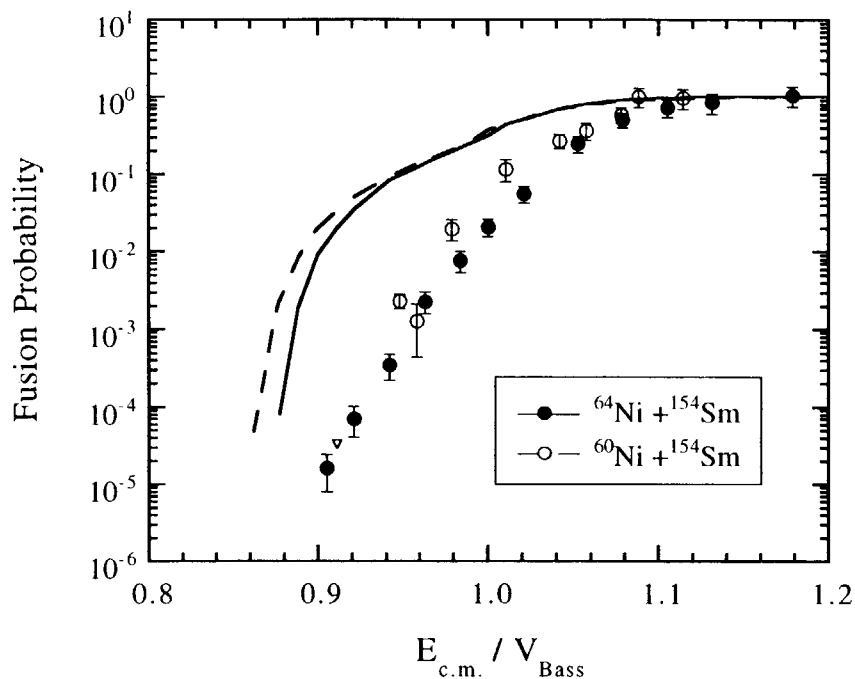
Fig. 1. Fusion probability for ^{64}Ni $+^{154}$Sm (solid circles) and ^{60}Ni$+^{154}$Sm (open circles) determined from the experimental evaporation residue cross sections. The curves are the calculated results by CCDEF.

References

[1] W. Nörenberg, Proc. Int. Workshop on Heavy-Ion Fusion, Italy (1994).

[2] A. Iwamoto et al., Nucl. Phys. **A596** (1996) 329.

[3] H. Ikezoe et al., Nucl. Instrum. and Methods **A376** (1996) 420.

[4] H. Ikezoe et al., JAERI Tandem & V.D.G Annual Report 1999, p41.

[5] S. Mitsuoka et al., Phys. Rev. C **62** (2000) 054603.

[6] W. Reisdorf and M. schädel, Z. Phys. **A343** (1981) 47.

[7] J. Fernandez-Niello et al., Comput. Phys. Commun. **54** (1989) 409.

3.4 MEASUREMENT OF EVAPORATION RESIDUE CROSS SECTION FOR ^{82}Se+^{150}Nd NEAR THE COULOMB BARRIER

K. NISHIO, H. IKEZOE, S. MITSUOKA and K. SATOU

We have recently found that the fusion reaction using largely deformed targets results in higher fusion probability than that using spherical nuclei near the Coulomb barrier energy region [1,2]. This conclusion was drawn from the measurement of evaporation residue (ER) cross sections for ^{76}Ge+^{150}Nd ($Z_1 Z_2$ =1920) and ^{82}Se+^{nat}Ce ($Z_1 Z_2$ =1972), both of which lead to compound nuclei of uranium isotopes. It would be interesting to extend this measurement to heavier systems. The pourpose of the present study is to measure the ER cross sections for ^{82}Se+^{150}Nd ($Z_1 Z_2$ =2040) which includes the prolately deformed target ^{150}Nd and forms the compound nucleus ^{232}Pu, and to find whether there is fusion hindrance at and above the Coulomb barrier in this system.

The experimental method and data analysis were similar to those described in [1,2]. Evaporation residue cross sections for ^{82}Se+^{150}Nd are shown in Fig.1 as a function of c.m. energy. The solid circles with the error bars indicates the observed cross sections. We show the upper limit of the cross section by the open triangle.

Statistical model calculation (HIVAP code [3]) was made to demonstrate ER cross section. This calculation assumes that there is no fusion hindracne in the entrance channel, and hence we expect no fusion hindrance when agreement between the experimental data and the calculation is observed. The partial wave cross section is calculated by the coupled channel calculation (CCDEF code [4]), which includes the static deformation of the target and couplings to vibrational states of both nuclei. The parameters describing deexcitation process is the same we have used in the previous papers [1,2,5].

Below the Coulomb barrier (V_B=221 MeV), the upper limits for the ^{230,229}Pu channels lie below the calculation, showing the fusion hindrance. The experimental data at $E_{c.m.}$=243 MeV (1.1V_B) agrees with the calculation for the channels of ^{227,226,225}U, indicating that there is no fusion hinsrance at this energy.

REFERENCES

[1] K. Nishio, H. Ikezoe, S. Mitsuoka and J. Lu, Phys. Rev. C62 (2000) 014602.
[2] K. Nishio, H. Ikezoe, S. Mitsuoka, K. Satou and S.C. Jeong, Phys. Rev. C63 (2001) 044610.
[3] W. Reisdorf and M. Schädel, Z. Phys. A343 (1992) 47.
[4] J.O. Fernandez and Niello, C.H. Dasso and S. Landowne, Comput. Phys. Commun. 54 (1989) 409.
[5] S. Mitsuoka, H. Ikezoe, K. Nishio and J. Lu, Phys. Rev. C62 (2000) 054603.
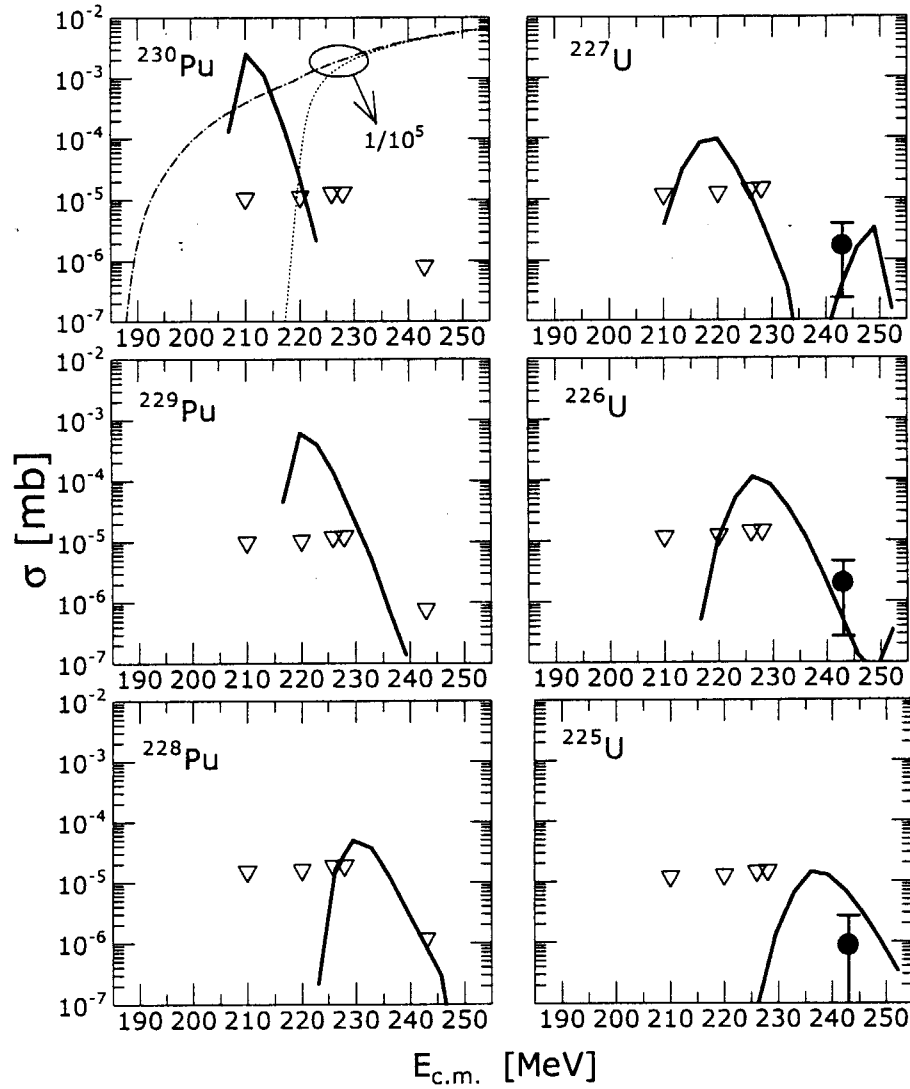
Fig.1. Evaporation residue cross sections for ^{82}Se+^{150}Nd. Thick solid curves are the calculated values by the statistical model. The thin dotted curve is the fusion cross section assuming one-dimensional barrier penetration model. The thin dash-dotted curve shows the fusion cross sections based on the coupled channel calculation.

3.5 MEASUREMENTS OF FUSION CROSS SECTIONS IN THE REACTIONS OF ^{82}Se + ^{138}Ba AND ^{82}Se + ^{134}Ba

K.SATOU[1], H.IKEZOE, K.NISHIO and S.MITSUOKA

Evaporation residue (ER) cross-sections for the reactions of ^{82}Se+^{138}Ba and ^{82}Se+^{134}Ba were measured by using ^{82}Se beams from JAERI-tandem booster accelerator, where ^{138}Ba has the neutron closed shell of N=82 while ^{134}Ba has no such neutron closed shell. Main purpose of these experiments is to investigate how strongly the fusion process is affected by the nuclear shell structure. All evaporation residues produced in the present fusion reactions are α-emitting nuclei and their energy and lifetimes of α-decay are known in the literature [1]. Therefore we can identify each evaporation residue by detecting its α-decay energy and lifetime event by event.

The targets were made by sputtering a barium oxide on an thin aluminum foil of the thickness of 1.3μm. The abundances of the mass 138 in a ^{138}Ba target and of the mass 134 in a ^{134}Ba target are ≈100% and 73.5%, respectively. The thicknesses of the targets were measured by the energy loss of α particles (5.486 MeV) from a ^{241}Am source, where the energy loss of α-particles in the barium target was calculated by the code TRIM [2]. The measured thicknesses of ^{138}Ba and ^{134}Ba targets were 410 and 500 μg / cm^2, respectively. The targets were mounted on a rotating frame and were rotated during the beam irradiation to prevent breaking from heating by ^{82}Se beam.

The evaporation residues emitted in beam direction were separated in-flight from the primary and scattered beams by the JAERI-recoil mass separator (JAERI-RMS). The separated ERs were implanted into the double-sided position-sensitive strip detector (DPSD) mounted at the focal position of the JAERI-RMS. The energy resolution of the DPSD was 75 KeV. The time-of-flight signal (TOF) of incoming particles was obtained by two microchannel-plate detectors mounted in front of the DPSD and 30 cm upstream the DPSD, respectively. The TOF signal was used to distinguish the α decay events from the incoming particles. Moreover, the rough estimation of a mass number of the incoming particles was obtained by using a two-dimensional spectrum of the energy of the incoming particles versus the TOF signal. A silicon surface barrier detector was set at 45° with respect to the beam direction in the target chamber to measure the elastic scattering of the ^{82}Se beam from the barium targets. The elastic scattering events were used to determine the absolute values of the evaporation residues cross section.

We identified some specific channels by detecting ER-α1 and α1-α2 correlation chains, where α1 and α2

---

[1]Department of Physics, Tsukuba University

are the parent and daughter α decay event, respectively. The correlated event in position was identified under the condition $(\Delta X, \Delta Y)=(0.6, 0.6)$ mm, where the ΔX and ΔY are the position uncertainties in the horizontal (x) and vertical (y) directions. Figure 1 shows a two-dimensional spectrum of α particle energy and the time interval between ER and α event, and Figure 2 shows the two-dimensional spectrum of $\alpha 1$ energy versus $\alpha 2$ energy. In order to obtain the absolute cross sections of ERs, the transport efficiency of the ER through the JAERI-RMS was estimated by the method described in Refs. [3,4]. The estimated transport efficiency for each ER was obtained by taking into account the charge fraction calculated by Ref. [5]. The obtained transport efficiency was about 0.35 for the xn channel. Furthermore the probability of
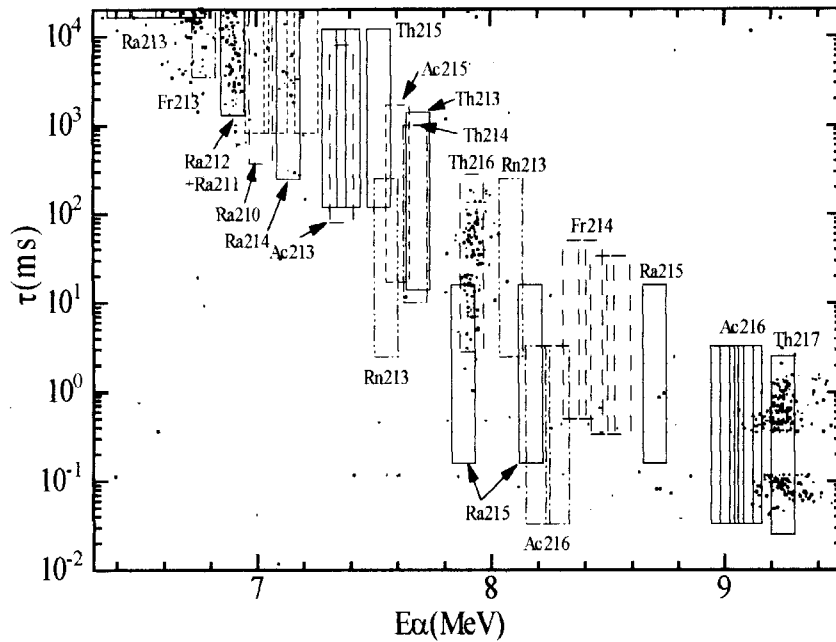
Fig.1. Two-dimensional spectrum of the energy versus the detected time interval between the α decay particle and the position-correlated ER, whose position difference was within $\Delta X=\Delta Y=0.6$mm
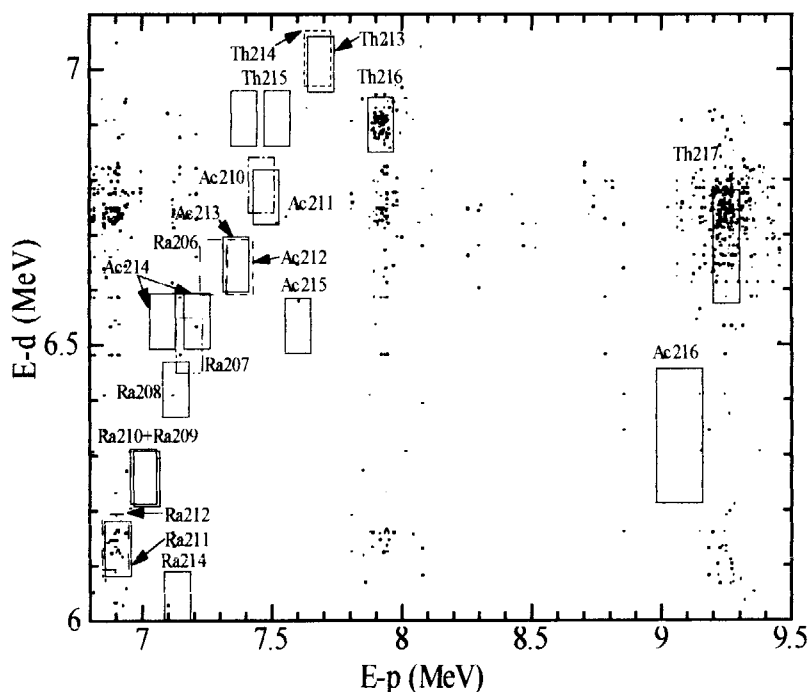
Fig.2. Two-dimensional matrix showing the correlated $\alpha 1$-$\alpha 2$ chain between parent and daughter α.

Boxes in Fig. 1 and in Fig. 2 indicate the eyes guide for each α-decay property of decay energy $E\alpha$ and half lifetime $T_{1/2}$. ($E\alpha$ - 50 KeV $\leq E \leq E\alpha$ + 50 KeV, $T_{1/2} / 10 \leq \tau \leq T_{1/2} \times 10$)

detecting the α decay of ER implanted in the DPSD was also estimated. The probability of full energy absorption of α particle from ^{216}Th was 0.64, for example, at the beam energy of 323 MeV.

The obtained evaporation residues cross sections (xn channels) for the reactions of ^{82}Se+^{138}Ba and ^{82}Se+^{134}Ba are shown in Figure 3 as a function of c.m. energy determined in the middle of the target layer. The error includes both statistical and systematical contribution. The systematical uncertainty was 40% coming from the transport efficiency and the charge distribution of ER.
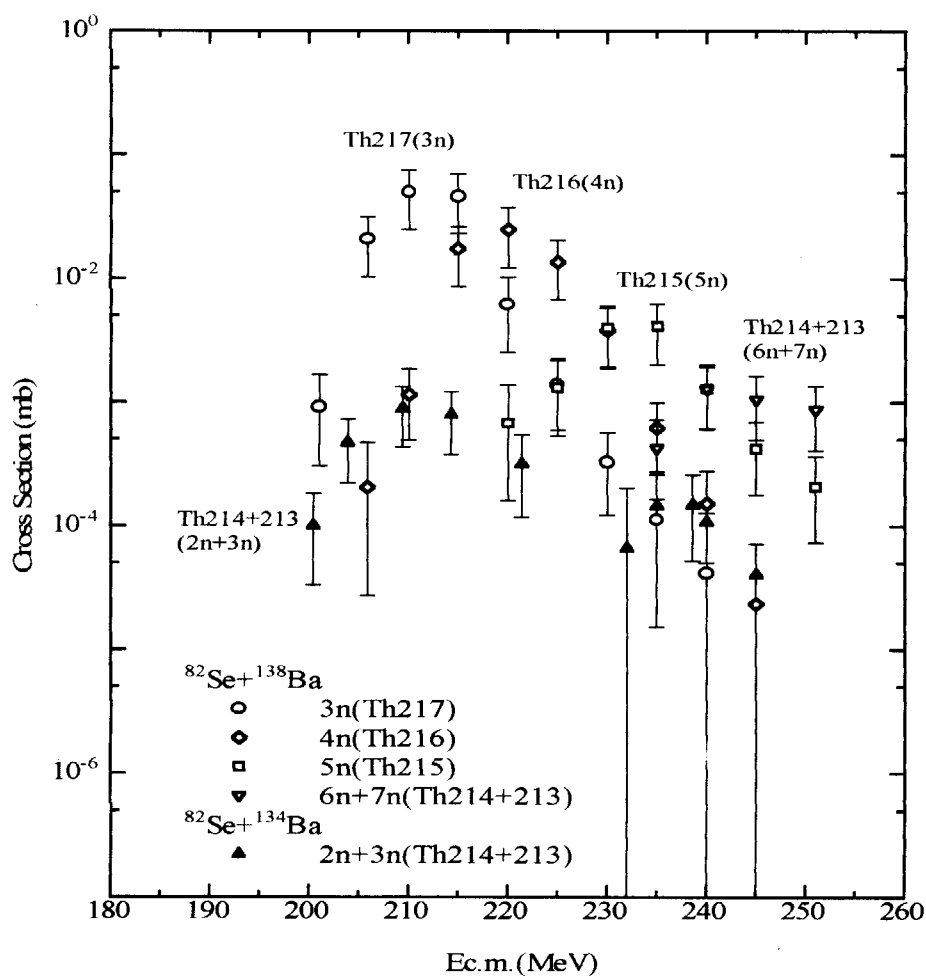
Fig. 3. Evaporation residues cross sections of xn channels for ^{82}Se+^{138}Ba and ^{82}Se+^{134}Ba reaction are shown together.

From Figure 3, we can see that the 2n+3n cross sections in the reaction of ^{82}Se+^{134}Ba are about a hundred times smaller than the 3n cross sections in the reaction of ^{82}Se+^{138}Ba at the low energy region of $E_{cm} < 210$ MeV. It is noted that at the high-energy region of $E_{cm} > 220$ MeV the small contamination of heavier masses 138,137,136,135 of the present target (these contaminations are 5.26%, 1.94%, 4.03%, 15.24%, respectively) comes into play in the ^{82}Se+^{134}Ba experiment. The analysis is now proceeding by using the statistical model code HIVAP [6] to simulate the deexcitation process of the excited compound nucleus.

References

[1] R. B. Firestone et al.; Table of Isotopes 8th ed. John Wiley, New York (1996)

[2] The computer code to calculate the transport of ions in matter; see "The stopping and range of ions in solid" by J. F. Ziegler, J. P. Beersak, and U. Littnark Pergamon Press, New York (1985)

[3] K. Nishio, H. Ikezoe, S. Mitsuoka, and J. Lu, Phys. Rev. C 62 (2000) 014602.

[4] T. Kuzumaki, H. ikezoe, S. Mitsuoka, T. Ikuta, S. Hamada, Y. Nagame, I. Nishinaka, and O. hashimoto, Nucl. Instrum. Methods Phys. Res. A 437 (1999) 107.

[5] K. Shima, T. Ishihara, and T. Mikuno, Nucl. Instrum. Methods 200 (1982) 605.

[6] W. Reisdorf and M. Schadel, Z. Phys. A 343 (1992) 47.

— 43 —

4. Nuclear Chemistry

This is a blank page.

4.1 SYNTHESIS OF THE METALLOFULLERENES ENCAPSULATING ACTINIDES

K. AKIYAMA[1], K. SUEKI[1], Y-L. ZHAO[2], H. HABA, M. ASAI, K. TSUKADA,
K. KIKUCHI[1], T. OHTSUKI[3], Y. NAGAME, H. NAKAHARA[1], and M. KATADA[1]

The metallofullerene is one of the most interesting materials because of its endohedral nature. The atmosphere in the fullerene cages is expected to be very reductive by π electrons that exist abundantly on fullerene cages. For this reason, it is possible that the metal atom encapsulated in fullerenes takes unusual oxidation states that we can't observe in aerobic atmosphere. We reported previously about the production of some metallofullerenes encapsulating actinides (for uranium, neptunium and americium) and unusual characters of these encapsulated atoms [1]. In this paper, we report the HPLC elution behavior of metallofullerenes of thorium and protactinium and discuss the chemical state of these atoms encapsulated in the fullerenes.

The metallofullerenes encapsulating thorium and protactinium were produced by the arc discharge method using carbon rods absorbing radiotracers of these elements [1,2]. The radiotracers of ^{234}Th and ^{233}Pa were prepared from the α decay of ^{238}U and ^{237}Np, respectively. These tracers were dissolved in ethanol and mixed with lanthanum nitrate as a carrier and a cerium tracer for comparison with each data. The ethanol solution was absorbed into porous carbon rods and then dried. The carbon rod was sintered for 3 h at 800 °C and mounted on the chamber as an anode for the arc discharge. The arc discharge for the fullerene synthesis was performed with the direct current of 110 A about 0.05 MPa of He atmosphere. The soot containing fullerenes was collected from the chamber by washing the wall with CS_2 and filtered to remove the insoluble substance. The CS_2 solution containing the thorium and protactinium metallofullerenes were dried, re-dissolved in toluene, and then developed to the Buckyprep and 5PBB columns with toluene as the eluting agent.

Figure 1 shows the HPLC chromatograms of Th and Pa metallofullerenes on the a) Buckyprep and b) 5PBB columns; for comparison, the previous results on those of uranium, neptunium, americium, and cerium are also plotted in the figure. The retention time of the metallofullerenes of Th and Pa was found to be different from those of the previously reported. As a result of the TOF/MS measurement, the observed elution peak for Th species has been

[1]Department of Chemistry, Graduate School of Sciences, Tokyo Metropolitan University

[2]Accelarator Research Center, The Institute of Physical and Chemical Research (RIKEN)

[3]Laboratory of Nuclear Science, Tohoku University
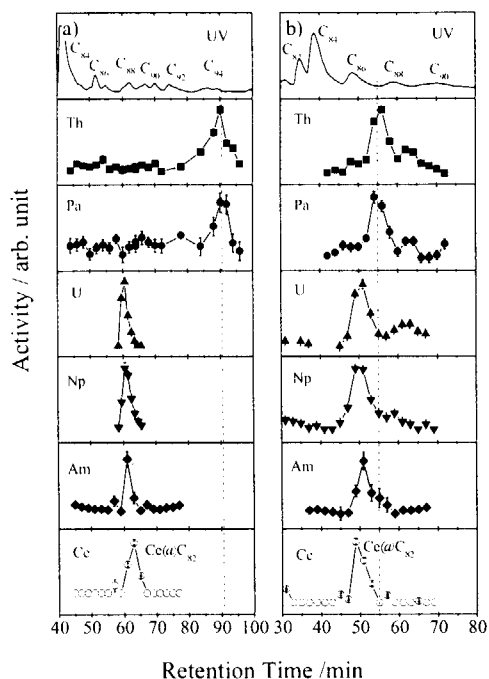
Figure 1. HPLC elution behavior of actinide fullerenes: (a) the HPLC elution curve for the Buckyprep column elution with toluene at 3.2 ml/min. (b) the HPLC elution curve for the 5PBB column elution by toluene at 6 ml/min. The major elution peaks of Th and Pa species are observed at the retention time of around 55 min.

Figure 2. Number of π electron vs. retention time on 5PBB column: The formal π electron number on fullerene cage is about 85 for U, Np, and Am and 87 for Th and Pa.

found to be Th@C_{84}, and that for Pa species is also considered to be Pa@C_{84} because of the similarity of chromatographic behaviors on both the columns. Stevenson et al [3] reported the correlation between the retention time and the number of electrons on the fullerene cage for the 5PBB column development. According to their logic, it can be said that the number of electrons on the cage of Th@C_{84} is the same as that of C_{87} because this species was eluted between C_{86} and C_{88} (See Figure 2). Thus, extra three electrons are moved to the C_{84} cage from the encapsulated metal atom. In conclusion, the oxidation state of the encapsulated Th and Pa atoms inside C_{84} would be 3+, and the reductive oxidation state of the encapsulated metal atoms is affected by the reductive environment of the inside of the fullerenes.

References

[1] K. Akiyama, Y.-L. Zhao, K. Sueki, K. Tsukada, H. Haba, Y. Nagame, T. Kodama, S. Suzuki, T. Ohtsuki, M. Sakaguchi, K. Kikuchi, M. Katada and H. Nakahara, J. Am. Chem. Soc. **123** (2001) 181.

[2] K. Sueki, K. Kikuchi, K. Akiyama, T. Sawa, M. Katada, S. Ambe, F. Ambe and H. Nakahara, Chem. Phys. Lett. **300** (1999) 140.

[3] S. Stevenson, P. Burbank, K. Harich, Z. Sun, H.C. Dorn, P.H.M. van Loosdrecht, M.S. deVries, J.R. Salem, C.-H. Kiang, R.D. Johnson and D.S. Bethune, J. Phys. Chem. A **102** (1998) 2833.

4.2 PRODUCTION CROSS SECTIONS OF ^{262}Db AND ^{261}Rf IN THE ^{248}Cm+HI REACTION SYSTEMS

K. TSUKADA, M. ASAI, H. HABA, I. NISHINAKA, S. GOTO, M. SAKAMA,
S. ICHIKAWA, Y. NAGAME, H. W. GÄGGELER[1], A. TÜRLER[1]
and M. SCHÄDEL[2]

To investigate chemical behavior of the transactinide elements, such as Rf and Db, the nuclides 78-s ^{261}Rf and 34-s ^{262}Db must be efficiently produced by bombarding heavy radioactive actinide targets with high-intensity heavy-ion beams. We have developed some experimental apparatuses for producing and detecting them, including a beam-line safety system for the radioactive ^{248}Cm target, a gas-jet transport system and a rotating wheel catcher apparatus for the measurement of the α and SF decays. Recently we have successfully produced the ^{261}Rf and ^{262}Db by using the ^{248}Cm(^{18}O, 5n) and ^{248}Cm(^{19}F, 5n) reactions, respectively, at the JAERI tandem accelerator facility, and their excitation functions have been measured.

The ^{248}Cm target of 590 μg/cm^2 in thickness and 5 mm in diameter was prepared by electrodeposition on to a 2.1 mg/cm^2 thick beryllium backing foil. The ^{18}O and ^{19}F beam intensities were 200 pnA and 300 pnA, respectively. The recoiling products attached to KCl aerosol generated by sublimation of KCl powder at 620 °C were continuously transported through a Teflon capillary and deposited on polyethylene terephthalate foils of 0.12 mg/cm^2 in thickness and 20 mm in diameter at the periphery of an 80-position stainless wheel of 80 cm in diameter. The transport yield was deduced to be about 35% based on the production of ^{252}Fm ($T_{1/2}$=25 h) by using ^{238}U(^{19}F, xn) reaction. The wheel was periodically rotated and the sources on the wheel were measured at six pairs of Si PIN photodiodes. The efficiency of each detector was approximately 40% for α particles and the energy resolution was about 30 keV FWHM for the top detectors and about 150 keV FWHM for the bottom detectors. All events were registered together with the time information in an event-by-event mode for determination of the correlations between mother and daughter nuclide.

The maximum production cross section of ^{261}Rf was evaluated to be about 13±3 nb at 94 MeV beam energy, and that of ^{262}Db was about 1.5±5 nb at 103 MeV. The measured excitation functions are shown in Fig.1. The closed circle indicates the present data and the open symbols are data from the literature. The series of open circles from Ref. [1] were normalized the present values in this figure, since the absolute values have not been reported. The present shape of the excitation function is good agreement with that of the literature. In the chemical experiment for Rf the beam energy had been selected in 99 MeV [2], and the reported absolute value was 5 nb [3]. In the present data, however, the maximum cross section around 94 MeV is 1.5 times larger

[1] Paul Scherrer Institute (PSI), CH-5232 Villigen, Switzerland
[2] Gesellschaft für Schwerionenforschung (GSI), D-64291 Darmstadt, Germany

than that in 99MeV. The present cross section of ^{262}Db was one order magnitude larger than the literature value [3,4]. Therefore this reaction system will be available to study the chemical behavior of Db without a very rare and relatively short half-life target material ^{249}Bk ($T_{1/2}$=320 d). These results indicate that there is a good chance to start the study of transactinide chemistry in Japan.
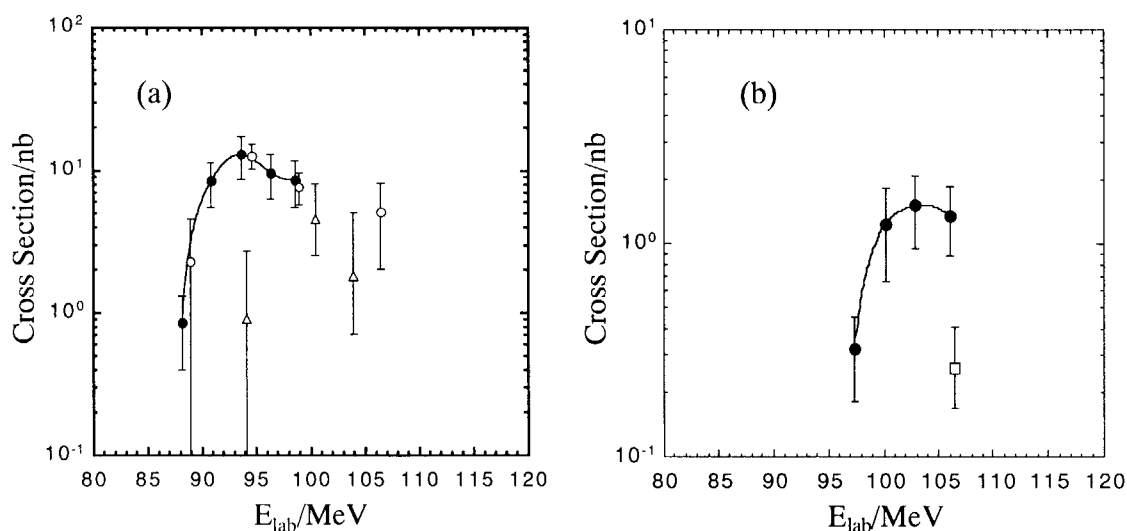
Fig.1. Measured excitation functions of the reactions (a) ^{248}Cm(^{18}O, $5n$)^{261}Rf and (b) ^{248}Cm(^{19}F, $5n$)^{262}Db. Open symbols are data from the literature: circle Ref. [1] (see text), triangle Ref. [3], square Ref. [4].

References

[1] A. Ghiorso et al., Phys. Lett. **32B** (1970) 95.

[2] E. Strub et al., Radiochim. Acta **88** (2000) 265.

[3] A. Türler, *Proc. Experimental Nuclear Physics in Europe*, edited by B. Rubio et al., CP495, AIP, New York (1999) p. 149.

[4] R. Dressler et al., Phys. Rev. **C59** (1999) 3433.

4.3 AQUEOUS CHEMISTRY OF Rf IN JAERI

H. HABA, K. TSUKADA, M. ASAI, S. GOTO[1], I. NISHINAKA, K. AKIYAMA[2],
A. TOYOSHIMA[3], M. HIRATA, S. ICHIKAWA, Y. NAGAME, T. KANEKO[1], H. KUDO[1],
A. YOKOYAMA[3], Y. SHOJI[3], A. SHINOHARA[3], Y. OURA[2], K. SUEKI[2], H. NAKAHARA[2],
M. SAKAMA[4], J. V. KRATZ[5], and M. SCHÄDEL[6]

We plan to study chemical properties of element 104 rutherfordium (Rf) in aqueous systems. The isotope ^{261}Rf was successfully produced in the ^{248}Cm(^{18}O,5n) reaction at the JAERI tandem accelerator [1]. For atom-at-a-time chemistry of ^{261}Rf, we have developed the **A**utomated **I**on exchange separation apparatus coupled with the **D**etection system for **A**lpha spectroscopy (**AIDA**). The chromatography unit is almost the same as that of the **A**utomated **R**apid **C**hemistry **A**pparatus (**ARCA**) developed by Schädel *et al.* [2]. It is equipped with two cartridges, each containing twenty micro-columns (1.6 mm in diameter, 8 mm long). The reaction products are transported by the He/KCl gas-jet system through a Teflon capillary (2.0 mm in diameter, 20 m long) on a mechanical slider. The KCl aerosol is dissolved with a desired solution and fed onto one of the micro-columns. The flow of eluents is directed through the column by computer control of chromatographic pumps, valves, and mechanical sliders. The effluent collected on a Ta disk is evaporated to dryness with hot He stream and a halogen heat lamp. The Ta disk is automatically subjected to α spectrometry by eight 600 mm^2 PIPS detectors.

On-line test experiments with AIDA were performed using the Rf homologues Zr and Hf. The isotopes ^{89m}Zr and ^{165,167}Hf were produced in the ^{89}Y(p,n) and ^{152}Gd(^{18}O,xn) reactions, respectively. MCI GEL CK08Y and CA08Y both with a particle size of about 20 μm supplied by Mitsubishi Chemical were used as cation and anion exchange resins, respectively. The distribution coefficients (K_d) for Zr and Hf on CK08Y and CA08Y were measured in 0.1 M HNO$_3$ / 5×10^{-4}–0.1 M HF solutions, because the ion exchange behaviors of Zr, Hf, Th, and Rf in this system were well investigated by Strub *et al.* [3]. Details of the experimental and analytical procedures are almost the same as described in Ref. [3]. The variations of the K_d values on CA08Y and CK08Y in 0.1 M HNO$_3$ are shown as a function of the HF concentration in Figs. 1a and 1b, respectively. The present on-line data for Zr and Hf are shown by closed circles and closed squares, respectively. The solid, dotted, and dashed curves indicate the off-line batch

[1] Department of Chemistry, Faculty of Science, Niigata University

[2] Department of Chemistry, Graduate School of Science, Tokyo Metropolitan University

[3] Department of Chemistry, Graduate School of Science, Osaka University

[4] Department of Radiological Technology, School of Medical Sciences, Tokushima University

[5] Institut für Kernchemie, Universität Mainz

[6] Gesellschaft für Schwerionenforschung

results for Zr, Hf, and Th, respectively, and the open squares and open triangles represent the on-line data for Hf and Rf, respectively, all of which are taken from Ref. [3]. It seems that the present results reproduce the off-line trend well, though the K_d values for CA08Y are two orders of magnitude higher at > 0.01 M HF than those reported in Ref. [3]. This discrepancy may be explained as the difference in the performance of anion exchange resins.

We first intend to perform ion exchange experiments of Rf in simple acid systems such as HNO_3 and HCl, where it may be easy to understand ion exchange behavior and to perform theoretical molecular orbital calculations. It is important to investigate chemical properties of Rf homologues Zr and Hf and its tetravalent actinide pseudo-homologue Th in order to predict a suitable experimental system for Rf and to verify the influence of the relativistic effects. For this purpose, carrier-free radiotracers ^{88}Zr and ^{175}Hf were produced in the ^{89}Y(p,2n)^{88}Zr and ^{175}Lu(p,n)^{175}Hf reactions, respectively, at the JAERI tandem accelerator. ^{234}Th was obtained as a daughter of the naturally occurring radioactive ^{238}U. By using these radiotracers, the K_d values on ion exchange resins were measured systematically in 1–11 M HCl and 1–14 M HNO_3 with the batch method. It was found that the K_d value for Th (510 ml/g) on the anion exchange resin CA08Y is more than one order of magnitude higher than those for Zr (8.0 ml/g) and Hf (12 ml/g) at 8 M HNO_3, reflecting the difference in the complex structures. On the other hand, the K_d values for Zr, Hf, and Th on CA08Y in 9.5 M HCl are 540, 60, and 0.56 ml/g, respectively, and they are all quite different from each other. Therefore, we will investigate the anion exchange behavior of Rf in both 8 M HNO_3 and 9.5 M HCl to obtain information useful to extract the ionic radius of Rf and to verify the influence of relativistic effects. The first experimental result on the ion exchange behavior of Rf in these aqueous systems will be reported elsewhere.
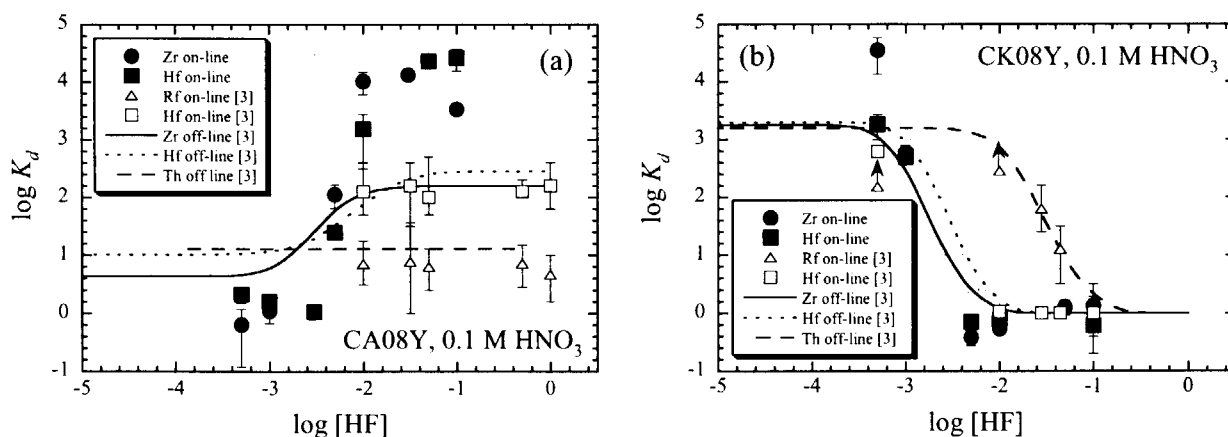
Fig. 1. Variation of the distribution coefficient (K_d) for Zr, Hf, Th, and Rf on (a) CA08Y and (b) CK08Y in 0.1 M HNO_3 as a function of the HF concentration.

References

[1] H. Haba et al.: Radiochim. Acta (in press).

[2] M. Schädel et al.: Radiochim. Acta 48(1989)171.

[3] E. Strub et al.: Radiochim. Acta 88(2000)265.

4.4 MEASUREMENTS OF LONG-LIVED NUCLIDES USING MULTI-PARAMETER COINCIDENCE METHOD

Y. HATSUKAWA, Y. TOH, M. OSHIMA, T. HAYAKAWA,

N. SHINOHARA, K. KUSHITA, T. UENO

Multi-parameter coincidence γ ray spectroscopy methods are widely used in the field of nuclear spectroscopic studies, and have produced many successful results. In order to scrutinize the ability of the multi-parameter coincidence method for activation analysis of long-lived nuclides, $^{129}I/^{127}I$ ratios in algae samples were measured.

^{129}I is a long-lived (half-life 1.57×10^7 y) radionuclide. During atmospheric nuclear explosion test, large amounts of ^{129}I have been released into the environment. ^{129}I is also formed in the nuclear fuel cycle. A reliable and practical method for the identification of ^{129}I is required from the viewpoint of environmental science.

In this study, we applied multi-parameter γ ray coincidence method with an array of 12 Ge detectors for identification of long-lived iodine, ^{129}I. Iodine was collected from algae samples. The algae samples were dried, and carbonized. After chemical purification, the iodine was precipitated as PbI_2, and irradiated in JRR-4 reactor. Gamma rays from PbI_2 samples were measured with an array of 12 Ge detectors with BGO Compton suppressors, GEMINI. Contents of ^{129}I are obtained from the intensity of γ–γ coincidence peak from ^{130}I produced by the $^{129}I(n,\gamma)$ ^{130}I reaction. Amount of stable iodine, ^{127}I is obtained from γ ray measurement of ^{126}I, produced by the $^{127}I(n, 2n)^{126}I$ reaction. Isotopic ratios of $^{129}I/^{127}I$ obtained in this study are listed in Table 1. Detection limit of this method is estimated at $^{129}I/^{127}I = 10^{-12}$.

Table 1 Isotopic ratio of $^{129}I/^{127}I$ in Japanese algae

Sample	Location	$^{129}I/^{127}I$
Kajime	Ibaraki	$3.5(5) \times 10^{-10}$
Konbu	Rishiri, Hokkaido	$7(3) \times 10^{-11}$

4.5 MEASUREMENT OF MASS YIELD DISTRIBUTIONS
IN PROTON-INDUCED FISSION OF MINOR ACTINIDES

N. SHINOHARA, H. HABA, Y. HATSUKAWA, M. OSHIMA, Y. TOH,
J. KATAKURA, O. IWAMOTO, K. NISHIO, Y. NAGAME, K. TSUKADA
and I. NISHINAKA

Fission product yields of minor actinides have been the subject of interest, because they are essential data in management of radioactive waste from nuclear power plants.   Although there are a lot of data on the fission of uranium and plutonium nuclides, the number of measured data on minor actinides is limited [1].   In the present study, the fission product yields of low-energy proton-induced fission of ^{241}Am and ^{243}Am were measured by γ-ray spectrometry in order to construct the mass yield distributions from the measured values.

Enriched targets of ^{241}Am and ^{243}Am were prepared by radiochemical method and irradiated by proton beams with the energies of 25 and 30 MeV for several hours at the JAERI tandem accelerator.   After irradiation, the fission products implanted into an aluminum catcher foil put behind the target were identified and determined by γ-ray spectrometry.

About forty fission products were determined in the p (25 MeV) + ^{243}Am reaction. Figure 1 shows the mass yield distribution constructed from the measured formation cross sections of the nuclides by correcting the charge distributions.   Systematic trends of the mass yield distributions in the proton-induced fission of the minor actinides will be discussed quantitatively in a separate paper.

Fig. 1.   Mass yield distribution for the fission of ^{243}Am with 25-MeV protons.
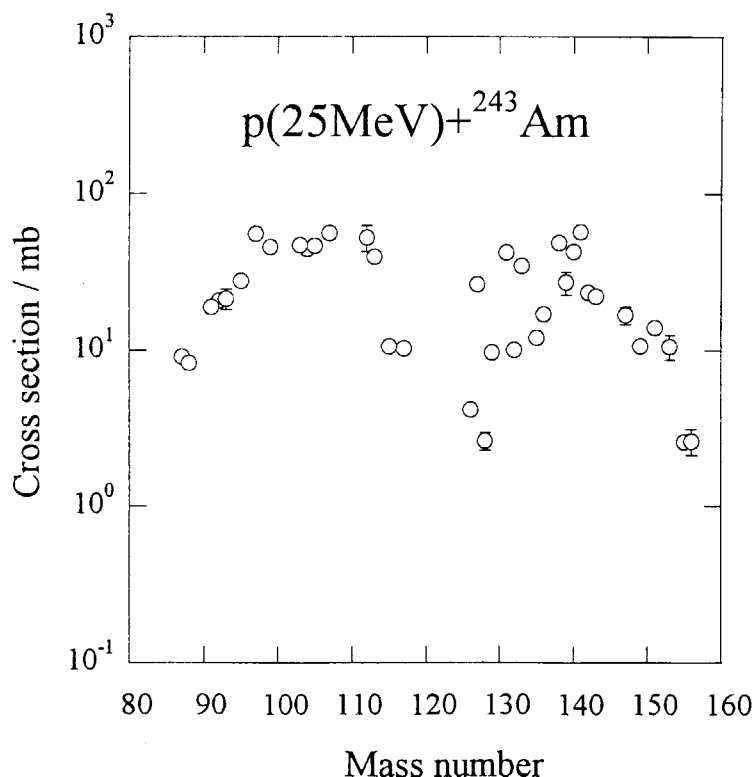
Reference

[1] Z. Qin et al., Radiochim. Acta **84** (1999) 115.

4.6 MASS AND ENERGY DISTRIBUTIONS OF FRAGMENTS IN THE PROTON-INDUCED FISSION OF ACTINIDES

S. GOTO[1], I. NISHINAKA, Y. NAGAME, S. ICHIKAWA, K. TSUKADA, M. ASAI, H. HABA,
S. MITSUOKA, K. NISHIO, M. SAKAMA[2], Y. L. ZHAO[2], K. SUEKI[2], H. NAKAHARA[2],
K. TANIKAWA[3], K. TAKAMIYA[4], Y. HAMAJIMA[5],
D. KAJI[1], and H. KUDO[1]

In the low-energy fission of actinides, it has been demonstrated that there exist at least two independent deformation paths; one leads to a symmetric elongated scission conifguration, and the other leads to a compact scission configuration with reflection asymmetry [1]. From the detailed analysis with respect to the asymmetric mass distributions in the proton-induced fission of ^{232}Th, ^{238}U, ^{244}Pu, and ^{248}Cm, it has been found that the lighter side of the heavier asymmetric mass distributions converges on $A = 126$–128, but on the other hand the heavier side of those distributions broadens with the fissioning nucleus mass number. Those features of the asymmetric mass distribution would be caused by the shell structure of the fragments: heavy fragments with $Z = 50$ and the $N = 50$ shell structure of the complementary light fragments. If the systems with different N/Z are studied, it is expected that the features of the asymmetric mass distribution will become different from those in the above systems because the fragment mass number corresponding with $Z = 50$ and $N = 50$ changes. Thus, to study systematically the relation between the asymmetric mass distribution and the shell structure of the fragments, the fragment mass and total kinetic energy distributions in the proton-induced fission of uranium isotopes, ^{233,235,238}U ($N/Z = 1.52, 1.54, 1.57$), and plutonium isotopes, ^{239,242,244}Pu ($N/Z = 1.53, 1.56, 1.58$), are precisely measured.

Each target of the uranium and plutonium isotopes on 0.1 μm Ni backing foils was bombarded with 13 and 15-MeV proton beams at the JAERI tandem accelerator. Fission fragment velocities were measured by the double time-of-flight (TOF) method. Detailed conditions are described in Ref. [2]

From the measured velocities of the complementary fragments, the mass and the total kinetic energy (TKE) of the fragments were determined. Details of analysis were described in Ref. [1]. Furthermore, mass distributions were decomposed into symmetric and asymmetric components by a two component analysis of TKE distributions [3]. In Fig.1, the preliminary results on the heavy asymmetric mass distributions in the 13-MeV proton-induced fission of ^{233,235,238}U are shown. It is found that the peak position shifts to heavier mass number with the fissionig nucleus mass number. The heavier wing shifts to the heavy mass side with the fissioning nucleus mass A_f as expected. More detailed analysis considering the light wings of the distributions and that in the other reaction systems are in progress.

[1] Department of Chemistry, Niigata University
[2] Department of Chemistry, Tokyo Metropolitan University
[3] Department of Chemistry, The University of Tokyo
[4] Research Reactor Institute, Kyoto University
[5] Department of Chemistry, Kanazawa University

References

[1] Y. Nagame *et al.*, Phys. Lett. **B387** (1996) 26.

[2] S. Goto *et al.*, JAERI-Review 2000-018 (2000) 49.

[3] Y. L. Zhao *et al.*, Phys. Rev. Lett. **82** (1999) 3408.
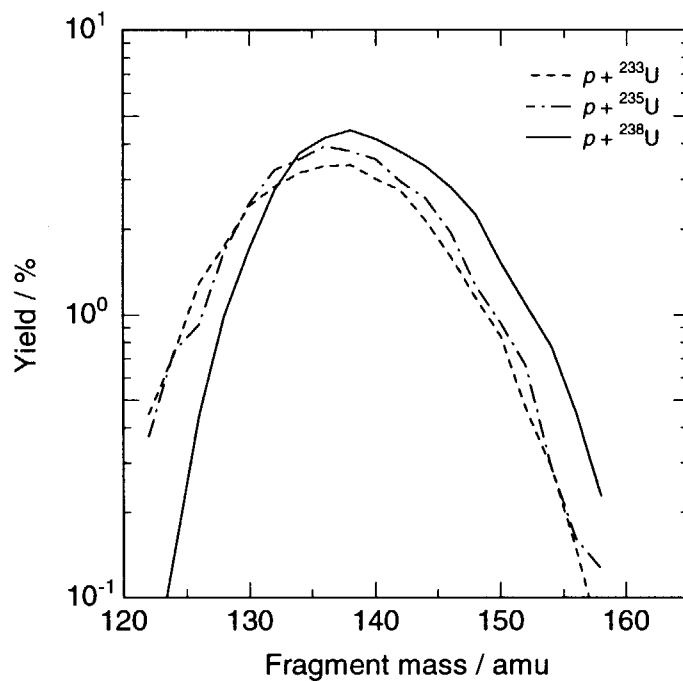
Fig. 1. Heavy asymmetric mass distributions of the 13 MeV $p+^{233,235,238}$U systems.

4.7 EMISSION PROBABILITY MEASUREMENT OF PRINCIPAL GAMMA RAYS FOR [147]Eu

H. MIYAHARA[1], N. MARNADA[2], Y. KATOH[2], K. KATOH[2], K. FUJIKI[2],
S. ICHIKAWA, K. TSUKADA, I. NISHINAKA, H. HABA, Y. NAGAME, M. SAKAMA

Gamma-ray emission probability is one of the important decay parameters for radionuclide, because it informs absolute number of quantum gamma rays derived from a gamma-ray pulse height spectrum. Many nuclides have been studied to determine the decay parameters, but very few of the studies concern with direct investigation of gamma-ray emission probability. In addition, the reported results show still large uncertainties and large spread in the absolute values, especially for proton-rich nuclides. The failure in providing precise gamma-ray emission probabilities in the measurements or evaluation might be caused mainly by imprecise beta-ray branching ratios. To improve the certainty the gamma-ray emission probability is to be determined from the gamma-ray intensities and disintegration rate. The purpose of the present study is to establish emission probabilities of principal gamma rays for [147]Eu by using $4\pi\beta$-γ coincidence apparatus.

Preparing sample source with high specific activity is important for precise measurement because presence of non-active materials affects the certainty of disintegration rate. [147]Eu sources were produced by 10 MeV proton irradiation of enriched [147]Sm (enrichment : 98.34%), and the suitable proton energy was determined from pre-experiment and calculation by the ALICE code [1]. At the energy over 10 MeV [146]Eu was produced by the [147]Sm(p,2n) reaction, and at the lower energy the yield of [147]Eu decreased gradually.

The irradiated sample was dissolved in dilute HCl solution and [147]Eu sources were prepared on thin metallised VYNS films stretched on brass mounts. Measurements were carried out by a $4\pi\beta$ pressurised proportional counter, an HPGe gamma-ray detector with relative efficiency of 23%, and coincidence apparatus using a two-dimensional data-acquisition system [2]. Gamma-ray detection efficiencies were calibrated by measuring the gamma-ray spectra and disintegration rates of standard sources of [57]Co, ^{60}Co, [133]Ba, [134]Cs and [152]Eu. The gamma-ray emission probailities adopted for these nuclides were the evaluated values taken from an IAEA report [3]. The measured data were corrected for cascade summing effect. A fourth-order polynomial function was fitted to the logarithms of the energy and efficiency by a method of least squares incorporating a covariance matrix.

Fig. 1 shows an example of gamma-ray spectrum and the principal photopeaks of the 121.3, 197.4, 601.4, 677.6, 798.9, 857.1, 933.2, 955.9 and 1077.2 keV gamma rays are clearly seen. If [146]Eu was contained in the source, the photopeak of 747 keV gamma ray (emission probability : 98%) could be recognised. Therefore, this spectrum shows that the sample contained less than 0.1% of [146]Eu. The disintegration rate was determined from the coincidence efficiency functions obtained for the gates set of the 121.3, 601.4 and 677.6 keV gamma rays.

---

[1] Department of Radiological Technology, School of Health Sciences, Nagoya University

[2] Department of Nuclear Engineering, Graduate School of Engineering, Nagoya University

The emission probabilities of the principal gamma rays were calculated from the disintegration rate, gamma-ray intensities and gamma-ray detection efficiencies. The results are shown in Table 1 together with the evaluated data. The evaluated values show large uncertainties close to 10%, but the present work gives uncertainties of about 1%. Furthermore, the evaluated values are larger than the present ones by about 20%, 10% and 5% at low, middle and high energy regions, respectively.

References

|1| M. Blann and H.K. Vonach, Phys. Rev. **C28** (1983) 229.

|2| H. Miyahara, K. Ikeda and N. Marnada, J. Nucl. Sci and Technol. **38** (2001) 270.

|3| IAEA, X-ray and gamma-ray standards for detector calibration, IAEA-TECDOC-619, Vienna (1991)

|4| E. Browne and R.B. Firestone, Table of Radioactve Isotopes, Wiley, New York (1986)

|5| E. der Mateosian and L.K. Peker, Nucl. Data Sheets, **66** (1992) 705.
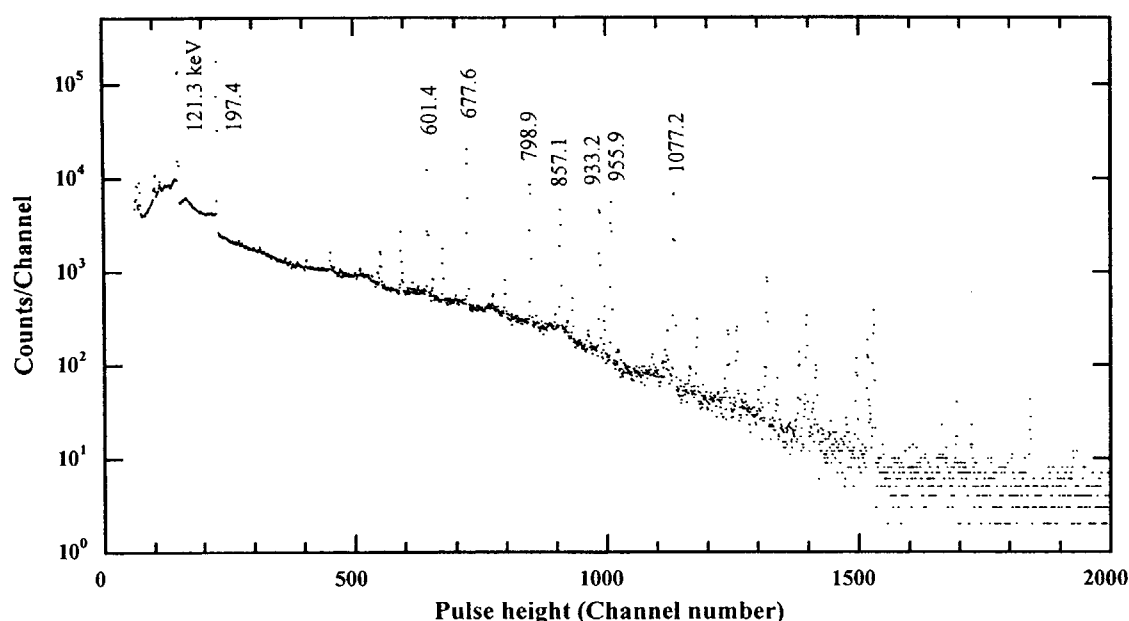
Fig. 1   An example of gamma-ray pulse height spectrum of ^{147}Eu source

Table 1   Measured and evaluated emission probabilities of principal gamma rays (%)

Energy (keV)	Table of Radioactive Isotopes [4]	Nuclear Data Sheets [5]	Present result
121.3	22.7(31)	22.9(21)	18.48(13)
197.4	26.0(26)	26.5(22)	21.62(15)
601.4	6.8(9)	5.9(5)	5.32(4)
677.6	10.7(13)	9.8(9)	8.97(6)
1 077.2	6.4(8)	6.1(5)	5.80(4)

— 57 —

5. Nuclear Theory

This is a blank page.

5.1 ANALYSIS OF LOW-LYING COLLECTIVE LEVEL STRUCTURE, B(E2) AND NUCLEON INTERACTION DATA OF ^{56}Fe BY SOFT-ROTATOR MODEL

E.Sh. SOUKHOVITSKII[1], S. CHIBA, J-Y LEE[2], Y-O LEE[2], J. CHANG[2] and O. IWAMOTO

We applied the soft-rotator model[1] to analyze the collective level structure, nucleon interaction and B(E2) γ - transition data for ^{56}Fe in the unified framework. The essence of the coupled-channels formalism based on the soft-rotator model is in the account of the enhancement of the coupling strengths as compared with the conventionally used rigid-rotator model [2], which arises because the dynamic variables appearing in the expansion of the deformed potential are averaged over the appropriate nuclear wave functions which are eigenfunctions of the soft-rotator Hamiltonian, describing rotational-vibrational states of non-axial deformed nuclei.

The experimental low-lying collective levels of ^{56}Fe nucleus are described by adjusting the Hamiltonian parameters in the soft-rotator nuclear model. Figure 1 shows comparison of the theoretical and experimental nuclear energy levels for ^{56}Fe. The experimental levels denoted with thin lines are not included in the present calculations. Rotational structure is not very prominent in case of ^{56}Fe nucleus: nevertheless we could describe the first five low-lying collective levels and some other lying above, necessary for creating coupling scheme of coupled-channel calculations, with average energy accuracy better than 5%.

Nuclear wave functions of the soft-rotator model with the adjusted nuclear Hamiltonian parameters were used to construct the coupling among eight collective levels of ^{56}Fe, 0^+(G.S.), 2_1^+(0.847 MeV), 4_1^+(2.085 MeV), 2_2^+(2.658 MeV), 0_2^+(2.942 MeV), 2_3^+(3.748 MeV), 3_1^+(3.445 MeV), and 3_1^-(4.510 MeV), in the coupled-channel (CC) calculations.

The optical potential parameters were searched by minimizing χ^2 involving neutron and proton scattering data and neutron total cross sections. Figure 2 shows the calculated total neutron cross sections for ^{56}Fe compared with the experimental data up to incident energy 160 MeV. The theoretical results are in good agreement with the experimental data over the energy range region.

Elastic and inelastic angular distributions both for neutrons and protons are described with good accuracy. Figure 3 shows the typical quality of angular distributions predictions. Calculated proton nonelastic cross section is also in good agreement with experimental data.

Determined soft-rotator nuclear Hamiltonian parameters can be used to calculate γ - transition probabilities with the account of nuclear non-axiality and softness (for details see:[1]) to be compared with available experimental ones[3, 4]:

Value for B(E2; 2_1^+(0.847MeV) $\rightarrow$ 0^+(G.S.)) transition probability, calculated with account of inner dynamic variables taken up to square terms is equal to $0.0208e^2b^2$, while experimental value is $0.0214\pm0.0009e^2b^2$[3] , calculated B(E2; 4_1^+(2.085MeV) $\rightarrow$ 2_1^+(0.847MeV)) is $0.0360e^2b^2$, while experimental value is $0.031\pm0.006e^2b^2$[3]. Calculated quadrupole moment of 2_1^+(0.847MeV) level Q_{2_1} is -0.289eb, which can be compared with experimental value[4] is equal to -0.249$\pm$0.0586eb.One can see, that soft rotator model describes G.S. rotational band level properties rather accurately. We can conclude that γ - transition values give evidence that ^{56}Fe nucleus is a relatively soft prolate rotator and its softness should be taken into account. The same values calculated for ^{56}Fe

in 2p-2h shell model plus inert ^{56}Ni core are[4]: B(E2; 2^+_1(0.847MeV) $\rightarrow$ 0^+(G.S.))=0.0115e^{2}b^2; B(E2; 4^+_1(2.085MeV) $\rightarrow$ 2^+_1(0.847MeV))=0.0161 e^{2}b^2, Q_{2_1} = -0.215eb.

References

[1] S. Chiba, O. Iwamoto, Y. Yamanouti, M. Sugimoto, M. Mizumoto, K. Hasegawa, E. Sh. Sukhovitskiĭ, Y. V. Porodzinskiĭ, and Y. Watanabe, Nucl. Phys. A **624**(1997)305.

[2] T. Tamura , Rev. Mod. Phys. **37**(1965)679.

[3] Huo Junde, Nuclear Dater Sheets **67**(1992)523.

[4] P.N.S. Lesser et al., Nucl. Phys., **A190** (1972)597.
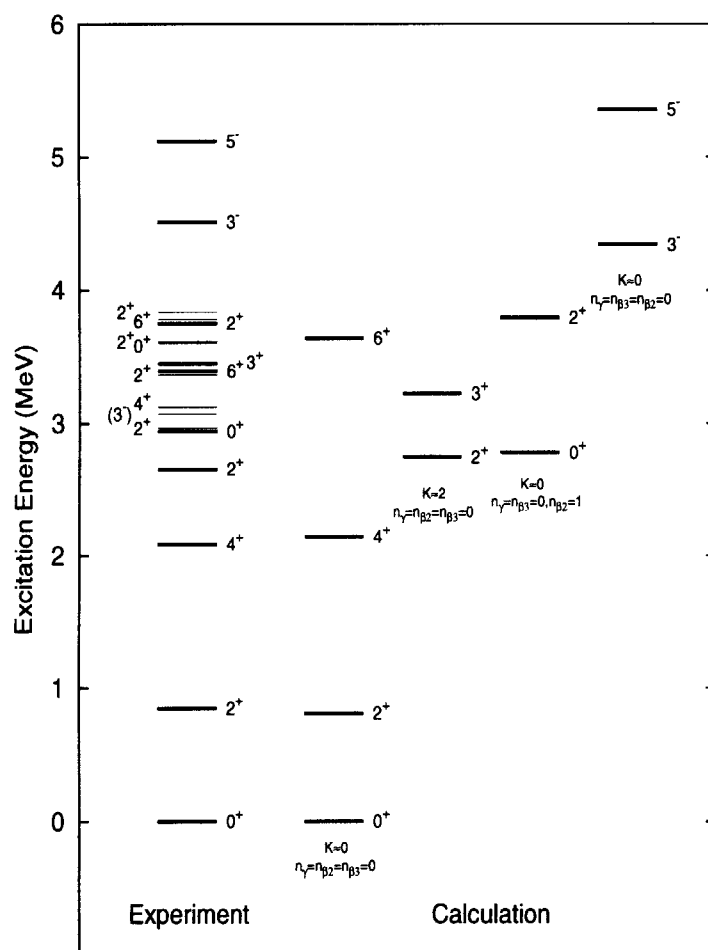
Figure 1. Comparison of the theoretical and experimental levels for ^{56}Fe nucleus. The experimental levels denoted with thin lines are not included in the present calculations.
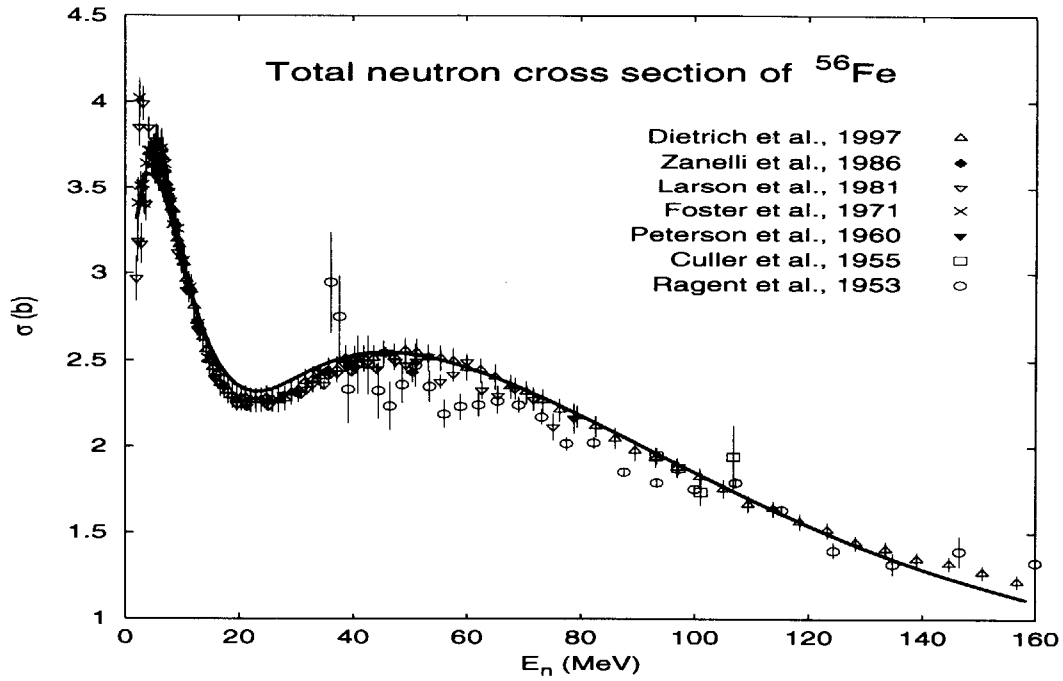
Figure 2. Comparison of the theoretical (solid lines) and experimental total neutron cross sections for ^{56}Fe up to 160 MeV neutron incident energy.
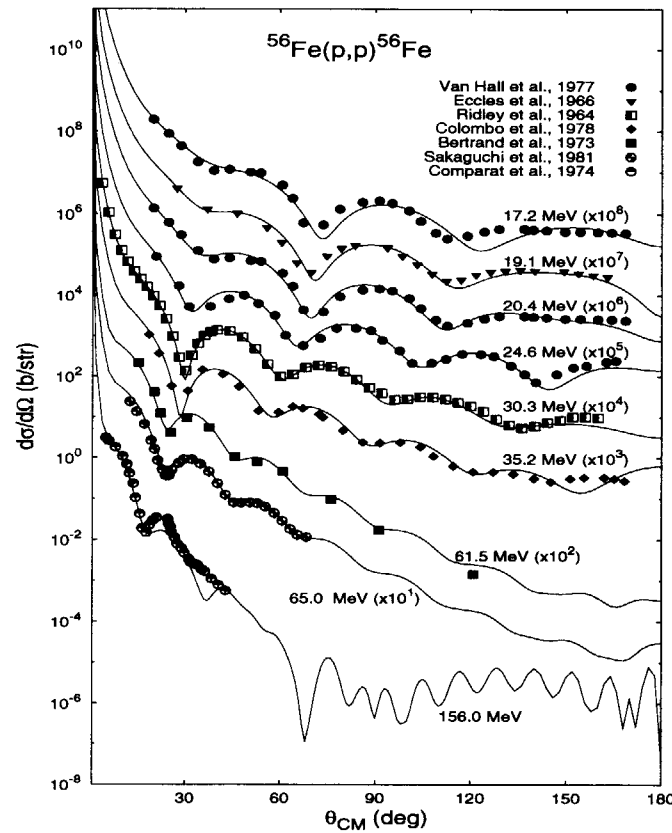
Figure 3. Comparison of the theoretical and experimental angular distributions for protons elastically scattered by ^{56}Fe.

5.2 NUCLEAR FRAGMENTATION BY TUNNELING

T. MARUYAMA, A. BONASERA [1] and S. CHIBA

For a long time the problem of spontaneous fission (SF) has been of large interest for both experimentalists and theorists [1]. Both the N-particle nature of the system, i.e. the atomic nucleus, and the quantum aspect, i.e. penetration of a barrier, have stimulated a huge literature production and still the problem is largely unsolved from a quantum mechanical point of view. To a minor extent, the "inverse process" of SF i.e. subbarrier fusion has also stimulated many workers [1, 2]. Our present purpose is to suggest a similar problem which involves the quantum N-body features as well as the possibility of critical phenomena. The multifragmentation in heavy-ion collisions has been one of the most attractive problems in nuclear physics. Many authors have discussed the reaction mechanism as a phase transition where many liquid fragments are formed from hot gas when the temperature of the system decreases. Another mechanism can be a cracking of the system. In both cases multifragmentation can take place only when the energy of the system is high enough to overcome the barrier against the expansion. On the other hand, when the energy of the system is too low, the expansion will come to an halt and the system will shrink back. Simply assuming the expansion is spherical, we could roughly describe it with a collective coordinate $R(t)$, the radius of the system at time t and its conjugate coordinate $P(t)$. We can imagine that connected to the collective variable $R(t)$ there is a collective potential $V(R)$. Thus, at low energies fragmentation by tunneling through the collective potential $V(R)$ can be considered. When this happens, fragments will be formed at very low T not reachable otherwise than through the tunneling effect.
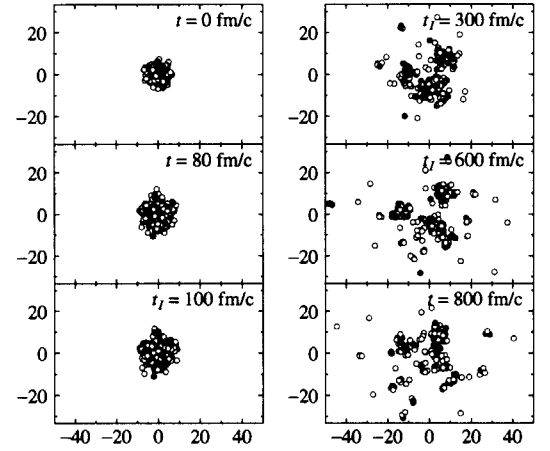
Figure 1: Snapshot of tunneling fragmentation of ^{230}U with $E^* = 6.8$ MeV/u. White circles represent neutrons and gray ones protons. The time in the simulation t is shown in each panel. After the system enters the tunneling region, the time is written as t_I.

We combine imaginary-time prescription with quantum molecular dynamics model [3] to simulate fragmentation of finite system with relatively low excitation energy E^*. At sufficiently low E^*, fragmentation occurs via tunneling. In Fig. 1 we display snapshots of a typical tunneling event. The collective coordinate $P(t)$ becomes zero at $t = 100$ fm/c. At this stage we turn to imaginary times and the tunneling begins. Notice that the system indeed expands and its shape can be rather well approximated to a sphere at the beginning. The corresponding probability II of tunneling event is calculated using the action S during the tunneling process. Unfortunately the calculated probability is found to be very small. Figure 2 (a) shows the calculated probability of fragmentation with fragment multiplicity of 2 and 3 vs. E^*/E_0. Here E_0 is the threshold for having real events with $M = 3$. The value E_0 depends on the detail of the force and in our case $E_0 = 7$ MeV.

[1] INFN-LNS, Via S. Sofia 44, Catania 95123, Italy.

Although the probability of tunneling fragmentation is very small, one possible observable may be the fragment mass distribution. In Fig. 2 (b) we plot the average fragment mass for intermediate mass fragment multiplicity M of 2 and 3. Although we see slight difference between imaginary and real events, the values are too close to be distinguished. However, if we plot the average momentum of produced fragments in Fig. 2 (c), we see significant difference between imaginary and real events. It is rather natural that real events have larger value of fragment momenta since the eventual difference of kinetic energy of the expansion determines whether the system experiences the imaginary process or not. However, the difference of the process itself has some effects on the resulting fragment momenta: in the real events the fragments momenta are larger for cases with large fragment multiplicity $M = 3$ compared to $M = 2$. This is due to the different Q-value for events with $M = 3$ and 2. In fact the difference of the total kinetic energy of large fragments for two types of events, which amounts to about 30 MeV, almost exactly corresponds the difference of their Q-values estimated by a simple liquid-drop model. In imaginary events, on the contrary, fragment momenta for $M = 3$ and 2 are almost the same though there are large fluctuations due to the poor statistics. This is due to the fact that below the threshold, the system must use all the excitation energy to form the final fragments. In order to do that the final fragments keep the lowest possible kinetic energy. The final kinetic energy is essentially due to Coulomb repulsion at the second turning point (end of tunneling region). Thus precise experimental information on the final kinetic energies will give us an insight on the densities at freeze out. The comparison of fragment momenta between the fragment multiplicity $M = 2$ and 3 may give a signature of the tunneling fragmentation [4].
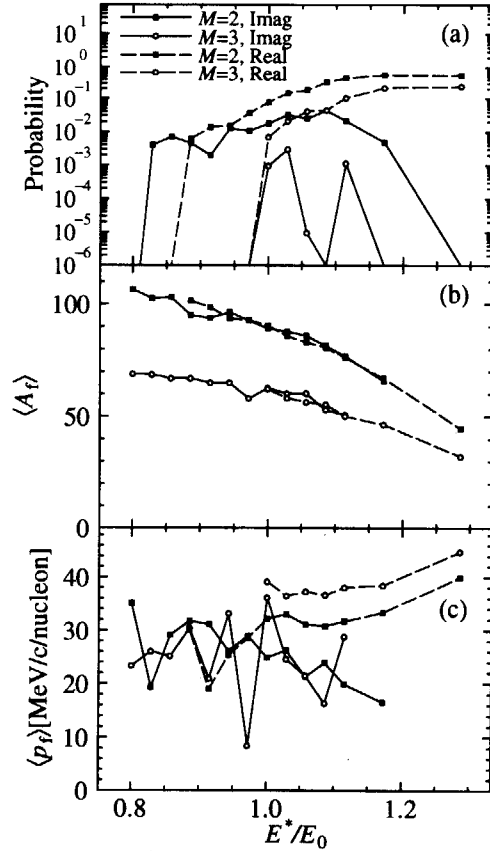
Figure 2: (a) Reaction probability; (b) average mass of large fragments ($Z \geq$ 3); (c) average momenta of large fragments. The abscissa is scaled by E_0.

References

[1] *Proceedings of the International Conference on Fifty Years Research in Nuclear Fission, Berlin April 1989*, edited by D. Hilscher et al. [Nucl. Phys. **A502** (1989) 1c-639c].

[2] A. Bonasera and V. N. Kondratyev, Phys. Lett. B. **339** (1994) 207; A. Bonasera and A. Iwamoto, Phys. Rev. Lett. **78** (1997) 187.

[3] T. Maruyama, K. Niita, K. Oyamatsu, T. Maruyama, S. Chiba, and A. Iwamoto, Phys. Rev. C **57** (1998) 655.

[4] T. Maruyama, A. Bonasera and S. Chiba, Phys. Rev. C **63** (2001) 057601.

5.3 NEW PARALLEL COMPUTER SYSTEM "HELIOS" INSTALLED IN JAERI TANDEM

Y. UTSUNO, T. HAYAKAWA and M. OSHIMA

Since the 1990's, a parallel-computing technique in which a single computational task is divided into a number of factors performed in each individual processor has been developed in the field of numerical computation very rapidly. In many cases, each processor used in the parallel computing is scalar-type one. On the other hand, a large-scale numerical computation was carried out mainly with a supercomputer consisting of a vector-type processor before. For instance, the situation is shown in the so-called TOP500 list [1] where names of the fastest 500 computers are listed in the order of their performance of the numerical computation. In the list, the number of computers comprised of vector-type processors decreases from 332 in 1993 to 50 in 2000, out of the fastest 500 computers. This is mainly because, for scalar-type processors, the ratio of the price to their performance is decreasing very rapidly. Thus, one can increase the number of processors keeping the total price reasonable. This is why the parallel computing becomes popular in the numerical computation. Many scientific calculations are quite suited for the parallel computing, including a Monte Carlo calculation, one which needs a number of results with different parameters, etc.

A parallel computer system was newly installed in the building of the JAERI tandem facility in January 2001, and was open for users in this April. This system was named Helios. It aims mainly at experimental and theoretical analyses of the results obtained from an experiment with the tandem accelerator, as well as theoretical calculations related to researches with it. The Helios system is made of personal-computer components which are available rather inexpensively. The system consists of two servers, a a boot and a file server, and 69 nodes all of which have no hard disk. The numerical computation is performed on each node, and input/output data are stored in the hard disk of the file server. The nodes are booted up using the floppy disk. The CPU of each node is the AMD Athlon processor whose clock frequency is 900 MHz. As for the network, the nodes are connected by the 100Base-TX Ethernet. Because of the limitation associated with the above configuration, the Helios system is not suitable for a calculation which requires very frequent and/or heavy network traffic and file access.
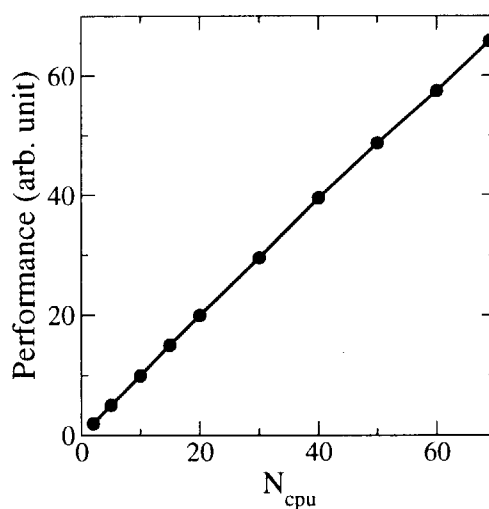
Fig. 1. Performance of the Helios computer system as a function of the number of computing nodes. The Monte Carlo shell-model code is used. The performance is defined as the inverse of the elapsed time. Unit is fixed so as to be 2 in the case of the configuration with 2 computing nodes and the servers.

We tested the performance of the Helios system as a parallel computing system, measuring the elapsed time in changing the number of the computing nodes from 2 to 69. We used the Monte Carlo shell-model [2] code as a benchmark test. The Parallel Virtual Machine (PVM) library is used as a tool supporting the parallel computing in the Monte Carlo shell-model calculation. As an alternative tool, one can use the Message Passing Interface (MPI). In the Monte Carlo shell model, three-dimensional numerical integration is very frequently performed in the process of the angular momentum projection. In this numerical integration, each coordinate axis is divided into $N_{mesh} = 20\text{-}30$ mesh points. Then, $N_{mesh}^3 \sim 10^4$ individual computations are totally carried out per three-dimensional integration. The parallel computing is performed by distributing these computational tasks into each node. In the present case, other computational time is negligibly short. If the parallel computing works most efficiently, the peformance defined as the inverse of the elapsed time should be proportional to the number of the computing nodes. The performance of the Helios system was measured with the Monte Carlo shell-model code. Figure 1 shows the variation of the performance as a function of the number of nodes. One sees that the performance increases almost proportional to the number of nodes. Indeed, in the case of the maximum number of CPU's (69 CPU) the performance reaches about 96% of the "ideal" value, i.e., the performance extrapolated from the 2-CPU elapsed time. In the present benchmark test, an about 10kB datum is transfered among the nodes per ~ 3 seconds for the 69-CPU calculation. The result shows that delay due to the network trafic is quite small compared to the total computational time.

Presently, 12 users have their accounts of the Helios system. We hope that more and more researchers are interested in the parallel computing and that the system helps their study.

References

[1] TOP 500 Supercomputer Sites, http://www.top500.org.
[2] T. Otsuka, M. Honma, and T. Mizusaki, Phys. Rev. Lett. **81** (1998) 1588, and references therein.

5.4 FEASIBILITY FOR AN ODD-A NUCLEUS ^{31}Na OF THE MONTE CARLO SHELL MODEL

Y. UTSUNO, T. OTSUKA,[1] T. MIZUSAKI[2] and M. HONMA[3]

Since anomalous properties of ^{31}Na concerning the mass [1] and the ground-state spin and magnetic moment [2] were observed in the 1970's, the structure of neutron-rich nuclei around $N = 20$ has attracted much interest, particularly concerning vanishing of the $N = 20$ magic number. Based on the Monte Carlo shell model (MCSM) [3], we performed a systematic shell-model calculation for even-even $N \sim 20$ exotic nuclei with full mixing between the normal, intruder, and higher intruder configurations for the first time [4], and gave a comprehensive picture of the region. Here, the MCSM implies applications of the quantum Monte Carlo diagonalization (QMCD) method to the nuclear shell model. As for odd-A nuclei, since we should adopt J-compressed bases [3] which require much computational time in the MCSM calculation, such a calculation was not practical until we used a parallel computer. In 2001, a parallel computing system "Helios" was installed in JAERI, enabling us to perform a systematic calculation including odd-A nuclei and ones which need a more extended model space. In the present study, the structure of a neutron-rich odd-A nucleus ^{31}Na, which is expected to be in the "island of inversion" [5], is studied by the MCSM [6].

We first examine whether or not the MCSM calculations can be performed for odd-A nuclei with a small number of bases similarly to even-even nuclei. The number of bases adopted in the MCSM calculation is referred to as the QMCD basis dimenasion. We compare energy levels of ^{25}Mg obtained by the MCSM and the exact shell-model result in Fig. 1. The total $M = 1/2$ shell-model dimension is 44 133, which is much more than the QMCD basis dimension. Figure 1 shows that the MCSM results come close to the exact ones for the dimension ~ 40, indicating the feasibility of the MCSM.
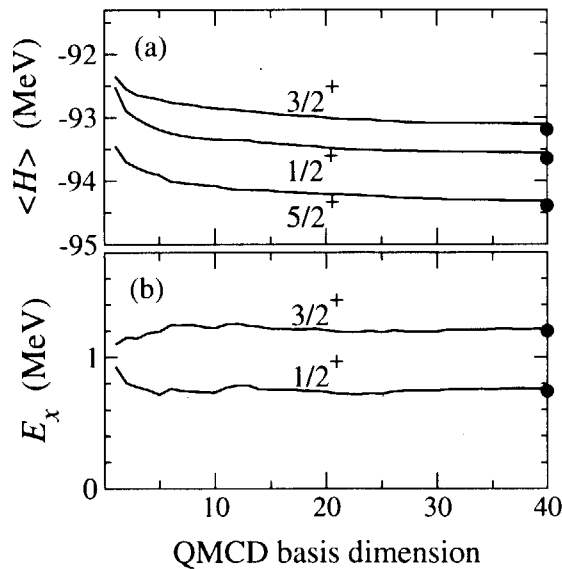
Fig. 1. (a) Total energies and (b) excitation energies of ^{25}Mg calculated by the MCSM as a function of the QMCD basis dimension. Circles denote exact solutions.

The energy levels of ^{31}Na are shown in Fig. 2. The ground-state spin $3/2^+$ agrees with an experi-

ment, in contrast to the sd-shell model prediction of $5/2^+$. The calculated magnetic moment of the ground state is 2.17 μ_N with free-nucleon g factors being consistent with the experimental value of 2.283(38) μ_N [2]. The present study shows that, while the ground state is dominated by the 2-particle 2-hole ($2p2h$) excitations from the $N = 20$ core, $4p4h$ and higher excited configurations are mixed and lower the ground-state energy by more than 700 keV. This energy gain gives rise to a better two-neutron separation energy. The first excited state obtained by the MCSM calculation is a $5/2^+$ state located at 310 keV, in good agreement with a recent measurement of 350±20 keV [7]. On the other hand, this level lies around 200 keV in the $0p0h+2p2h$ truncation. The comparison between the truncated and full calculations indicates the importance of the higher intruder configurations (i.e., $4p4h$ and higher excited configurations from $N = 20$ core): these configurations lower the energy of the ground state more than that of the first excited state, giving rise to a better agreement with experiment. The higher intruder configurations occupy the ground state by about 10%. The $B(E2; 3/2^+ \rightarrow 5/2^+) = 200~e^2~\text{fm}^4$ is obtained with the effective charges $e_p = 1.3e$ and $e_n = 0.5e$, suggesting a strong deformation similarly to the adjacent even-A nucleus ^{32}Mg. This $B(E2)$ value corresponds to $\beta_2 = 0.53$ by assuming an axially symmetric rotor with $K = 3/2$. The present result also implies the validity of the model space and effective interaction for unstable nuclei around $N = 20$.
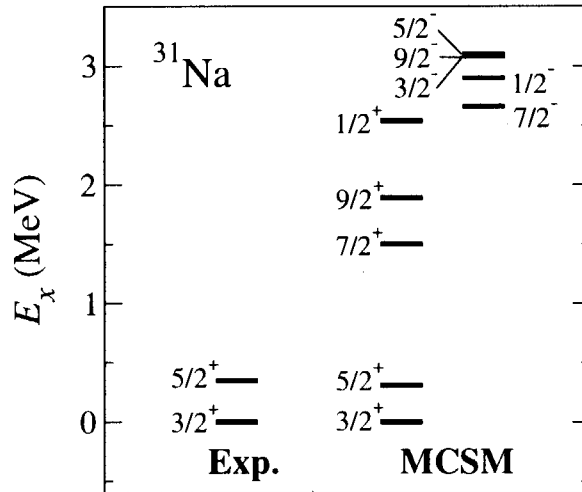
Fig. 2. Experimental energy levels of ^{31}Na (Exp.) [7] compared with those of the MCSM calculation (MCSM) for $J = 1/2$ to $9/2$.

References

[1] C. Thibault et al., Phys. Rev. C **12** (1975) 644.

[2] G. Huber et al., Phys. Rev. C **18** (1978) 2342.

[3] T. Otsuka, M. Honma, and T. Mizusaki, Phys. Rev. Lett. **81** (1998) 1588, and references therein.

[4] Y. Utsuno, T. Otsuka, T. Mizusaki, and M. Honma, Phys. Rev. C **60** (1999) 054315.

[5] E.K. Warburton, J.A. Becker, and B.A. Brown, Phys. Rev. C **41** (1990) 1147.

[6] Y. Utsuno, T. Otsuka, T. Mizusaki, and M. Honma, Phys. Rev. C **64** (2001) 011301(R).

[7] B.V. Prityckenko et al., Phys. Rev. C **63** (2001) 011305(R).

5.5 INSTANTON PROPERTIES IN COLOR MAGNETIC FIELD

M. FUKUSHIMA

The Quantum chromodynamics (QCD) includes various infrared phenomena such as the color confinement, the dynamical chiral-symmetry breaking and the large η' mass. It is necessary to clarify nonperturbative phenomena of the QCD vacuum composed of quarks and gluon fields with non-abelian nature. The topological aspects may provide a useful approach for descriptions of the nonperturbative QCD properties, although the usual perturbative expansion is not applicable any longer in this infrared region. The instanton is a classical solution of Euclidean Yang-Mills field equations with a finite action, which belongs a nontrivial homotopy group [1, 2]. The $U_A(1)$ anomaly and the large η' mass is interpreted as such topological effects [3]. Witten and Veneziano indicated an approximate relation between the η' mass and the topological susceptibility in the context of the $1/N_c$ expansion [4, 5]. Chiral-symmetry breaking could be interpreted also as the instanton effect [6]. Therefore, topological excitations like instantons are important objects for nonperturbative hadron physics at the low energy.

The classical instanton solution is well known as the 't Hooft ansatz [2]. The SU(2) instanton has the 8 collective coordinates corresponding to the size ρ, the 4-dim. central position z_μ and the global color orientation O^{ab} in the color space. The single instanton action density has a point-like peak at its center with the 4-dimensionally spherical symmetry $O(4)$ in the space-time $\mathbf{R}^4$. In the quantum level, the 't Hooft ansatz is no longer solution of QCD, the quantum vacuum is actually filled with many instantons and anti-instantons superposed in highly complicated way. Actually, one can investigate instantons directly from the QCD vacuum by using lattice QCD simulations with the recent computational progress. Lattice QCD simulations provide the average instanton size $\bar{\rho} \simeq (0.33 - 0.4)$ fm and the instanton number density $(N/V) \sim \langle G_{\mu\nu}G_{\mu\nu}/32\pi^2 \rangle \simeq 1$ fm^{-4} corresponding to the gluon condensate. Additionally, the vacuum structure of QCD is studied analytically. Savvidy adopted the background field method for non-Abelian gauge theories. In the SU(2) Yang-Mills theory, the effective potential up to one loop order for an Abelian gauge field leads a nonzero constant color magnetic field instead of the perturbative vacuum. Furthermore, Savvidy's studies motivated Copenhagen group to describe the QCD vacuum including an aspect of the inhomogeneous magnetic structure.

Now, we show Figure 1 demonstrated the extraction of instanton configurations from the SU(2) QCD vacuum. It is noted that we does not consider quark's contributions in this paper. As shown in Fig. 1(a), even the pure gluon vacuum contains many kinds of fields fluctuations and thus instantons are indistinguishable in such a situation. The stability of instantons is guaranteed from the topological view points and therefore, one can eliminate short-range quantum fluctuations around such topological excitations by adopting a local cooling procedure, as shown in Fig. 1(b). It is reported that instantons in the vacuum seem to appear as deformed configurations even after the cooling.

The 't Hooft ansatz is not a solution of the Yang-Mills equation any longer in the presence of background fields, for example, other instantons effects, gluon condensate and inhomogeneous magnetic fields. Therefore, we would like to clarify instanton properties, *deformation mechanism*, in the "quantum" vacuum. To this end, we try to find the instanton solution in a external color electro-magnetic field numerically [7]. For simplicity, the external color field in the nontrivial topological sector is set to be a constant Abelian magnetic one along a direction. Starting from the superposed total gauge field of the 't Hooft ansatz and the external color field, we perform the numerical minimization of the total Yang-Mills action under the anisotropic scale transformation

(a)   (b)
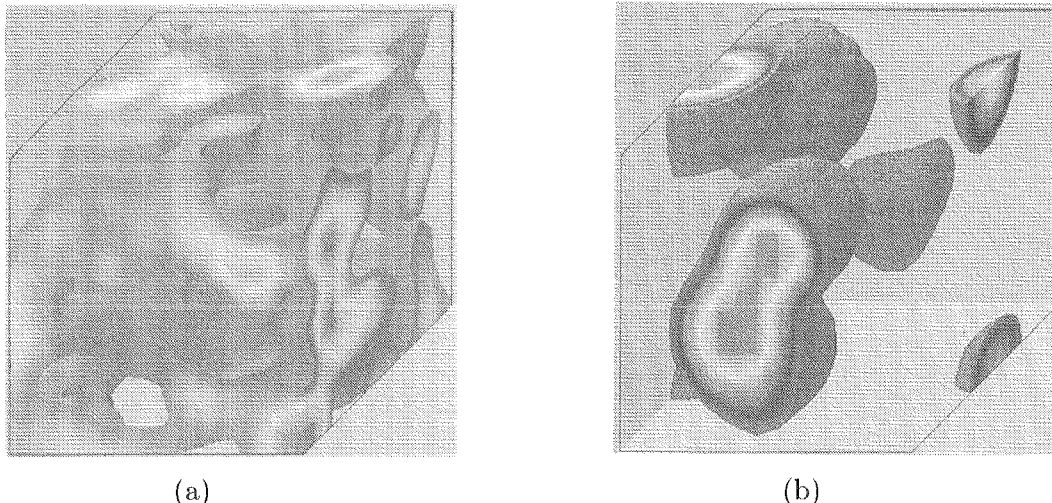
Figure 1: The action density in $\mathbf{R}^3$ of the SU(2) lattice QCD with $\beta = 2.25$ on 16^4 lattice. (a) a original pure gauge configuration and (b) a cooled one after 100 sweeps of the Cabibbo-Marinari cooling.

on the instanton configuration as $x_\mu \rightarrow \lambda_\mu x_\mu$. Here, λ_μ are the global re-scale parameters acting on the coordinates x_μ along the direction μ. The scale transformation affects directly on the changing of the instanton profile, which cannot be achieved by the gauge degrees of freedom on the instanton configuration. Since we are interested in a typical-size instanton $\bar{\rho}$, we impose a condition $\lambda_1 \lambda_2 \lambda_3 \lambda_4 = 1$, which means the volume conservation of the 4-dimensional instanton profile. The external field stabilizes the instanton profile with $\lambda_1 = \lambda_2 = \lambda = 1.3$ and $\lambda_3 = \lambda_4 = 1/\lambda$ [7]. Such a nontrivial conditions of λ_μ means the breaking of the $O(4)$ symmetry, namely the quadrupole-deformed instanton in $\mathbf{R}^3$.

We have obtained true instanton solution in the external color field by considering the minimization of total action. In this solution, the 4-dimension-rotational symmetry $O(4)$ is reduced into two 2-dimensionally rotational symmetries $O(2) \times O(2)$, due to the homogeneous external field. In the space $\mathbf{R}^3$ at a fixed t, we have found a quadrapole deformed instanton solution. In the magnetic field $\vec{H}$, the prolate deformation occurs along $\vec{H}$. In the electric field $\vec{E}$, the oblate deformation occurs along $\vec{E}$.

References

[1] A. A. Belavin, A. M. Polyakov, A. S. Shvarts, and Y. S. Tyupkin, Phys. Lett. **B59** (1975) 85.

[2] R. Rajaraman, *Solitons and Instanton* (1982) p.1.

[3] G. 't Hooft, Phys. Rev. Lett. **37** (1976) 8.

[4] G. Veneziano, Nucl. Phys. **B159** (1979) 213.

[5] E. Witten, Nucl. Phys. **B156** (1979) 269. (1990) 1.

[6] T. Schafer and E. V. Shuryak, Rev. Mod. Phys. **70** (1998) 323, hep-ph/9610451.

[7] M. Fukushima, H. Suganuma, *Dynamics of Gauge Fields, TMU-Yale Symposium*, (2000) 213.

This is a blank page.

− 71 −

6. Atomic Physics and Solid State Physics

This is a blank page.

6.1 HIGH–RESOLUTION ZERO–DEGREE ELECTRON SPECTROSCOPY (VII)

M. IMAI[1], M. SATAKA, K. KAWATSURA[2], K. KOMAKI[3], H. SHIBATA[4], and H. TAWARA[5,6]

Penetration of ions through solid target has been investigated in many aspects. Production of Rydberg states of fast projectiles interacting with foil target has provided attractive subjects among them [1]. The method of zero-degree electron spectroscopy [2] has proved to be one of the excellent tools to study collision dynamics of highly charged ions colliding with gaseous and solid targets. We have been devoted to measuring Coster-Kronig (C-K) electrons from Be-like Rydberg configuration $1s^2 2p(^2P_{3/2}°)nl$ $\rightarrow$ $1s^2 2s(^2S_{1/2})\varepsilon\ l'$ or $1s^2 2p(^2P_{1/2}°)nl$ $\rightarrow$ $1s^2 2s(^2S_{1/2})\varepsilon\ l'$ of S^{12+} ions excited through He or C-foil target, and studying the difference of the l-distribution between gas and solid phase targets [3], or the dependence of the l-distribution on foil thickness or projectile charge state [4]. We present here our latest results of C-K spectra for 80 MeV S^{7+}, S^{10+}, S^{12+} and S^{13+} ions penetrating through C-foil targets.

As the experimental apparatus has already been presented elsewhere [3–5], only the major parameters are given here. Measured are the electrons emitted from sulfur projectile passing through C-foil target of various thickness (1.1 - 6.9 μ g/cm^2). A beam of 2.5 MeV/u S^{7+} was provided by the accelerator and was guided directly into the target for S^{7+} injection case. As for other projectiles, a fraction of the primary S^{7+} beam was selected by switching magnet after passing a post stripper foil. Energy of electrons emitted from the projectile was analyzed by a tandem electrostatic analyzer at zero degree. Two spectra corresponding to the low and the high energy wings of the cusp were obtained from the measured spectrum by converting the laboratory frame spectrum in projectile rest frame, resulting in the energy resolution of 0.01 - 0.05 eV at the electron energy region of our interest ($\sim$2 eV).

Electron energy spectra from the C-K transition formed through 80 MeV S^{7+}, S^{10+}, S^{12+}, and S^{13+} ions colliding with C-foil targets of various thickness are shown in Fig. 1. The observed electron intensities have been normalized to the fixed number of the impinging ions utilizing the mean charge states of the projectile ions through the foils, estimated from the variations of current measured by Faraday cup as in Table 1. The vertical indicator bars on top show the C-K electron energies calculated with the Z-expansion method (MZ code) [6]. These calculated values are shifted by - 0.2 eV, which is mentioned in [6] to compensate the difference with experimental results for $n \leqq 19$. As a detailed qualitative description will be given elsewhere, only the shape of the peak and its change for each collision system are treated here. With a help of the energy calculations with MZ code, we consider the peak at around 1.25 eV to originate from $1s^2 2p9l$ configurations, whose l is larger or equals to d. The shoulder at around 1.15 eV, which can be seen in most of the spectra, is likely to come from configurations with lower angular momentum (l=p) value. In the S^{7+} collision, the shoulder is very standing as compared with the peak at around 1.25 eV for the target with 2.0 μ g/cm^2 thickness, and still stands at 6.9 μ g/cm^2 target. In the S^{10+} and S^{12+} collisions, the comparison of shoulder against 1.25 eV peak stands until target thickness grows to 2.0 μ g/cm^2, and turns less standing as the target thickness grows more. In the S^{13+} collision, there is no change of either peak shape or intensity on target thickness. In the S^{7+}, S^{10+} and S^{12+} collisions, the autoionizing Rydberg electron is considered to have its origin in projectile bound electrons, which once have been lost into continuum and having traveled inside the foil undergoing multiple collisions. The standing appearance of the shoulder until 2.0 μ g/cm^2 can be attributed to the l(=p)-enhancement of the entrained electrons, and the disappearance of that shoulder is due to the shift of l to higher value, reflecting multiple collisions of entrained electrons with target under the strong influence of projectile, as has been shown [7] for $1s^2 2p5l \rightarrow 1s^2 2s\varepsilon\ l'$ transition of 1.5MeV C^{2+} ion. In the

---

[1] Department of Nuclear Engineering, Kyoto University
[2] Department of Chemistry and Materials Technology, Kyoto Institute of Technology
[3] Institute of Physics, Graduate School of Arts and Sciences, University of Tokyo
[4] Research Center for Nuclear Science and Technology, University of Tokyo
[5] Department of Physics, Kansas State University
[6] Atomic Physics Division, National Institute of Standards and Technology

Table 1   The estimated mean charge for 80 MeV S^{q+} ions after passing through thin carbon foil with various thicknesses

Foil Thickness	Projectile Incident Charge			
(μ g/cm^2)	S^{7+}	S^{10+}	S^{12+}	S^{13+}
1.1	10.1	-	-	-
1.5	-	10.7	12.4	13.3
2.0	10.3	11.9	12.5	13.3
3.0	-	12.2	12.8	13.3
6.9	11.8	13.1	13.3	13.3
10	12.8	13.3	13.3	13.3

S^{7+} collision, projectile bound electrons are expected to be continuously released during foil penetration than in the case for collisions with higher initial charge state. In the S^{13+} collision, however, the release of projectile bound electron and following formation of entrained electrons are less expectable, and the autoionizing Rydberg state is preferably formed by electron capture from target continuum upon or near the exiting surface.

References

[1] Y. Yamazaki, Nucl. Instr. Meth. **B96**, 517 (1995).

[2] N. Stolterfoht *et al.*, Phys. Rep. **146**, 315 (1987).

[3] K. Kawatsura *et al.*, Nucl. Instrum. Methods **B48**, 103 (1990); Nucl. Instrum. Methods **B53**, 421 (1991); Nucl. Instrum. Methods **B124**, 381 (1997).

[4] M. Imai *et al.*, Nucl. Instrum. Methods **B67**, 142 (1992).

[5] M. Sataka *et al.*, Phys. Rev. **A44**, 7290 (1991); K. Kawatsura *et al.*, J. Electron Spectr. and Relat. Phenomena **88–91**, 83 (1998); M. Imai *et al.*, Physica. Scripta **T73**, 93 (1997); K. Kawatsura *et al.*, J. Electron Spectr. and Relat. Phenomena **88–91**, 87 (1998).

[6] I. Yu. Tolstikhina *et al.*, Physica Scripta **54**, 188 (1996).

[7] Y. Yamazaki *et al.*, Phys. Rev. Lett. **61**, 2913 (1988); J. Burgdörfer and C. Bottcher, Phys.Rev. Lett. **61**, 917 (1988).

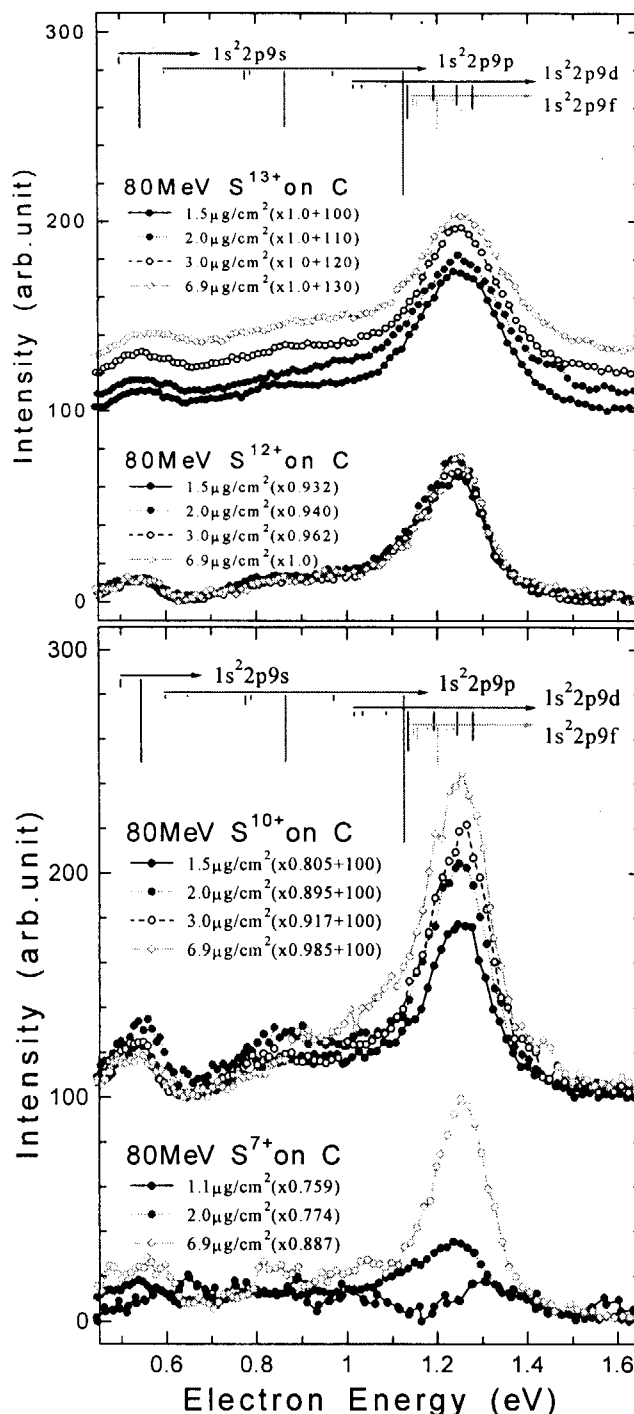Fig.1.   Electron energy spectra from Coster-Kronig transitions $1s^2 2p(^2P_{3/2}°)9l$ $\rightarrow$ $1s^2 2\varepsilon\, l'$ formed through 80 MeV S^{7+}, S^{10+}, S^{12+} and S^{13+} ions colliding with C-foil targets with various thicknesses.

6.2 B_Φ —DEPENDENCE OF TRANSPORT CRITICAL CURRENT DENSITY IN YBa2Cu3Oy CONTAINING COLUMNAR DEFECTS

N. ISHIKAWA, T. SUEYOSHI[1], A. IWASE, Y. CHIMI, T. FUJIYOSHI[1], K. MIYAHARA[1], and T. KISS[2]

There have been many studies on the change in the pinning properties by changing the density of vortices in YBa2Cu3Oy (YBCO) containing the columnar defects[1-3], while there have been only a limited number of systematic studies on the effect of changing the dose equivalent field, B_Φ, on the pinning properties. In order to avoid the sample dependence and to precisely measure the effect of changing B_Φ, in-situ measurement of the irradiation effect using one sample is indispensable.

A c-axis oriented YBa2Cu3Oy epitaxial thin film was irradiated with 200MeV ^{197}Au ions from a tandem accelerator at JAERI-Tokai. Inclined columnar defects were produced in the film by ion irradiation from the angle of $\theta_{irr}=45°$ off the c-axis. Irradiation doses are expressed in terms of the dose equivalent field, B_Φ, which is defined so that the average spacing between the columnar defects are equal to the spacing of vortex lattice under the magnetic field of $B=B_\Phi$. The irradiation temperature was about 80K. The in-situ measurements of transport critical current density, J_c, as a function of B and B_Φ were performed at T=80~82K without warming the sample above 83K. The transport current was always applied in the direction perpendicular to the magnetic field direction and c-axis direction.

Figure 1 shows the B_Φ-dependence of J_c for various magnetic fields parallel to the columnar defects ($\theta_{mag}=45°$) and that for the magnetic fields perpendicular to the columnar defects ($\theta_{mag}=-45°$). $J_c(\theta_{mag}=-45°)$ decreased monotonically with increasing B_Φ due to the increase in $t_{meas}=T_{meas}/T_c$. The behavior of $J_c(\theta_{mag}=45°)$ as a function of B_Φ is rather complicated but can be explained by the competition of the enhancement of pinning due to introduction of the columnar defects and the decrease in the superconducting condensation energy accompanied by the increase in t_{meas}. The effect of columnar defects as pinning centers can be extracted by defining $\Delta J_c=J_c(\theta_{mag}=45°)-J_c(\theta_{mag}=-45°)$. Assuming a direct sum of pinning force, the contribution of the columnar defects to the pinning force density is estimated as $\Delta F_p=\Delta J_c \times B$. Figure 2 shows ΔF_p as a function of B_Φ. Monotonic increase in ΔF_p with increasing B_Φ is observed up to $B_\Phi=2.3T$, although B is varied from 1T to 3T. In Fig.3, ΔF_p as a function of B is plotted for the sample irradiated up to $B_\Phi=1.6T$. It appears that the broad peak is observed at $B \cong B_\Phi$. The result is almost the same as that of Holzapfel et al. [4]. They have concluded that the maximum of ΔF_p at $B \cong B_\Phi$ is attributed to the matching between the density of vortices and that of the columnar defects. However, as shown in Fig.4, although B_Φ is varied in the wide range from B_Φ =0.6T to 2.3T, ΔF_p exhibits a peak at around $B=1.5\pm0.2T$ irrespective of the values of B_Φ, i.e. the peak field for ΔF_p seems to be almost independent on B_Φ. To clarify whether or not a maximum of ΔF_p vs B curve is attributed to the effect of matching between B and B_Φ, it is necessary to precisely measure the change in the behavior of ΔF_p vs B curve by varying

[1] Department of Electrical and Computer Engineering, Kumamoto University
[2] Graduate School of Information Science and Electrical Engineering, Kyushu University

wide range of B_{Φ}.

References

[1]L. Krusin-Elbaum, L. Civale, G. Blatter, A.D. Marwick, F. Holtzberg, and C. Field, Phys. Rev. Lett. **72** (1994) 1914.

[2]L. Krusin-Elbaum, L. Civale, J.R. Thomson, and C. Field, Phys. Rev. **B 53** (1996) 11744.

[3]A. Mazilu, H. Safar, M.P. Maley, J.Y. Couter, L.N. Bulaevskii, and S. Foltyn, Phys. Rev. **B58** (1998) R8909.

[4]B. Holzapfel, G. Kreiselmeyer, M. Kraus, G. Saemann-Ischenko, S. Bouffard, S. Klaumünzer and L. Schultz, Phys. Rev. **B48** (1993) 600.
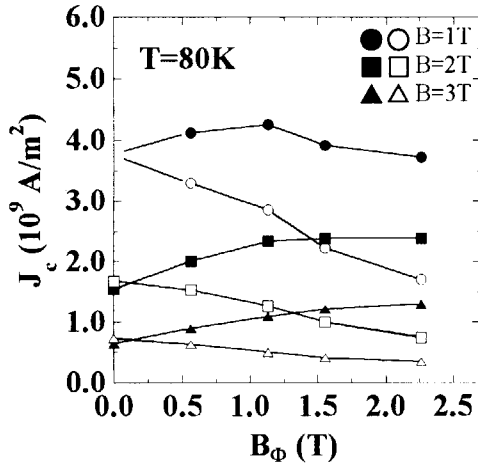
Fig.1. The B_{Φ}-dependence of J_c measured for the magnetic field parallel to the columnar defects (θ_{mag}=45°)and for the magnetic field perpendicular to the columnar defects (θ_{mag}=-45°). $J_c(\theta_{mag}$=45°) is shown as closed symbols, and $J_c(\theta_{mag}$=-45°) as open symbols.

Fig.2. ΔF_p as a function of B_{Φ} for various values of B.
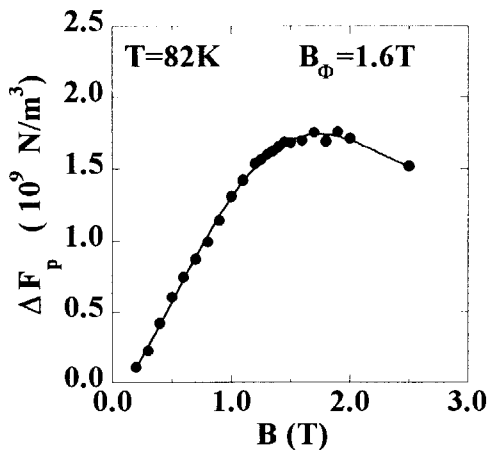
Fig.3. ΔF_p as a function of B for the sample irradiated up to B_{Φ}=1.6T. The measuring temperature is T=82K.
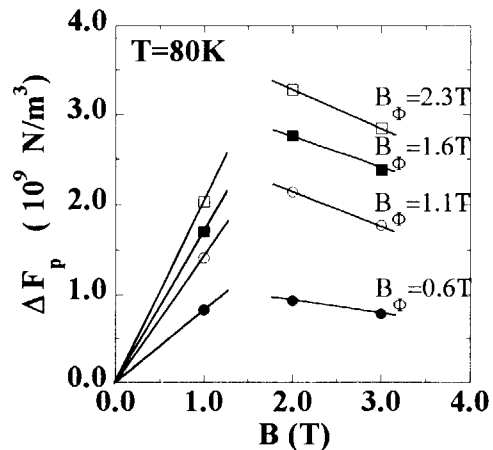
Fig.4. ΔF_p plotted against the magnetic field measured at T=80K. The solid lines are the guides for the eyes to show that the peak position is hardly changed, although the dose is varied from B_{Φ} =0.6T to 2.3T.

6.3 THERMAL RELAXATION OF HYDROGEN DISORDERING IN Pd-H SYSTEM IRRADIATED WITH HIGH-ENERGY IONS

Y. CHIMI, A. IWASE, K. ADACHI[1], N. ISHIKAWA, and K. YAMAKAWA[1]

In the Pd-H(D) system, an extraordinary behavior has been found near 50K in several properties such as specific heat, electrical resistivity and so on. Neutron diffraction measurements have shown that this anomaly is related to the order-disorder transition of hydrogen atoms [1]. We have reported that the thermally equilibrium ordered state at low temperatures is destroyed by the irradiation with high-energy ions, and that even at 10K, the disordered state appears [2]. In this report, we show the thermal relaxation of the irradiation-induced disordering of hydrogen atoms.

The specimen used in this experiment was a Pd foil, which was doped with hydrogen up to the atomic ratio of 0.6. First, the ordered state of hydrogen atoms was realized at 10K by cooling the specimen very slowly. Then, the disordered state of hydrogen atoms was introduced in the specimen by the irradiation with 60MeV ^{12}C ions. During heating the irradiated specimen up to 80K at a constant rate, the electrical resistivity was measured as a function of temperature. As the electrical resistivity is well correlated with the state of hydrogen atoms in the specimen, we can obtain the thermal relaxation of hydrogen disordering from the temperature dependence of the electrical resistivity.

Fig. 1 shows the thermal relaxation of hydrogen atoms from the irradiation-induced disordered state to the thermally equilibrium state (ordered state) as a function of temperature for each heating rate (2, 5 and 10 K/min). For comparison, the thermal relaxation behavior for frozen-in hydrogen disordering, which was obtained by cooling the specimen rapidly from 80K to 10K, is also shown. The figure clearly shows that the frozen-in disordering relaxes around 55-60K, while the irradiation-induced disordering relaxes around two temperature regions; 35-40K and 55-60K. The relaxation process around 55-60K for irradiation-induced disordering seems to be the same as for frozen-in disordering.

On the analogy of the result in Ni$_4$Mo irradiated with electrons [3], the present result can be explained as follows; the state frozen-in from 80K is not a completely disordered state but includes short-range order (SRO). The relaxation around 55-60K may correspond to the transition from SRO to the long-range order (LRO). On the other hand, high-energy ion irradiation can destroy not only LRO but also SRO. Therefore, the relaxation around 35-40K may correspond to the transition from the complete disorder to SRO, which subsequently relaxes to LRO around 55-60K.

The details of the experimental procedure and the data analysis are shown in ref. [4].

References
[1] O. Blaschko, J. Less-Common Met. **100** (1984) 307.
[2] K. Adachi, Y. Chimi, A. Iwase, N. Ishikawa, and K. Yamakawa, JAERI-Review 2000-018 (2000) p.94.
[3] S. Banerjee, K. Urban, and M. Wilkens, Acta Metall. **32** (1984) 299.

[1] Faculty of Engineering, Ehime University

[4] Y. Chimi, K. Adachi, A. Iwase, N. Ishikawa, and K. Yamakawa, J. Alloys and Compounds (2001) in press.
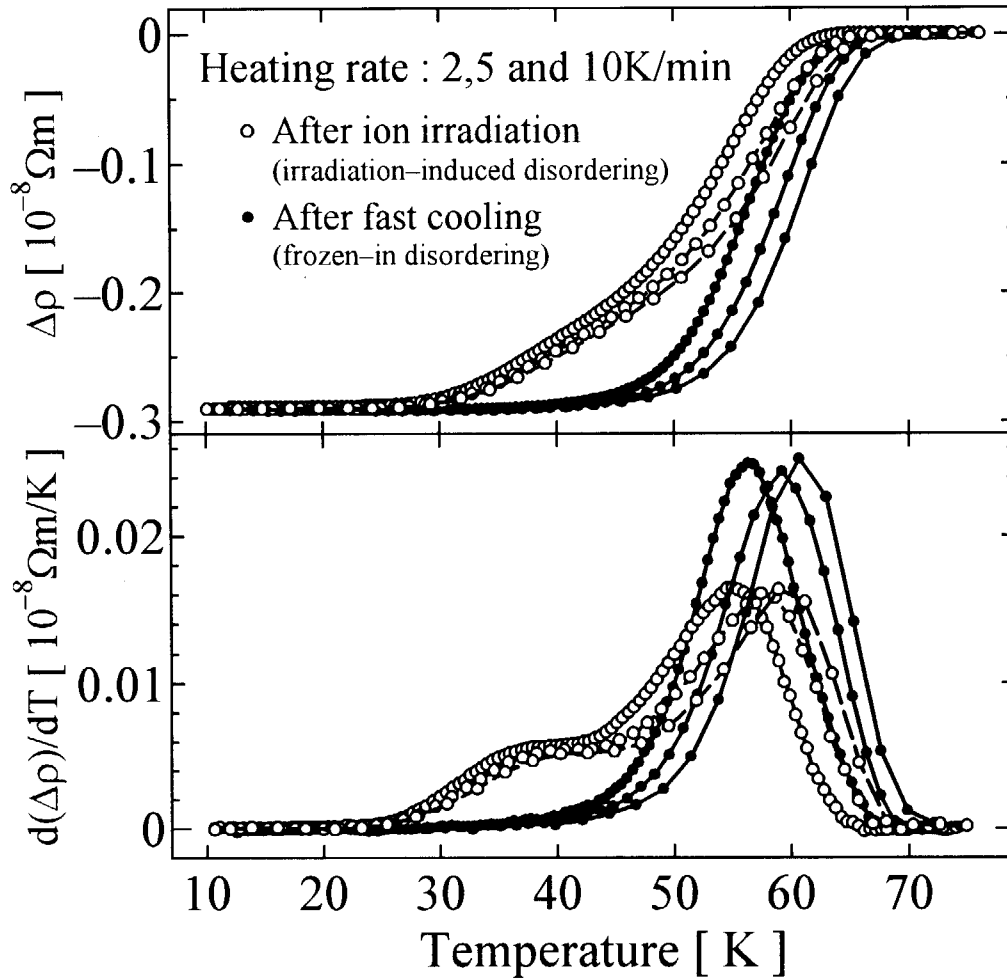
Fig. 1. Thermal relaxation of hydrogen disordering induced by ion-irradiation for heating rates of 2K/min (left curve), 5K/min (middle curve), and 10K/min (right curve). For comparison, thermal relaxation for frozen-in state is also shown.

6.4 ELECTRONIC EXCITATION EFFECT
IN THE SECONDARY ION EMISSION FROM SOLID SURFACE
BOMBARDED BY ENERGETIC HEAVY IONS

T. SEKIOKA[1], M. TERASAWA[1], M. SATAKA and S. KITAZAWA

The importance of the electronic excitation effect in solid materials has been attracting great interest. In almost all researches on the electronic excitation effect, the materials are limited to insulators. There have been few researches on conductive materials, because it has been believed that electronic excitation in the conductive materials is rapidly neutralized by free electrons. We have been studying the secondary ions mass spectra from thin conductive solid targets irradiated with heavy ion beams from the JAERI tandem accelerator at the energy region where the electronic stopping power is dominant.We have found remarkable dependence on the electronic stopping power of secondary ion yield for copper targets irradiated by Au ions with energies of 100, 150 200 and 240 MeV. We are now preparing a paper on these experimental results.

The experimental procedures are as follows. The thin metal foil targets evaporated on C-foils of $10\mu g/cm^2$ were irradiated with high-energy heavy ions beam from the tandem accelerator. The secondary ions ejected from the front surface of the target were collected by a time of flight (TOF) mass spectrometer by applying an acceleration voltage of $-500V$ and detected by an electron multiplier. Secondary electrons from the backside of the target were detected by another electron multiplier and this signal was used as the start signal of the TOF. In the secondary ions mass spectra, there were contaminant peaks which were mainly hydrocarbons, and we needed deconvolution to separate these peaks to obtain the secondary ion yield of target metal atoms.

In order to obtain more precise data of secondary ion yield, it is highly desirable to clean the surface of targets to suppress the contaminant peaks, which are mainly hydrocarbons. We have equipped a heater system which is so designed that with a special guide rod, infrared radiation is transmitted from the heating source on the atmosphere side and is introduced into an ultrahigh vacuum chamber to enable clean heating of a sample alone in the ultrahigh vacuum at an optional temperature.

A demonstration of the cleaning effect is given in fig.1, which shows secondary ions mass spectra from an Au foil target of 1000Å thickness evaporated on C-foils of $10\mu g/cm^2$ irradiated with 200MeV Au^{13+} ions, before cleaning and after cleaning by infrared radiation heater at 330°C. The peak assignments and the channel position where the Au^+ peak should appear are given in the figure. We can see the heavy hydrocarbon peaks have been hindered remarkably. The improvements of this heater system are now in progress.

With this cleaning system we are planning to measure secondary ion yield from metals such as Au or Ag, or the one from Cu at low electronic stopping power, where secondary ions yield is very low and cleaning procedure is indispensable.

---

[1] Faculty of Engineering, Himeji Institute of Technology
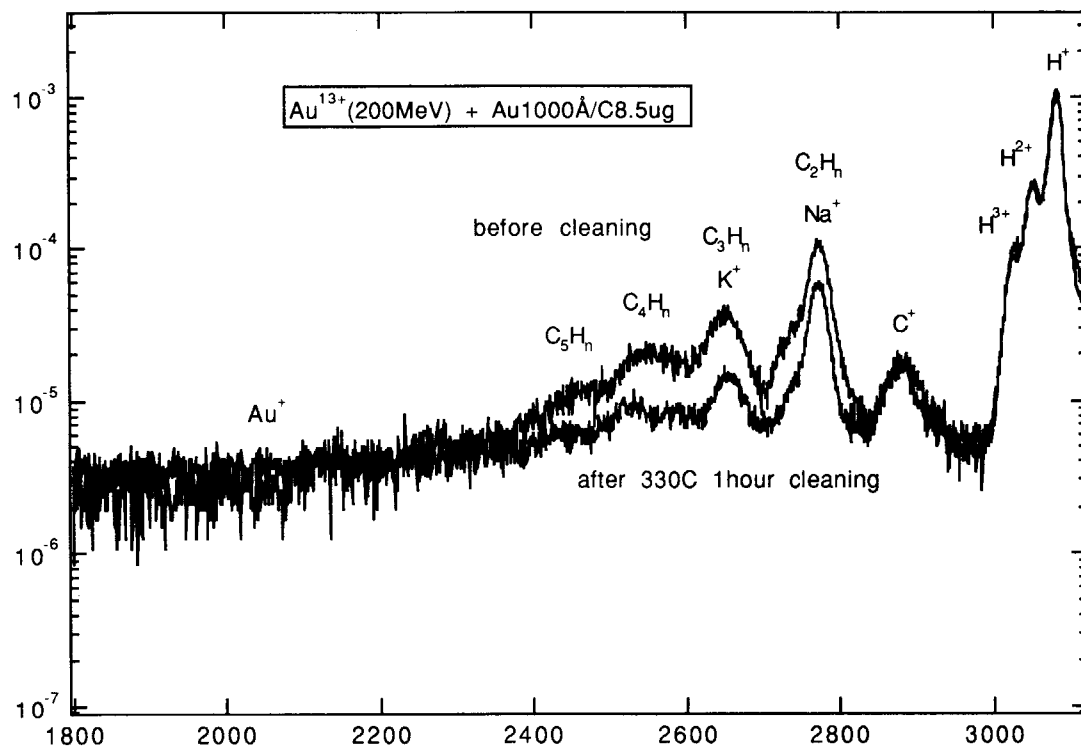
Fig. 1. A demonstration of the cleaning effect. The secondary ion mass spectra from an Au foil target before and after cleaning are shown.

6.5 ELECTRONIC EXCITATION EFFECTS ON OXIDES BY HIGH ENERGY HEAVY IONS

N. MATSUNAMI[1], M. SATAKA and A. IWASE

One of the key quantities of ion irradiation effects is the number of atomic displacements per ion and quantitative understanding of electronic excitation effects on atomic displacement is an interesting subject. In order to investigate the effects in oxides, we adopt sputtering yield measurement, which is a "direct" method for the observation of atomic displacements. We have applied a carbon (C)-film(~100 nm)-collector method [1] to measure the sputtering yields Ys of $YBa_2Cu_3O_{7-\delta}$ (YBCO), $SrCe_{0.95}Yb_{0.05}O_{3-\delta}$ (SCO) and amorphous(a-) SiO_2 by using 200 MeV I, 90 MeV Ni, 70 MeV Ni, 80 MeV S and 200 MeV Xe ions. YBCO and SCO films (~100 nm) were prepared on MgO by rf sputter-deposition and pulsed- laser deposition methods, respectively. The amount of sputtered atoms collected in the C-films (A) during ion irradiation (10^{13}- 10^{14} /cm^2) in vacuum of ~10^{-5} Pa was analyzed by 1.8 MeV He Rutherford backscattering spectroscopy (RBS). Results of SCO by Ni ion are shown in Fig. 1. It appears that A is approximately linear with the ion dose, indicating insignificance of surface contamination. The slope of A vs dose was employed to evaluate the sputtering yield for each component.

The collection efficiency of the C-films, fc, was calibrated by 120 keV Ne^+ ions using the same assembly as for high energy heavy ion irradiation. Sputtering yields of YBCO, SCO and SiO_2 by 60 keV Ne^+ ions (60 keV energy loss in C-films) are taken as 1.1, 0.61 and 0.5, and stoichiometric sputtering is assumed in fc evaluation. The fc values are obtained as 0.048(Y), 0.076(Ba), 0.061(Cu), 0.55(Sr), 0.25(Ce), 0.25(Yb), 0.35(O) and 0.48(Si). The validity of the present C-film-collector method is supported by the fact that the measured sputtering yields of Au by high energy heavy ions (fc for Au = 0.2) agree reasonably with Ys of calculation based on the elastic collision cascade.

With the values of fc mentioned above, the experimental sputtering yields Yexp (atoms per ion = sum of sputtering yield of each component) are evaluated as 1027 (198 MeV $^{127}I^{12+}$), 579 (69 MeV $^{58}Ni^{6+}$) and 100 (80 MeV $^{32}S^{7+}$) for YBCO [1], 294 (198 MeV $^{127}I^{12+}$), 453 (198 MeV $^{136}Xe^{14+}$), 212(69 MeV $^{58}Ni^{5+}$) and 21(80 MeV $^{32}S^{7+}$) for SCO, and 404(198 MeV $^{136}Xe^{13+}$), 120 (89 MeV $^{58}Ni^{9+}$) and 9.7 (80 MeV $^{32}S^{7+}$) for a-SiO_2. Here, the energy loss in the C-film-collector (less than 2 MeV) is taken into account and Yexp includes the oxygen contribution. Firstly, we find that Yexp of the oxides is larger by three order of magnitude than Ys of calculation based on the elastic collision cascade. This indicates significant contribution of the electronic excitation effects on the sputtering of the oxides.

Secondly, Figure 2 shows Yexp vs the electronic stopping power Se and the data are fitted by Yexp $\propto$ Se^n. We obtained n = ~2, 2-3 and ~3 for YBCO, SCO and a-SiO_2, respectively. Now, the electronic excitation density (EED) dependence is discussed. Se /(π Rad^2) is an estimate of EED, where Rad is the adiabatic radius (=Planck constant $\cdot$ ion velocity / {2 π $\cdot$ I}). Here the mean excitation energy I was taken as 20 eV and it is assumed that δ -ray

---

[1] Dept. Energy Engineering and Science, School of Engineering, Nagoya University

contribution to Se are the same for all ions used in this study. We find EED^n dependence with n~1 for YBCO, and n~2 for SCO and a-SiO$_2$, respectively. Thirdly, the sputtering is roughly stoichiometric for SCO and a-SiO$_2$, while the deviation is appreciable for YBCO. Fourthly, considerable mixing was observed between YBCO or SCO film and MgO substrate for heavier ion at higher doses. The equilibrium charge in the C-film is estimated as 30 (200 MeV I and Xe), 18 (70 MeV Ni) and 13 (80 MeV S) [2]. The charge state effect on sputtering and the mechanism of the electronic sputtering is under investigation.

We thank Prof. M. Ishigame and Dr. N. Sata for supplying us SCO samples.

REFRENCES
[1] N. Matsunami, M. Sataka, A. Iwase, Nucl. Instrum. Meth. B175-177(2001)56.
[2] K. Shima, N. Kuno, M. Yamanouchi, H. Tawara, At. Data Nucl. Data Tables 51(1992)173.
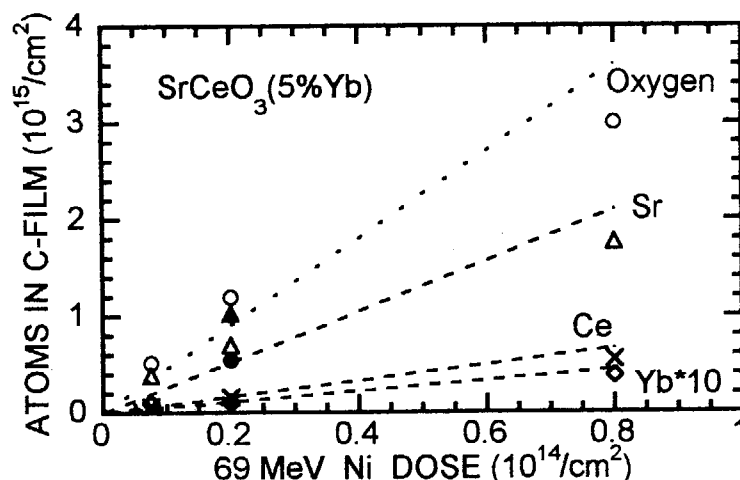
Fig. 1. Sr($\triangle$), Ce(x), Yb($\diamondsuit$) and O($\bigcirc$) atoms collected in C-films vs dose of 69 MeV Ni ion on SCO films. Also plotted are Sr($\blacktriangle$), Ce(+), Yb($\blacklozenge$) and O($\bullet$) atoms from thick polycrystalline SCO sample. Average is drawn by dashed lines.
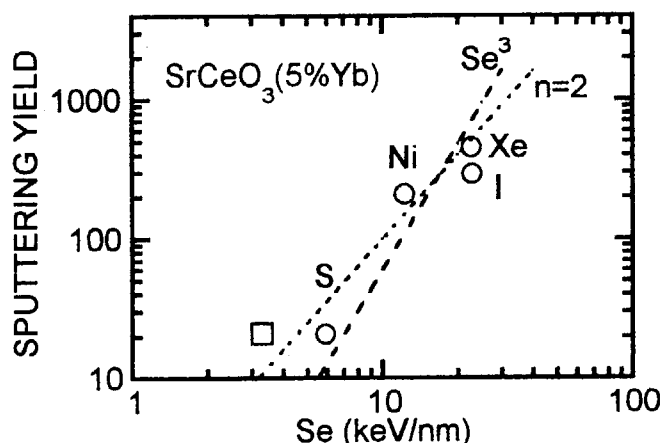
Fig. 2. Sputtering yield Yexp (atoms per ion) of SCO vs the electronic stopping power Se (open circles). Open square represents the corrected data of S ions for illustrating the electronic excitation density (EED) dependence. The dotted and dashed lines indicate Se^3 and EED^2 dependence, respectively.

7. Radiation Effects in Materials

This is a blank page.

7.1 EFFECT OF ION VELOCITY ON COLUMNAR DEFECTS FORMATION WITH HIGH-ENERGY HEAVY ION IRRADIATION IN Bi-2212

M. SASASE[1], S. OKAYASU, H. YAMAMOTO, H. KURATA AND K. HOJOU

When high energy heavy ions are irradiated to materials, most of their energy is dissipated through the electronic excitation process. In high-T_c superconductors, these ions produce columnar defects through this process [1].

In the formation of columnar defects, it has been considered that the electronic stopping power (S_e) mainly affects columnar defect morphology. However, other parameters might affect columnar defects formation because it is hard to explain observed data exactly by using S_e as only one physical parameter. Some research groups have found that the S_e is not only key parameter and ion-velocity also plays a very important role in the formation of columnar defects [2,3]. Recent studies also show that ion-velocity dependence has been observed in the defect production even for the constant S_e conditions [3,4].

In the present study, we have investigated the influence of the ion-velocity on the columnar defects formation under the fixed S_e. The relationship between the defects size, which is obtained from Transmission Electron Microscope (TEM) observation, and the ion-velocity has been discussed.

Specimens used in this study were $Bi_2Sr_2CaCu_2O_8$ (Bi-2212) single crystals (T_c=90 K). The specimens were irradiated with the following ions at room temperature: 60 MeV Au^{8+}, 120 MeV Au^{10+}, 180 MeV Au^{12+}, 240 MeV Au^{14+} and 300 MeV Au^{24+} ions; 90 MeV I^{8+} and 600 MeV I^{29+}; 180 MeV Ni^{11+} and 190 MeV Br^{12+} with a fluence of 2.0 x 10^{10} ions/cm^2 using the tandem accelerator at JAERI. The projected range and S_e of irradiating ions in the Bi-2212 were calculated by using the TRIM code [5]. We investigated the effect of various combinations of S_e and ion-velocity on the defects formation in the Bi-2212. Irradiation defects were observed by using TEM (JEOL JEM-2000F type).

The diameter of the columnar defects depends on both of the atomic number and the energy of the irradiating ions. Particular, the diameter has often been discussed in terms of S_e value [6], since the columnar defects are observed only for high-energy heavy ion irradiation. In the present study, their sizes were measured on TEM micrographs of lattice images surrounding the amorphous columns from regions less than 50 nm. We observed the columnar defects with the diameter from 9 to 15 nm, which were produced by the irradiation from 60 to 300 MeV Au^{24+} ions. From this results, the size of the columnar defects depended on the S_e [7]

On the other hand, ion-velocity dependence has also been observed in the defect production even for the constant S_e in recent studies [3,4]. The S_e was not only key parameter and ion-velocity also plays a very important role in the columnar defects formation.

In Fig. 1 and Table 1, comparison of defect size is made for three irradiations with same S_e value (11.5, 14.5 and 23 keV/nm) but much different velocities. Even though the size of the columnar defects depend on the S_e [7], these results reveal that irradiating ions which have higher ion-velocity produce smaller columnar defects under the fixed S_e condition, showing the "velocity effect". A similar effect has been also reported in magnetic insulator $Y_3Fe_5O_{12}$[2] and high-T_c superconductor $EuBa_2Cu_3O_y$ films[3].

---

[1] present address : The Wakasa Wan Energy Research Center

The Bi-2212 single crystals were irradiated by various high energy heavy ions using a tandem accelerator. The relationship between the columnar defects size which is obtained from TEM observations, and S_e has been discussed but much different velocities. We find that ion-velocity is one of the dominant factors on the defects formation process. The results of columnar defects diameter show that the diameter becomes smaller for higher ion-velocities

Table 1 The species, energy, and velocity of various ions used in the present study and the electronic stopping power (S_e). D is the diameter of columnar defects measured by the TEM observations.

Ion	Energy (MeV)	Velocity (x10⁹ cm/sec)	S_e (keV/nm)	D (nm)
Au⁸⁺	60	0.76629	11.5	9.0
Ni¹¹⁺	180	2.43242	11.5	4.0
I⁸⁺	90	1.16934	14.5	9.0
Br¹²⁺	190	2.14203	14.5	5.0
Au¹²⁺	180	1.32776	23.0	12.0
I²⁹⁺	600	3.0192	23.0	6.5
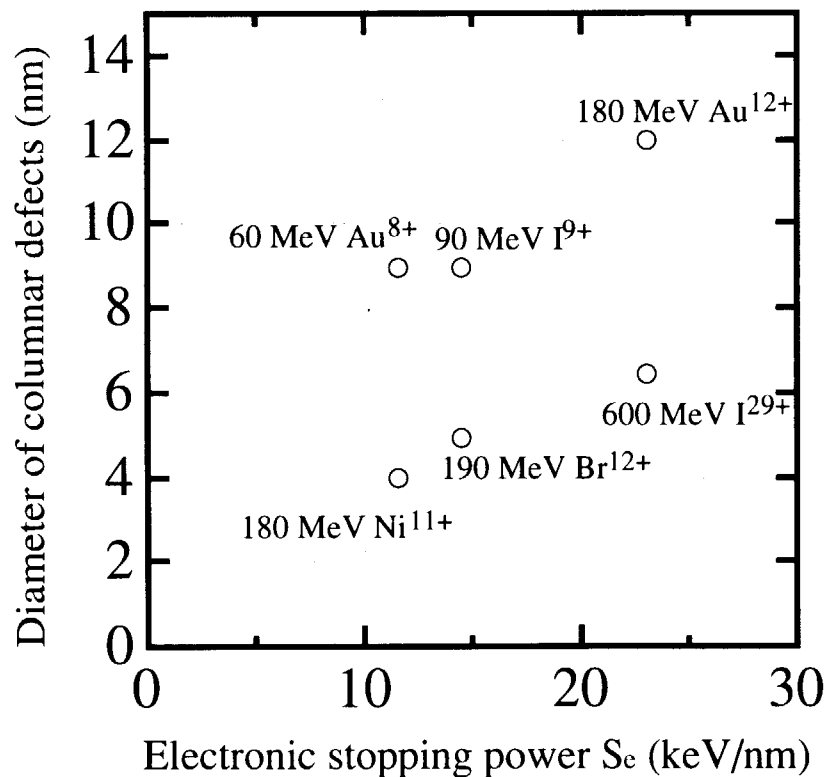
Figure 1 Dependence of the columnar defect diameters on the S_e in the Bi-2212. Comparison of defect sizes is made for three irradiations with same S_e value (11.5, 14.5 and 23 keV/nm) but much different velocities.

Acknowledgments

References

[1] e.g., M. Toulemonde, S. Bouffard and F. Studer, Nucl. Instrum. Method, *B91*(1994)108.

[2] A. Meftah, F. Brisard, J. M. Constantini, M. Hage-Ali, J. P. Stoquert, F. Studer and M. Toulemonde et. al., Phys. Rev. *B48*(1993)920.

[3] N. Ishikawa, Y. Chimi, N. Kuroda, A. Iwase and T. Kambara, Physica Scripta, *T80*(1999) 559.

[4] V. Hard, D. Groult, M. Hervieu, J. Provost and B. Raveau, Nucl. Instrum. Method, *B54*(1991) 472.

[5] J. F. Ziegler : Handbook of Stopping Cross Section for Energetic Ions in All Elements Pergamon, New York (1980)

[6] Y. Zhu, Z. X. Cai, R. C. Budhani. M. Suenaga and D. O. Welch, Phys. Rev. *B48*(1993)6436.

[7] M. Sasase, T. Satou, S. Okayasu, H. Kurata and K. Hojou, International Symposium on Superconductor (ISS'99) Proceedings (2000)314.

7.2 CHANGE IN CRITICAL CURRENT DENSITY OF Bi$_2$Sr$_2$CaCu$_2$O$_{8+x}$ SINGLE CRYSTALS DUE TO HIGH-ENERGY HEAVY-ION IRRADIATION FOLLOWED BY THERMAL ANNEALING

K.OGIKUBO[1] , T.TERAI[1], S.OKAYASU and K.HOJOU

Particle-beam irradiation is one of the most effective methods to introduce strong pinning centers into high-T_c superconductors. In particular, high-energy heavy-ion irradiation produces columnar defects, which give very large pinning force for the vortices parallel to the defects. The size and the number of columnar defects as flux pinning centers can be changed by thermal annealing treatment after irradiation. This treatment is quite effective for the improvement of the superconducting properties in some cases for neutron irradiated specimens [1], because the superconducting properties are strongly affected by the defect structure in materials. It is considered that some overlapped defect clusters, which are produced by neutron irradiation, become complex defects due to thermal annealing. In this study, we investigated the thermal annealing effect in the critical current density of Bi-2212 superconductors irradiated with high-energy heavy-ions (200 MeV Au or 200 MeV Ag) up to the fluence of 5×10^{11} cm^{-2}.

Bi$_2$Sr$_2$CaCu$_2$O$_{8+x}$ (Bi-2212) single crystal specimens were prepared by the floating-zone method. Their size was about 1 mm × 1 mm × 50 μm (c-axis). All of the specimens were annealed at 1073 K for 72 h in air and were quenched to room temperature in advance. The specimens were irradiated with 200 MeV Au ions or 200 MeV Ag ions using a tandem accelerator at JAERI. Tokai (Japan Atomic Energy Research Institute). The irradiation temperature was room temperature. In this study, the specimens were irradiated up to the fluence of 5×10^{11} cm^{-2}. After the irradiation, the specimens were annealed in air at 673 K up to 6 h. Magnetization hysteresis curves were measured by using a vibrating sample magnetometer (VSM) at 20 K and 40 K as a function of applied magnetic field parallel to the c-axis of the specimen. The critical current density J_c in a-b plane of the specimen was calculated from the magnetization hysteresis curve using the extended Bean's model[2].

The ion-fluence dependence of J_c is shown in Fig.1. All the plotted values are normalized to J_{c0} which indicates the critical current density of the unirradiated specimen. For both 200 MeV Au-irradiated specimen and 200 MeV Ag-irradiated specimen, J_c once increased at the fluence of 5×10^{10} cm^{-2} and decreased at 5×10^{11} cm^{-2}. According to SRIM96 code calculation, the maximum values of the electronic stopping power of incident Au ion and Ag ion are 29.0(keV/nm) and 22.6(keV/nm), respectively. It is considered that these values of the electronic stopping power are high enough to make columnar defects which have a large diameter (> 10nm)[3,4]. Fig.2 shows the annealing time dependence of J_c for 200 MeV Au-irradiated specimen and 200 MeV Ag-irradiated specimen at the fluence of 5×10^{11} cm^{-2}. For both 200 MeV Au-irradiated specimen and 200 MeV Ag-irradiated specimen, J_c gradually decreased with the increase in annealing time at the measurement temperature of 20 K. On the other hand, J_c gradually increased with the annealing time at the measurement temperature of 40 K. It is considered that this different dependence of J_c on the annealing time between the measurement temperatures of 20 K and 40 K is attributed to the different kind of defects which contribute dominantly to the pinning effect at each temperature. It is considered that not only radiation-induced columnar defects but also intrinsic point defects, which exist in the specimen before irradiation, are still effective

---

[1] Department of Quantum Engineering and Systems Science. Graduate School of Engineering. The University of Tokyo.

as strong pinning centers even after irradiation at relatively lower temperature of 20 K. On the other hand, the only columnar defects contribute dominantly as effective pinning centers at 40 K, because the intrinsic point defects can hardly act as effective pinning centers at such a relatively higher temperature. This consideration is supported by the change in the enhancement ratio J_c/J_{c0} shown in Fig.1. The enhancement ratio J_c/J_{c0} at 5×10^{10} cm^{-2} mainly depended on the measurement temperature and it was larger at the higher temperature of 40 K than that at lower temperature of 20 K. The less change of J_c in the lower temperature of 20 K means that the intrinsic point defects are still dominant as effective pinning centers even after irradiation. On the other hand, the larger increase in J_c at the higher temperature of 40 K indicates that the contribution of the columnar defects becomes dominant. Therefore, after the thermal annealing treatment as shown in Fig.2, the increase in J_c at the measurement temperature of 40 K is considered to be due to the formation of secondary complex defects from several adjacent columnar defects, which produced with the very high irradiation fluence of 5×10^{11} cm^{-2}, by moving atoms constituting defects. On the other hand, the decrease in J_c at the measurement temperature of 20 K is considered to be due to the disappearance of the intrinsic point defects, which act as effective pinning centers before the thermal annealing treatment. These results suggest that the J_c decrease at 20 K due to the disappearance of the intrinsic point defects is larger than the J_c increase due to the formation of secondary complex defects. For both measurement temperatures of 20 K and 40 K, the change ratio of J_c after thermal annealing to J_c of the as-irradiated specimen is not so large (0.68 to 2.2). This means the columnar defects keep a somewhat stable structure at the annealing temperature of 673 K as well as form secondary complex defects.
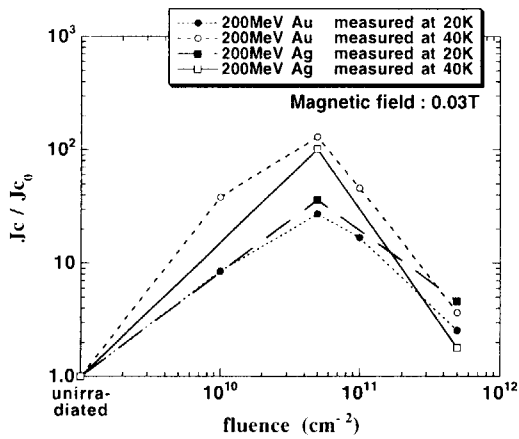
Fig.1.　Fluence dependence of J_c　　　Fig.2.　Annealing time dependence of J_c
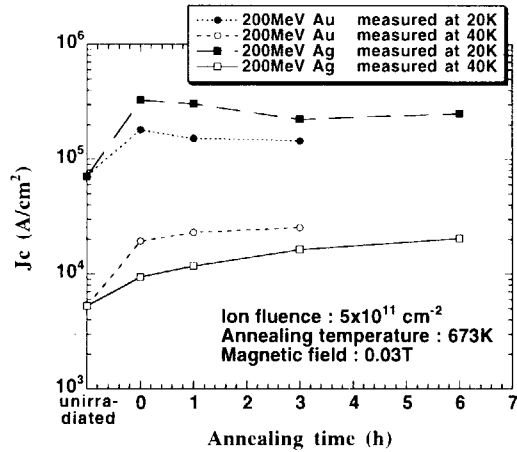
References

[1] K. Ogikubo et al., Physica C **341-348** (2000) 1469.
[2] E. M. Gyorgy et al., Appl. Phys. Lett. **55** (1989) 283.
[3] D.X. Huang et al., Phys. Rev. B **57** (1998) 13907.
[4] D.X. Huang et al., Phys. Rev. B **59** (1999) 3862.

7.3   OBSERVATION OF VORTICES AND COLUMNAR DEFECTS BY LORENTZ MICROSCOPY   II

K. HARADA[1,4], H. KASAI[1,4], O. KAMIMURA[1,4], T. MATSUDA[1,4], A. TONOMURA[1,4], S. OKAYASU, M. SASASE, Y. NAKAYAMA[2,4], J. SHIMOYAMA[2,4], K. KISHIO[2,4], T. HANAGURI[3,4] and K. KITAZAWA[3,4]

In high-T_c superconductors, because quantized vortices move very easily under current-induced force acting on them, pinning centers are very important to be used as dissipation free conductors.   Columnar defects produced by penetration of high energy heavy ions are considered as one of the most effective pinning centers [1].   Up to now only static observations of vortices have been done with scanning tunneling microscopy [2] and the Bitter decoration method [3].   The Lorentz microscopy using the 300-kV field-emission electron microscope is the only tool to observe vortex dynamics.   We have observed that each single vortex and their dynamic behavior at the TV frame rate of 1/30 s [4,5].   In our present work, simultaneous observation of single vortex and columnar defect has been carried out successfully with the Lorentz microscopy, and their interactions have also been investigated [6].

A single crystalline of $Bi_2Sr_2CaCu_2O_{8+\delta}$ (Bi-2212) was grown by the standard floating-zone technique and annealed at 800 °C to be slightly oxygen over-doped.   The critical temperature T_c was about 85 K [7].   The Bi-2212 thin films of thickness about 200 nm with a 100 × 100 μm^2 uniform area were cleaved as specimens for transmission electron microscopy (TEM) [5].   The thin film was irradiated by 240-MeV Au^{+15} ions with density of 2.5×10^7 ions/cm^2(1 Gauss).   The irradiation direction was tilted by 70 degrees from the c-axis of Bi-2212.   The ion irradiation in such a low dose was performed with a specially developed slit shutter system installed at the beam line of the Tandem accelerator of the Japan Atomic Energy Research Institute (JAERI) [8].   Then the prepared thin film was set on a low-temperature stage of electron microscope tilted by 30 degrees from electron beam in order to detect the vortex contrast in the micrograph.

Figure 1 is an in-focused electron micrograph which shows projected images of tilted columnar defects as black short lines.   The diameter of the tilted column is about 10 nm, which is almost the same as that of the perpendicular column.   However, the contrast of the tilted columns in the figure is enhanced by the Bragg condition between electron beam and crystallographic orientation of sample film, and it helps us to observe the columnar defects in such low magnified images.   Sparse distribution of columnar defects with the density of 5×10^6 columns/cm^2 are intentionally produced by tilted ion irradiation with the incidence angle of about 70 degrees.

[1]Advanced Research Laboratory, Hitachi, Ltd., Hatoyama, Saitama 350-0395
[2]Department of Applied Chemistry, University of Tokyo, Bunkyo-ku, Tokyo 113-8656
[3]Department of Advanced Materials Science, School of Frontier Science, University of Tokyo, Bunkyo-ku, Tokyo 113-0033
[4]CREST, Japan Science and Technology Corporation (JST), Kawaguchi, Saitama 332-0012

Figure 2 shows a Lorentz micrograph of the same region of Fig. 1 with the same size. Because of a large defocusing of about 150 mm, contrast of columnar defects disappeared and globule-like contrast of black-and-white features appeared instead. In Fig. 2, vortex density is about the same order of magnitude of the columnar density at about 9 K. From Figs. 1 and 2, we observe that there are two types of configuration between vortices and columnar defects:

(1) Trapped vortices at the columnar defects. (This configuration is indicated by arrows.)
(2) No relation between vortex position and columnar defect position.

The second type of behavior is probably oriented from the difference of distributions between magnetic field through vortices and columnar defects.

We are now planning to observe how the vortices are pinned by columnar defects and how the vortices behave dynamically through the defects.
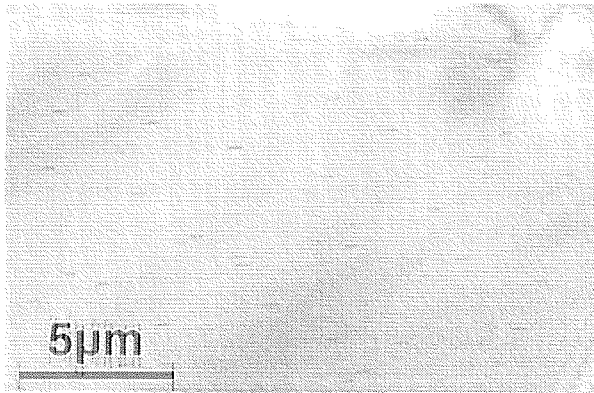
Fig. 1.   Electron micrograph of Bi-2212.   Fig. 2.   Lorentz micrograph at 9 K.
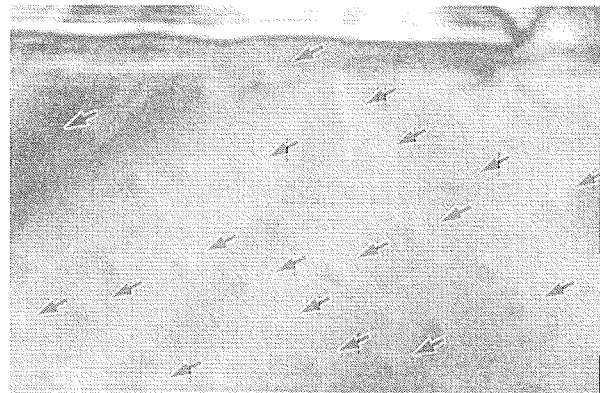
References
[1]   S. Oakayasu *et al.*, Physica B **194-196** (1994) 1881.
[2]   S. Behler, S. H. Pan, P. Jess, A. Baratoff, H. -J. Güntherodt, F. Lévy, G. Wirth and J. Wiesner, Phys. Rev. Lett. **72** (1994) 1750.
[3]   H. Dai, S. Yoon, J. Liu, R. C. Budhani and C. M. Lieber, Science **265** (1994) 1552.
[4]   A. Tonomura, H. Kasai, O. Kamimura, T. Matsuda, K. Harada, J. Shimoyama, K. Kishio and K. Kitazawa, Nature **397** (1999) 308-309.
[5]   K. Harada, H. Kasai, O. Kamimura, T. Matsuda, A. Tonomura, S. Okayasu and Y. Kazumata, Phys. Rev. B **71** (1996) 9400-9405.
[6]   In preperation.
[7]   Y. Kotaka, T. Kimura, H. Ikuta, J. Shimoyama, K. Kitazawa, K. Yamafuji, K. Kishio and D. Pooke, Physica C **235-240** (1994) 1529-1530.
[8]   K. Harada, H. Kasai, O. Kamimura, T. Matsuda, A. Tonomura, S. Okayasu M. Ssase, J. Shimoyama, K. Kishio and K. Kitazawa, JAERI Tandem Annual Report 1999, JAERI-Review **2000-018** (2000) 78-79.

7.4 RADIATION DEFECTS IN NANOCRYSTALLINE MATERIALS

H.OHTSUKA, H.SUGAI, K.HOJO, H.MAETA[1]

The aim of this study is to realize defect free material against radiation taking advantage of structural effects of the nanocrystalline. Within nano-scale structural crystals, annihilation of defects is expected to overcome the production of that owing to the diffusion of itself. Defect formation within nano-particles was investigated putting an emphasis on diffusion coefficient of defects. We have first observed a diffusion-limited reaction of defects in nano-particles. The results brought out a guide to damage-free materials.

In order to introduce defects, the nano-particles were irradiated by 200 MeV nickel ions using the JAERI tandem accelerator. The observation of the defects was carried out by using a transmission electron microscopy (TEM) operating at 200 kV. Gold nano-particles were used as the specimen. Figure 1-a shows TEM observation of a particle after the irradiation at room temperature with the calculated dpa about 0.6. Black spots are defect clusters. Among those spots triangle shaped ones are the stacking-fault tetrahedra. When the irradiation temperature was increased to 300℃, the feature of the clusters clearly changed. The size of the clusters increased and the distribution of those became sparse. These results imply that the diffusion-limited phenomenon took place in the particles. Hence, we needed to develop a simulation program for the cluster formation in order to analyze the phenomenon.

A tow-dimensional lattice model was developed applying the cellular automata method using Mathematica on IBM PC. A square shape of 100×100 lattice is the model of a particle, where at a time interval a point defect (i.e. vacancy) is created randomly in the lattice. The rules of the motion and the cluster formation are as follows. All single vacancies move 1 step at an another time interval. When they touch the boundary, they are annihilated. When a vacancy meets with another ones, they combine with each other. Tri-vacancy can not move and be a nucleus of the succeeding cluster formation. Because diffusion coefficient of single defects is strongly dependent on the temperature, we take that as the key parameter.

Figure 2-a/b shows the result of the simulation that aimed to show dependence of the pattern of clusters on diffusion coefficient of the point defect. In both cases 1200 point defects were created. The 'relative' diffusion coefficient of Fig.2-b case was 4000 times larger than that of Fig.2-a. In Figure 2-a small clusters distribute uniformly over the lattice (particle), that resembles Figure 1-a, and also we can find resemblance between Fig. 2-b and Fig. 1-b. So, we see good agreement

---

[1]Faculty of Engineering, Hiroshima Kokusai Gakuin Univ.

between the experiments and the simulation concerning the cluster formation. As to the size effect against the irradiation we note that the cluster formation has been hardly observed in small particles (<30nm) at the 300°C irradiation case. The simulation also supports this as shown in Fig. 2-c where the divided areas represent small particles. Those results suggest that the simulation model with further improvements will be able to use to predict operation condition of defect free against irradiation. This conclusion is a fruit of the present study.

Patterns in nature have attracted human interests because those are considered as the mystery of nature. The cellular automata method used in this study is one of theoretical tools to analyze the pattern formation in nature. It is worth to note that we analyzed the mystery of nature within the nano-particles.
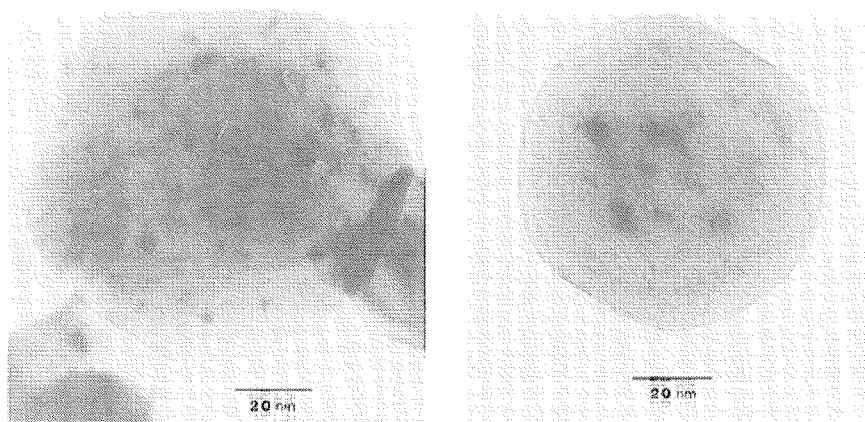
Fig.1 TEM observation of defect clusters in a nano-particle caused by high energy heavy ion irradiation: (a) room temperature and (b) 300°C irradiation, respectively.
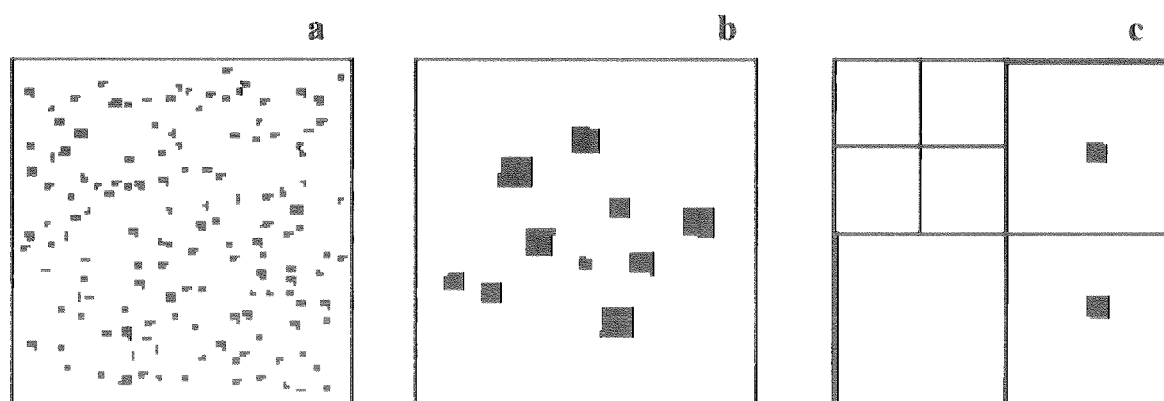
Fig.2. Simulation of cluster formation using the cellular automata method. The square frame represents the boundary of the particle. Clusters are shown in black spots. Dependence on the diffusion coefficient is shown in (a) vs (b). Diffusion coefficient of (b) is 4000 times larger than that of (a). (c) shows size effect where partitions are introduced to case (b) to simulate small particles. The diffusion-limited reaction is clearly exhibited.

7.5 DEFECT RECOVERY
IN ENERGETIC PARTICLE IRRADIATED IRON

Y. CHIMI, A. IWASE, and N. ISHIKAWA

Recovery of defects in energetic particle irradiated iron has been studied. Polycrystalline iron thin-film (~200nm thick) specimens were deposited on α-Al_2O_3 single crystal substrates. Specimens were irradiated at a low temperature (~77K) with several energetic particles; 2.0MeV electrons from a 3MV single-ended accelerator at TIARA, JAERI-Takasaki, 0.5-2.0MeV ^{1}H-^{40}Ar ions from a 2MV Van de Graaff accelerator and 84-200MeV ^{12}C-^{197}Au ions from a 20MV tandem accelerator both at JAERI-Tokai. Each irradiation was ceased when the increment in electrical resistivity of the specimen reached a certain value (~0.3$\mu\Omega$cm). After each irradiation, recovery behavior of irradiation-produced defects was observed during heating the specimen at a constant rate (2K/min).

In the present report, we are focusing on the recovery stage-I, where interstitial atoms can move and recombine with vacancies. Fig. 1 shows the fraction of the stage-I recovery as a function of primary knock-on atom (PKA) median energy, $T_{1/2}$ [1,2], which is a kind of the weighted average of the PKA energy. For electron and low-energy (~1MeV) ion irradiations, the fraction of the stage-I recovery decreases as $T_{1/2}$ increases. This indicates that more complicated defects are produced by a PKA with higher $T_{1/2}$. On the other hand, for high-energy (~100MeV) ion irradiations except for ^{12}C ion irradiation, the fraction of the stage-I recovery is much smaller than that for low-energy ion irradiations at the same $T_{1/2}$. This reduction of the stage-I recovery suggests that electronic excitations induce radiation annealing during the high-energy ion irradiations [3]. In Fig. 2, the reduction of the stage-I recovery is plotted against the electronic stopping power, S_e. The fraction of the stage-I recovery reduces with increase in S_e at lower S_e (<~30MeV/(mg/cm^2)). At higher S_e, however, the data points are scattered and not well scaled with S_e. Therefore, it appears that S_e is not appropriate for describing the radiation annealing. Here, we tried to scale the present data with the primary ionization rate, dJ/dx, as well as in the case of other electronic excitation effects [4]. The dJ/dx dependence of the data is shown in Fig. 3. As can be seen in the figure, the fraction of the stage-I recovery begins to increase with increase in dJ/dx at higher dJ/dx. This result implies that high-density electronic excitation induces the stage-I defect production, and the radiation annealing may be triggered by the ion explosion mechanism.

References

[1] R.S. Averback, R. Benedek, and K.L. Merkle, Phys. Rev. B **18** (1978) 4156.

[2] R.S. Averback, R. Benedek, K.L. Merkle, J. Sprinkle, and L.J. Thompson, J. Nucl. Mater. **113** (1983) 211.

[3] Y. Chimi, A. Iwase, N. Ishikawa, N. Kuroda, and T. Kambara, Nucl. Instrum. Methods **B164-165** (2000) 408.

[4] Y. Chimi, A. Iwase, N. Ishikawa, N. Kuroda, and T. Kambara, JAERI Tandem Annual Report 1999, JAERI-Review 2000-018 (2000) 95.
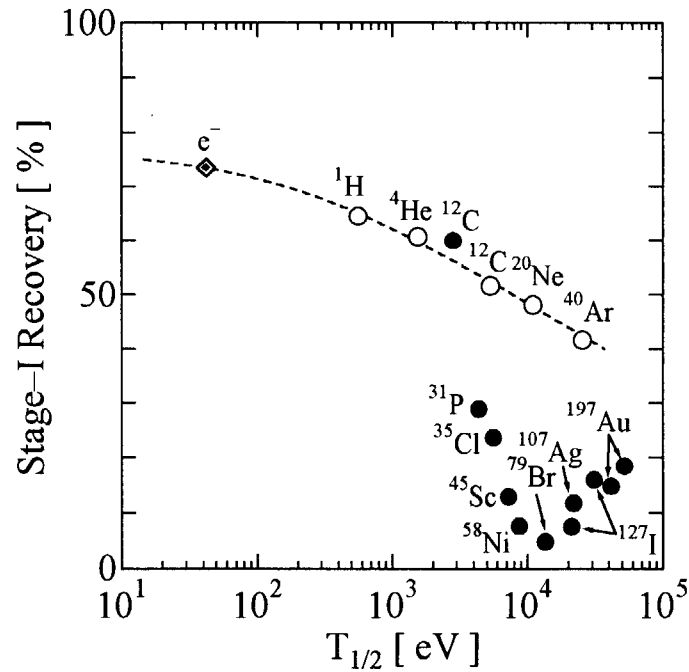
Fig. 1. Fraction of stage-I recovery as a function of PKA median energy, $T_{1/2}$. Open and closed circles represent low-energy (~1MeV) and high-energy (~100MeV) ion irradiations, respectively.
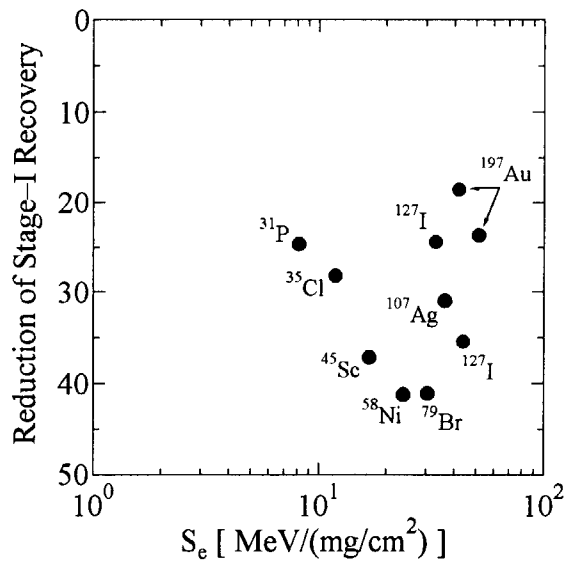
Fig. 2. Reduction of stage-I recovery for high-energy ions plotted against electronic stopping power, S_e.
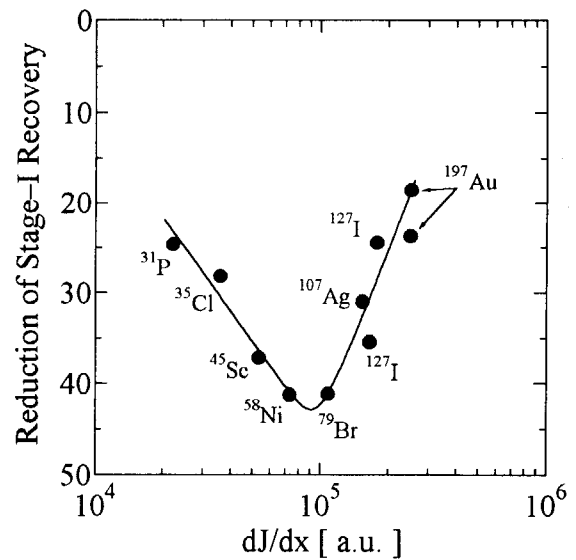
Fig. 3. Reduction of stage-I recovery for high-energy ions as a function of primary ionization rate, dJ/dx.

7.6 "*IN SITU*" ELECTRICAL RESISTIVITY MEASUREMENT OF Fe-Cu ALLOYS IRRADIATED WITH ENERGETIC HEAVY IONS

T.HASEGAWA[1], S.ISHINO[2], Y.CHIMI, N.ISHIKAWA, T.TOBITA, M. SUZUKI, AND A.IWASE

Although a reactor pressure vessel is one of the components which are required to have extremely high reliability, the mechanism of its irradiation embrittlement has not been clarified. Elucidation of the mechanism is of great current concern from the aspect of a plant life extension. We have reported in previous papers that ion irradiation experiment is very useful for the mechanistic understanding of irradiation embrittlement in reactor pressure vessel steels. In the present paper, we report the new result of the post-irradiation *in situ* electrical resistivity measurement of Fe-Cu alloys performed along this line.

Samples prepared in the present experiment were two kinds of Fe-Cu alloys, Cu concentrations of which were 0.02 and 0.6 wt%, respectively. The alloys about 30μ m thick were cut into a strip of 5mm × 10mm. Irradiations were performed at 7K and at 300K with 100MeV carbon ions using JAERI-Tokai tandem accelerator. Irradiation dose (dpa) was calculated by using the measured ion-fluence and the TRIM code [1]. The electrical resistivity was measured as a function of irradiation dose by a conventional four probe method. For the samples irradiated at 7K, we also carried out the isochronal annealing experiment.

Fig 1 shows the change in electrical resistivity, $\triangle \rho$, at 7K   for the two kinds of alloys as a function of calculated dpa. For both alloys, the resistivity increases clearly with increasing the irradiation dose. However, the resistivity change rate for Fe-0.6%Cu alloy is more than twice larger than for Fe-0.02%Cu alloy. This result implies that there is a certain interaction between Cu atoms and interstitial Fe atoms. For the irradiation at 300K, as can be seen in Fig.2, Fe-0.02%Cu alloy shows the increase in resistivity, while for Fe-0.6%Cu alloy, the resistivity decreases remarkably with increasing the dose. This result suggests the formation of Cu atom clusters and/or precipitates through the irradiation enhanced diffusion mechanism. Fig.3 shows the defect recovery curve after irradiation at 7K and their temperature derivatives for the two alloys. The defect recovery for Fe-0.02%Cu alloy is almost the same as that for the electron-irradiated pure Fe [2]. We can see that the major recovery occurs near 100K for each alloy. The amount of the recovery near 100K for Fe-0.6%Cu alloy is, however, less than that for Fe-0.02%Cu alloy, while the

1 Course of Applied Science, Graduate School of Engineering, Tokai University
2 Department of Nuclear Engineering, School of Engineering, Tokai University

recovery around 200K for Fe-0.6%Cu alloy is larger than for Fe-0.02%Cu alloy. This result may be explained as due to the interaction of Cu atoms with Fe interstitial atoms.

References

[1] J.T.Biersack and L.G.Haggmark, Nucl.Instr.Meth, B174(1980) 257.

[2] S.Takaki, J.Fuss, H.Kugler, U.Dedek and H.Schultz, Rad.Eff. 79(1983) 87.

Fig.1.Dose dependence of resistivity change at 7K.

Fig.2.Dose dependence of resistivity change at 300K.

ANNEALING TEMPERATURE , K

Fig.3.Defect recovery and temperature differential curves. The dose is nearly 1.9×10^{-5} dpa.

7.7 DEPTH-DEPENDENT AND SURFACE DAMAGES IN MgAl₂O₄ AND MgO IRRADIATED WITH ENERGETIC IODINE IONS

T. ARUGA, Y. KATANO, T. OHMICHI, S. OKAYASU AND Y. KAZUMATA

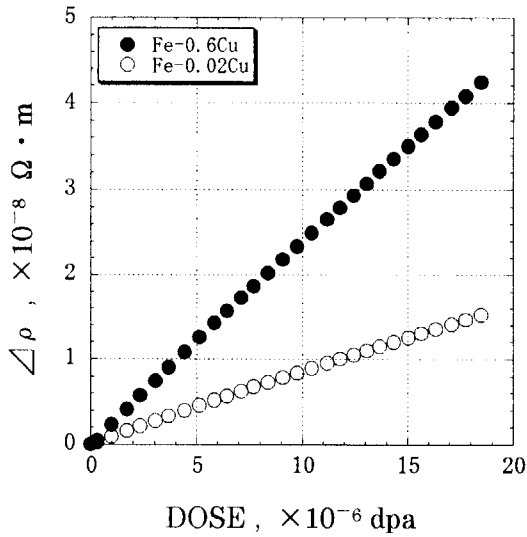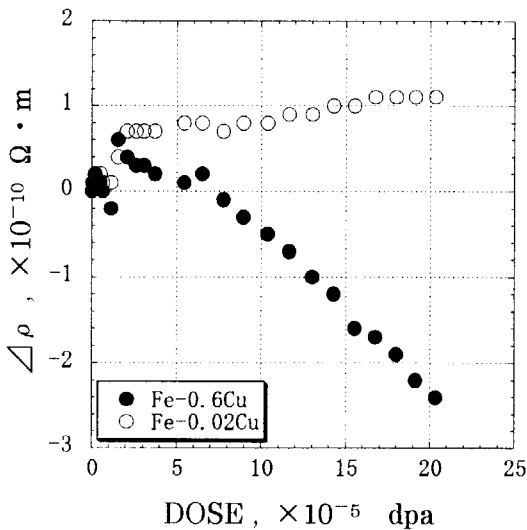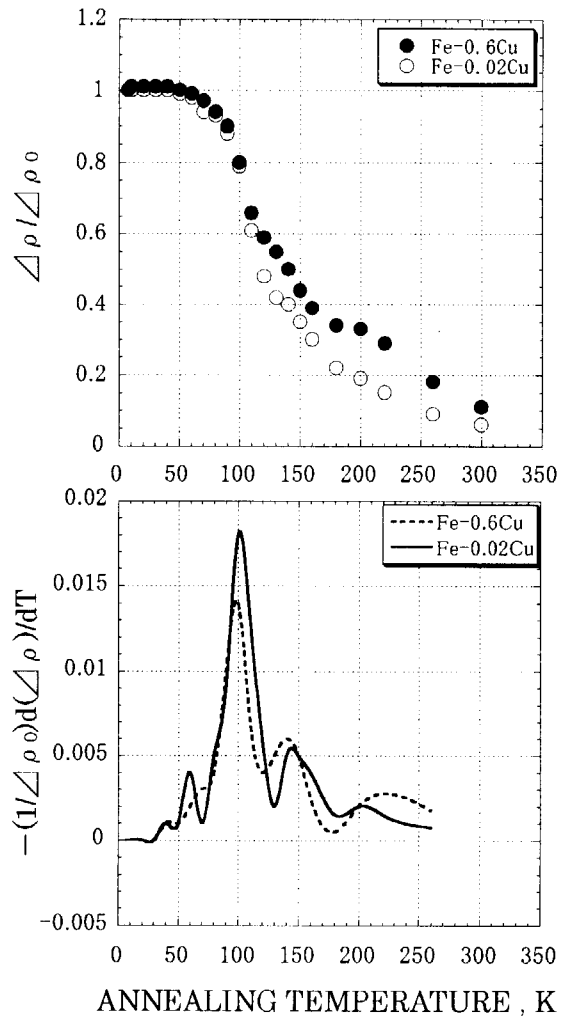We have already observed that polycrystalline alumina is amorphized by the irradiation with 85 MeV I^{7+} ions to a dose of $1.2 \times 10^{19}/m^2$ at the ambient temperature and that amorphization is entirely due to an electronic energy deposition[1]. It is of a physical and practical interest to elucidate the relation between a bonding nature of oxides and the tendency for these oxides to be amorphized under swift ion irradiation.

Samples of polycrystalline sintered ceramics of $MgAl_2O_4$ and MgO were irradiated at the ambient temperature with 85 MeV I^{7+} ions to doses up to $1.2 \times 10^{19}/m^2$. The $MgAl_2O_4$ sample is observed to be amorphized up to depths around 6 μm from the ion-incident surface for a dose of $1.2 \times 10^{19}/m^2$, through a cross-sectional transmission electron microscopy, as shown in Fig. 1. No defect clusters are observed around 9 μm, where displacement damages due to the nuclear energy deposition are predicted to be peaked to be 1.5 dpa, as illustrated in Fig. 2 based on a calculation by an extended E-DEP-1.EXT [2] code. The thickness of the amorphized layer is larger by 1 μm, as compared with that observed in polycrystalline Al_2O_3. Moreover, no preferred amorphization along grain boundaries nor grains having moved into the amorphized region are observed around depths of 6 μm, which have been observed in Al_2O_3 sample[1]. Instead a sharp boundary between amorphized and crystalline regions is observed.
A step height of 1 μm is observed across the border between the masked and irradiated regions of the surface using a laser profilometry. The height of the step is observed to increase sharply from the irradiated area towards the edge at the border, forming a peak as tall as 1.5 μm; while the step decreased gradually towards the edge at the border of Al_2O_3 sample. The differences observed in the depth profiles of amorphization behaviors and the manner of step height formations are attributable to the difference in the viscosities of the amorphized phases under the iodine irradiations.

Note that neither amorphization, nor defect clusters nor step heights are observed for the MgO sample irradiated with iodine ions to the same dose. The fact demonstrates that a higher ionicity of chemical bonding and its isotropic nature in MgO instantly recover the lattice agitations produced by electronic energy depositions. Instead, a X-ray diffractometry revealed an enhancement of the diffraction peak for (200), (400) reflections, as compared with those before irradiation, indicating that an atomistic re-arrangement may occur along ion's paths to form a new surface with the lowest surface energy or {100} planes from the ion-incident surface.

A glossy, silver-gray film with a thickness less than 0.1 μm is unexpectedly observed to have formed on the surface of samples of $MgAl_2O_4$ and MgO, but not of Al_2O_3, after about 3.5 y of aging or being left untouched in the air. The film is easily peeled off from the surface along grain boundaries, and found to be amorphous from the electron diffraction pattern. The EDS (energy dispersive X-ray spectroscopy) analysis reveals that the film from $MgAl_2O_4$ sample contains Al, Mg and Si. Silicon, which is one of impurities and is included to less than 0.1 mass %, may be enriched at the surface. These facts suggest that a long-term migration of atoms of Al, Mg and Si occurs in the layer in close proximity to the surface, where oxygen atoms bonding with or associated with magnesium atoms would be lost preferentially during the irradiation, then the thin film formation occurs in the near-surface region of depths for $MgAl_2O_4$ and MgO, but not for Al_2O_3.

References
[1] T. Aruga, Y. Katano, T. Ohmichi, S. Okayasu, Y. Kazumata, Nucl. Instr. Methods. Phys. Res. B 166-167 (2000) 913.
[2] T. Aruga, K. Nakata, S. Takamura, Nucl. Instr. Methods Phys. Res. B 33 (1988) 748.
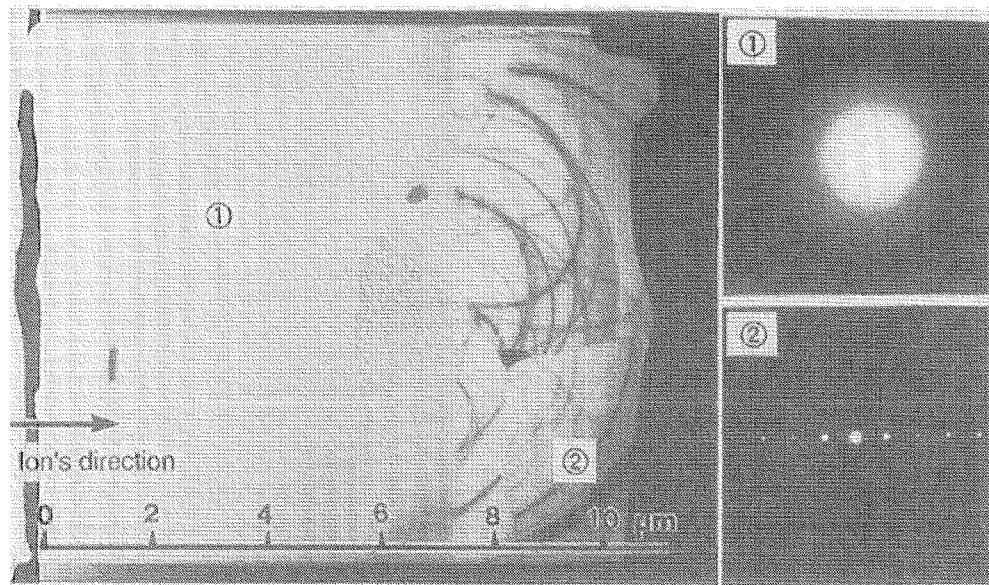
Fig. 1. Structural changes in the polycrystalline $MgAl_2O_4$ sample irradiated with 85 MeV I^{7+} ions to $1.2 \times 10^{19}/m^2$, as observed in a transmission electron microscopy as a function of depth along a direction of incident ion's direction. Selected area diffraction patterns taken for positions designated by ① and ② are also shown.
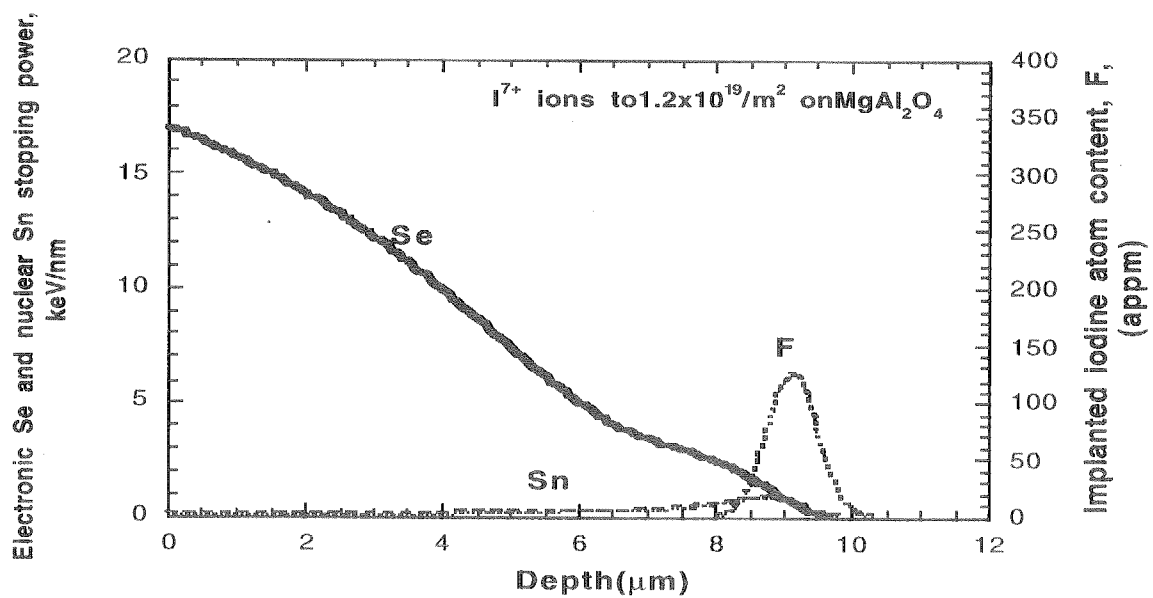
Fig. 1. Electronic and nuclear stopping powers, and implanted iodine atom concentration as a function of depth for $MgAl_2O_4$ sample irradiated with 85 MeV I^{7+} ions to $1.2 \times 10^{19}/m^2$, as calculated by extended E-DEP-1 code.

7.8 ION IRRADIATION EFFECTS ON MECHANICAL PROPERTIES OF DIFFERENT CARBON FIBERS

A. KURUMADA[1], T. OKU[2], Y. IMAMURA[1], M. ISHIHARA, K. HAYASHI, S. BABA and J. AIHARA

In order to apply carbon/carbon composites to the next fusion experimental reactor, it is needed to be studied on the materials for the changes in microstructures and mechanical properties with radiation damage. These studies lead us further development of new C/C composites with radiation-resistant properties. On the other hand, thermal and mechanical properties of C/C composites are well known to depend on those of carbon fibers since carbon fibers in C/C composites are generally less crystalline than the carbon matrix part. Thus, the effects of ion irradiation damage on the tensile properties of carbon fibers were evaluated in this study.

In this study, three grades with nine kinds of carbon fibers were selected, which were polyacrylonitrile (PAN) based fibers (M55JB, M40JB, T700SC by Toray Corp.), mesophase pitch based fibers (YS-70-60S, XN-70-60S, YS-15-60S by Nippon Graphite Fiber Corp.) and pitch based fibers (K13C2U, K1392U, K1352U by Mitsubishi Chemical Co.). They were irradiated by high energy carbon and argon ions. Carbon ions ($^{12}C^{+6}$) of 100 MeV with 0.5 μ A were irradiated to 6×10^{-6} dpa using the TANDEM accelerator in Tokai, JAERI, and argon ions ($^{40}Ar^{+8}$) of 175 MeV with 1 μ A were irradiated to 1.1×10^{-3} dpa using the Azimuthally Varying Field (AVF) cyclotron in JAERI Takasaki on four kinds of carbon fibers in those described above. The ranges of carbon and argon ions calculated by TRIM-98 code were 221 and 52.8 μ m, respectively. Irradiation damages in the carbon fibers were expected to be uniform across the cross section, because the carbon fibers, with about 20 μ m in diameter, were smaller enough than the ranges.

Figure 1 shows changes in cross sectional areas of different carbon fibers after ion irradiation. The cross sectional areas increased due to ion irradiation except for the XN-70-60S and tended to increase with increasing radiation damage. One of the causes of the increases is the swelling of carbon basal planes due to lattice defects in the graphite interlayer. Table 1 shows changing ratios on mechanical properties of different carbon fibers after ion irradiation. The tensile strengths and Young's moduli tend to decrease with the irradiation. The mechanism of radiation damage effects on the carbon fibers has not been completely illustrated.

Within the limits of this study, the tensile strength and Young's modulus of the YS-15-60S mesophase pitch based fiber were stable to radiation damage. Also it seemed that the tensile strengths and Young's moduli of the carbon fibers with random structure were comparatively more stable to radiation damage than those with radial structure.

---

[1] Faculty of Engineering, Ibaraki University

[2] The University of the Air
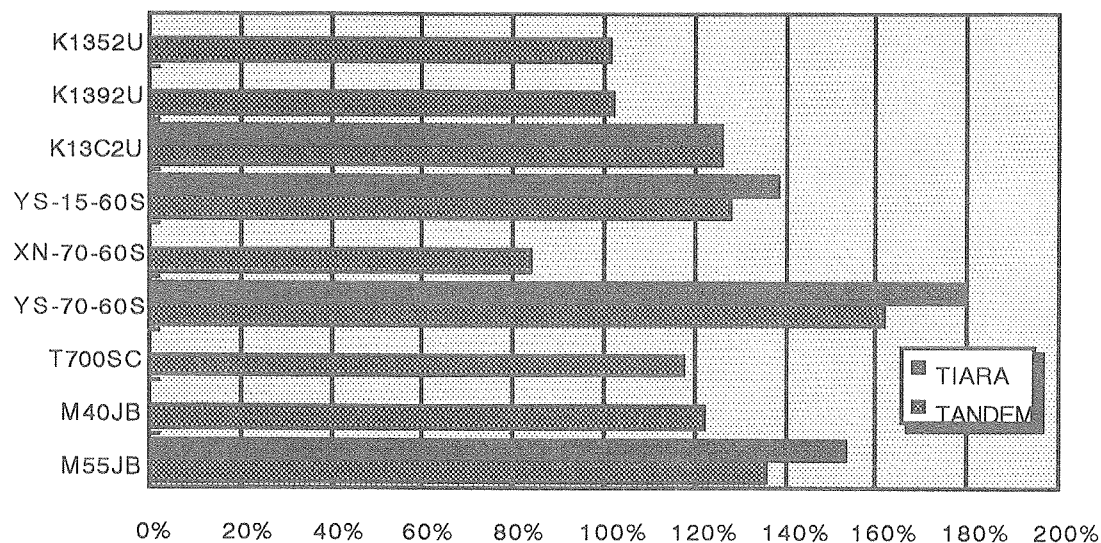
Fig. 1.   Changes in cross sectional areas of different carbon fibers after ion irradiation.

Table 1.   Changing ratios on mechanical properties of different carbon fibers after ion irradiation using TANDEM.

	Changing ratio on cross-sectional area	Changing ratio on Young's modulus	Changing ratio on tensile strength
K1352U (Pitch based fiber)	1.01 (-)	1.09 (-)	0.98 (-)
K1392U (Pitch based fiber)	1.02 (-)	0.99 (-)	0.86 (-)
K13C2U (Pitch based fiber)	1.26 (1.26)	0.72 (0.94)	0.65 (0.75)
YS-15-60S (Mesophase pitch based fiber)	1.28 (1.38)	1.01 (1.05)	1.00 (1.03)
XN-70-60S (Mesophase pitch based fiber)	0.84 (-)	1.17 (-)	1.04 (-)
YS-70-60S (Mesophase pitch based fiber)	1.62 (1.79)	0.78 (0.92)	0.76 (0.80)
T700SC (PAN based fiber)	1.17 (-)	0.85 (-)	0.71 (-)
M40JB (PAN based fiber)	1.22 (-)	1.16 (-)	1.08 (-)
M55JB (PAN based fiber)	1.36 (1.53)	1.04 (0.90)	1.00 (0.75)

Values in parenthesis indicate the effects of argon ion irradiation using TIARA.

7.9 THE CORRELATION BETWEEN THE TOLERANCE OF SINGLE EVENT BURNOUT AND THE DESIGN PARAMETER OF POWER MOSFETS

H. SHINDO [1], T. HIRAO, S. KUBOYAMA [1]
H. ITO, T. HIROSE [2], T. ABURAYA [1]
H. OHIRA [2], Y. NAGAI [2] and S. MATSUDA [1]

Single-event effects (SEE) are the most serious problem in applying highly sophisticated modern electronic devices in space environments. Single Event Burnout (SEB) was identified as a possible catastrophic failure mode for Power MOSFETs. SEB is triggered when a heavy ion passes through a power MOSFET biased in the OFF state. Transient current generated by a heavy ion turns on a parasitic bipolar transistor (BJT) inherent to the device structure, creates a short-circuit between the source and drain and destroys the device [1]. In order to analyze the mechanisms behind SEB and to develop SEB-tolerant devices for space use, we started the high-energy heavy ion irradiation tests for various test sample devices.

To determine the suitable design parameters of Power MOSFET for space use, we aim at the width of P^{++}-type diffusion region and the thickness of the epitaxial layer in Power MOSFET as one of the protection structures of SEB. We started to investigate the relationship between these design parameters and the tolerance of SEB in Power MOSFET. Tests were performed by using Energetic Particle Induced Charge Spectroscopy (EPICS) system [2]. Fig.1 shows the block diagram of EPICS system. EPICS is a specially designed pulse-height analyzer (PHA) system to characterize the charge collection characteristics in semiconductor devices. By using this measurement system, we can observe the SEB signal of Power MOSFET non-destructively during irradiation testing.

In the irradiation test, we used Ni ions (LET=28.0[MeV/(mg/cm^2)]) from a TANDEM accelerator in JAERI. The beam current was about 1.0 nA. The primary ion beam was scattered by an Au foil to obtain uniform beam intensity over the surface of the samples. Energy Spectrum and beam flux were monitored by SSD before the test. We prepared various test samples in which the width of the P^{++} region and the thickness of the epitaxial layer were altered. These samples were manufactured based on Power MOSFET 2SK3041 which the NASDA had developed for space use. EPICS measurements were performed at various drain-source voltages V_{DS}. Test results are summarized and are depicted in Fig. 2 and Fig. 3.
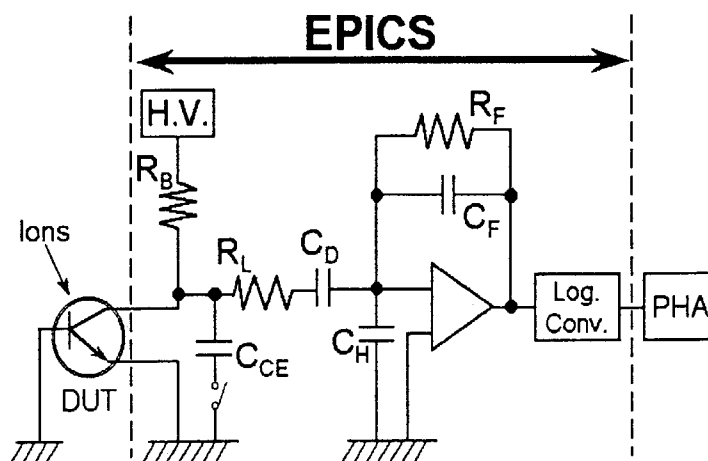
Fig. 1. Block diagram of the EPICS system

[1] Electronic and Information Technology Laboratory, Office of Research and Development, National Space Development Agency of Japan.
[2] Components Engineering Section, Engineering Dept., RYOEI TECHNICA Corporation.

Figure 2 shows the relationship between the width of the P^{++} region and the SEB threshold Voltage, V_{DS}. Δ Wp++ means the expansion width of the P^{++} region from the reference sample based on 2SK3041. Figure 3 shows the relationship between the thickness of epitaxial layer (t-epi) and the SEB threshold V_{DS}.
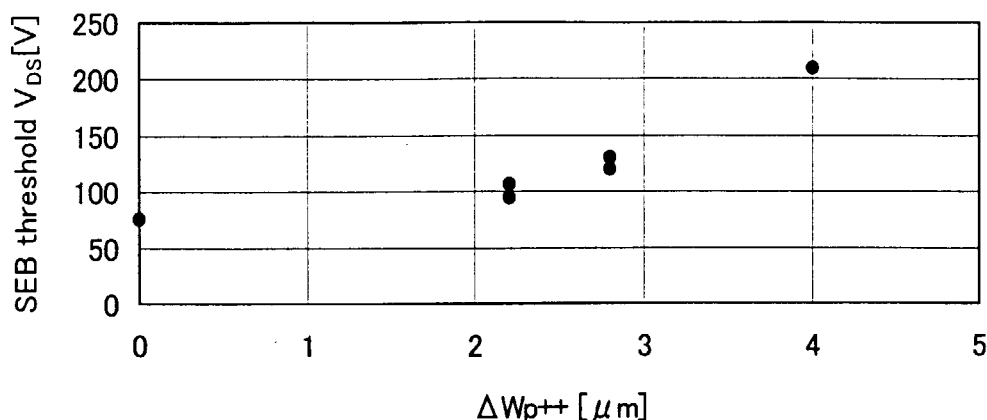
Fig. 2.V_{DS} - Δ Wp++ characteristic
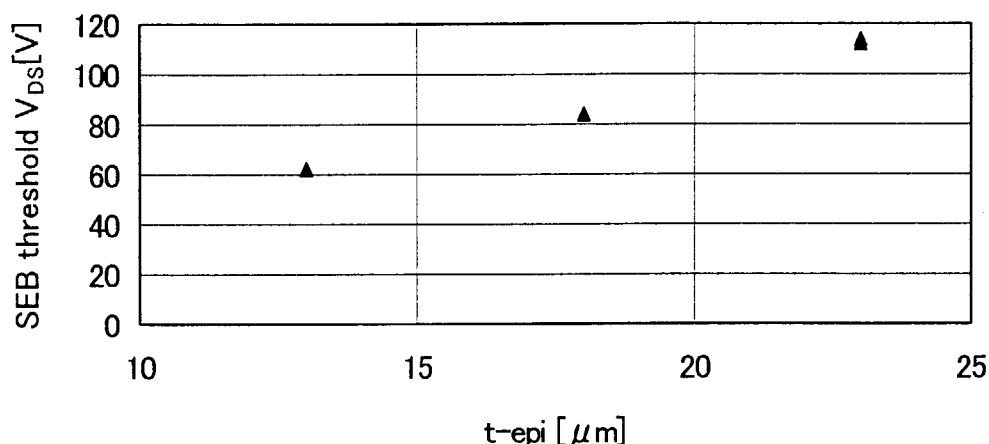
Fig. 3.V_{DS} - t-epi characteristic

As indicated on Fig. 2, an increase of Δ Wp++ to 4μm raises the threshold V_{DS} from 76V to 210V. This means that Δ Wp++ is one of the effective design parameters to improve the tolerance of SEB. It is also found (see Fig. 3) that as the t-epi becomes thicker, the threshold V_{DS} increases from 62V to 114V. It seems that the t-epi is also the effective design parameter to improve the tolerance. However, it is known that an increase of t-epi leads to an increase of the resistance of ON state and degrades the electrical characteristics of Power MOSFET. Thus the optimum value of t-epi must be fixed when designing the device. For further study, we are planning to evaluate the other design parameters such as the resistance of epitxical layer in order to determine the suitable design parameter set of Power MOSFET for space use. These tests also connect with making the mechanism of SEB clear. We expect that these test results are quite useful to develop high SEB tolerance Power MOSFETs.

References

[1] M.Allenspach, et al, IEEE. Trans.Nucl.Sci., Vol.NS-43,No.6 (1996) 2927.
[2] S.Kuboyama, et al, IEEE. Trans.Nucl.Sci. Vol.NS-39,No.6(1992) 1698.

This is a blank page.

8. Publication in Journal and Proceedings, and Contribution to Scientific Meetings

This is a blank page.

ACCELERATOR OPERATION AND DEVELOPMENT

Journal/Proceedings

Takeuchi, S.

Status of superconducting heavy-ion booster linac at JAERI

Proceeding of the 3rd Superconducting Linear Accelerator Meeting in Japan,

Tsukuba (May 25-26, 2000)p.16.

Meetings

Ichikawa, S.

New projects and special requrements: the Japanese way

TWIST II Workshop on Target and Ion Source Technology,

GANIL, Caen, France (Jun. 15-16, 2000)

Ichikawa, S., Osa, A., Tsukada, K., Nagame, Y.

Ion source development of the on-line isotope separator at JAERI

ISOL'01, Oak Ridge, USA (Mar. 11-14, 2001)

Osa, A., Matsuda, M., Ichikawa, S.

Study of neutron-deficient nuclei beam for Coulomb excitation

Science of Low Energy Short-lived Nuclei Beam 2001,

Tsukuba (Mar. 14, 2001)

Osa, A., Matsuda, M., Tsukada, K., Ichikawa, S.

Ion source development for on-line mass separation of fission products

Materials Science Symposium "Heavy ion Science in Tandem Energy Region",

Tokai (Jan. 9-10, 2001)

Takeuchi, S.

Status of superconducting heavy-ion booster linac at JAERI

The 3rd Superconducting Linear Accelerator Meeting in Japan,

Tsukuba (May 25-26, 2000)

Takeuchi, S., Matsuda, M., Yoshida, T.

Project of beam intensity increase for JAERI-tokai tandem booster

The 13th Workshop on Tandem Accelerators and Associated Technology,

Mutsu, Aomori (Jun. 8-9, 2000)

Yoshida, T., Kanda, S., Takeuchi, S., Hanashima, S., Ohuchi, I., Horie, K.,

Tsukihashi, Y., Abe, S., Ishizaki, N., Tayama, H., Matsuda, M.

The status of the JAERI tandem accelerator

13th Workshop on Tandem Accelerator and Associated Technology,

Mutsu, Aomori (Jun. 8-9, 2000)

Yoshida, T.

Electrostatic accelerator on the accelerator group and its recent utilization

Matrerials Science Symposium "Heavy ion Science in Tandem Energy Region",

Tokai (Jan. 9-10, 2001)

Yoshida, T.

JAERI tandem booster and its cryogenic system

Wrokshop on Accelerator Operation 2001, CERN,

Villars-sur-Ollon, Switzerland (Jan. 29- Feb. 2, 2001)

NUCLEAR STRUCTURE

Journal/Proceedings

Asai, M., Sakama, M., Tsukada, K., Ichikawa, S., Haba, H., Nishinaka, I.,

Nagame, Y., Goto, S., Kojima, Y., Oura, Y., Nakahara, H.,

Shibata, M., Kawade, K.

Spectroscopic studies of mass-separated heavy nuclei

Proc. of Tours Symposium on Nuclear Physics IV,

Tours, France, 2000 (AIP, New York, 2001)p.358.

Asai, M., Ishii, T., Makishima, A., Hossain, I., Ogawa, M., Ichikawa, S.

Nanosecond isomers in neutron-rich ^{67}Cu and ^{64}Co and a fast E3 transition in ^{67}Cu

Phys. Rev. **C 62** (2000) 054313.

Hatsukawa, Y., Oshima, M., Hayakawa, T., Toh, Y., Shinohara, N.

Application of multidimensional spectrum analysis for neutron activation analysis

J. Radioanal. Nucl. Chem. **248** (2000) 121.

Hayakawa, T., Oshima, M., Hatsukawa, Y., Katakura, J., Iimura, H.,

Mitarai, S., Shinohara, N., Tho, Y., Shizuma, T., Sugawara, M., Kusakari., H.

Yrast bands of N=91 isotones

Eur. Phys. J. **A9** (2000) 153.

Iimura, H., Ichikawa, S., Ishida, Y., Horiguchi, T.

Collinear laser spectroscopy on radioactive isotopes

Proc. First Symp. on Advanced Photon Research,

JAERI Conf 2000-006 (2000) 266.

Raman, S., Yonezawa, C., Matsue, H., Iimura, H., Shinohara, N.

Efficiency calibration of a Ge detector in the 0.1-11.0 MeV region

Nucl. Instr. Meth. in Phys. Res. **A454** (2000) 389.

Sakama, M., Tsukada, K., Asai, M., Ichikawa, S., Haba, H., Goto, S.,

Oura, Y., Nishinaka, I., Nagame, Y., Shibata, M., Kojima, Y., Kawade, K.,

Ebihara, M., Nakahara, H.

New isotope ^{233}Am

Eur. Phys. J. **A 9** (2000) 303.

Sugawara, M., Mitarai, S., Kusakari, H., Oshima, M., Hayakawa, T.,

Toh, Y., Hatsukawa, Y., Katakura, J., Iimura, H., Zhang, Y. H., Sugie, M.,

Sato, Y.

Rotational bands of ^{156}Gd

Nucl. Phys. **A686** (2001) 29.

Meetings

Hatsukawa, Y., Oshima, M., Hayakawa, T., Toh, Y., Shinohara, N.

Application of multidimensional spectrum analysis for neutron activation analysis

The Fifth Inter. Conf. on "METHODS AND APPLICATIONS OF RADIO-

ANALYTICAL CHEMISTRY" Kailua-Kona, Hawaii (Apr., 2000)

Hatsukawa, Y., Oshima, M., Hayakawa, T., Toh, Y., Shinohara, N., Kusita, K.,

Uneo, T.

Application of multidimensional analysis for neutron activation analysis-2,

The 44th Symposium on Radiochemistry, Kobe (Oct. 13, 2000)

Hatsukawa, Y., Oshima, M., Hayakawa, T., Toh, Y., Shinohara, N., Kusita, K.,

Uneo, T.

Measurements of long-lived nuclides by using multiparameter coincidence method

The second workshop on environmental radioactivity, Tsukuba (Mar., 2001)

Hatsukawa, Y., Oshima, M., Hayakawa, T., Toh, Y., Shinohara, N., Kusita, K.,

Uneo, T.

Application of multidimensional analysis for neutron activation method-Determination

of ^{129}I

2001 The Chemical Society of Japan Spring meeting, Kobe (Mar. 29, 2001)

Hayakawa, T., Toh, Y., Oshima, M., Hatsukawa, Y., Shinohara, N., Matsuda, J.,
Katakura, J., Iimura, H., Sugawara, M., Kusakari., H.

High spin states in ^{157}Dy

The 55th Annual Meeting of the Physical Society of Japan, Niigata (Sept. 22, 2000)

Hayakawa, T.

In-beam γ-ray spectroscopy using the GEMINI and the tandem accelerator at JAERI

The 25th memorial symposium of the Tandem accelerator in University of Tsukuba,
Tsukuba (Dec. 12, 2000)

Hayakawa, T., Toh, Y., Oshima, M., Hatsukawa, Y., Shinohara, N., Matsuda, J.,
Katakura, J., Iimura, H., Sugawara, M., Kusakari., H.

Coulomb excitation of ^{78}Se

The 56th Annual Meeting of the Physical Society of Japan, Tokyo (Sept. 27, 2000)

Ichikawa, S., Tsukada, K., Sakama, M., Asai, M., Shibata, M., Kojima, Y.,
Nishinaka, I., Nagame, Y., Oura, Y., Kawade, K.

Mass separation of neutron-deficient Am, Cm isotopes using the gas-jet
coupled JAERI-ISOL

The 55th Annual Meeting of the Physical Society of Japan, Niigata (Sept. 22, 2000)

Iimura, H., Ishida, Y., Koizumi, M., Shinohara, N., Shibata, T., Horiguchi, T.,
Schuessler, H. A.

Isotope shift measurements of La II by collinear laser spectroscopy

The 55th Annual Meeting of the Physical Society of Japan, Niigata (Sept. 22, 2000)

Iimura, H., Ishida, Y., Koizumi, M., Shinohara, N., Shibata, T., Horiguchi, T.,
Schuessler, H. A.

Isotope shift measurements of La II by collinear laser spectroscopy

The Second Symposium on Advanced Photon Research, Kyoto (Nov. 10, 2000)

Ishii, T., Asai, M., Matsuda, M., Ichikawa, S., Makishima, A., Hossain, I.,

Kleinheinz, P., Ogawa, M.

Nano-second isomers in neutron-rich Ni region produced by deep-inelastic collisions

International Conference on Nuclear Physics, XXXV Zakopane School of Physics,

Zakopane, Poland (Sept. 5-13, 2000)

Ishii, T., Asai, M., Makishima, A., Hossain, I., Kleinheinz, P., Ogawa, M.,

Matsuda, M., Ichikawa, S.

Gamma-ray spectroscopy of neutron-rich Ni region through heavy-ion

deep-inelastic collisions

International Symposium on Perspectives in Physics with Radioactive Isotope

Beams 2000 in Hayama, Kanagawa (Nov. 13-16, 2000)

Morikawa, T.

Nuclear structure study with low energy secondary beams

"Science of low-energy unstable nuclei beam 2001" KEK, Tsukuba (Mar. 10, 2001)

Morikawa, T.

Coulomb excitation experiments with low-energy unstable nuclear beams at CRIB

"Physics of low-energy RIB" CNS/RIKEN, Saitama (Aug. 23, 2000)

Morikawa, T., Oshimka, M., Toh, Y., Hayakawa, T., Hatsukawa, Y.,

Kusakari, H., Sugawara, M.

Coulomb excitation of ^{154}Sm

The Physical Society of Japan Kyushu Branch Meeting, Okinawa (Nov. 25, 2000)

Morikawa, T.

Plan of coulomb excitation experiment with low Energy secondary beams

The Physical Society of Japan Kyushu Branch Meeting, Okinawa (Nov. 25, 2000)

Tsukada, K., Sakama, M., Asai, M., Ichikawa, S., Haba, H., Nishinaka, I.,

Nagame, Y., Goto, S., Kojima, Y., Oura, Y., Nakahara, H.,

Shibata, M., Kawade, K.

EC/ α -decay properties of neutron-deficient Am and Cm isotopes
The 5th International Conference on Nuclear and Radiochemistry,
Pontresina, Switzerland (Sept. 3-8, 2000)

Sakama, M., Tsukada, K., Asai, M., Ichikawa, S., Oura, Y., Haba, H.,
Nishinaka, I., Nagame, Y., Goto, S., Shibata, M., Kojima, Y., Kawade, K.,
Ebihara, M., Nakahara, H.
α -decay properties of neutron-deficient actinide isotopes
The 44th Symposium on Radiochemistry, Kobe (Sept. 12-14, 2000)

Sugawara, M.
Study on the medium high spin states of β -stable neutron rich nuclei
"Science of low-energy unstable nuclei beam 2001" KEK, Tsukuba (Mar. 14, 2000)

Sugawara, M., Toh, Y., Oshima, M., Hayakawa, T., Hatsukawa, Y.,
Katakura, J., Kusakari, H.
Coulomb excitation of the ^{70}Ge beam
The 55th Annual Meeting of the Physical Society of Japan, Niigata (Sept. 22, 2000)

Sugawara, M., Mitarai, S., Kusakari, H., Oshima, M., Hayakawa, T.,
Toh, Y., Hatsukawa, Y., Katakura, J., Iimura,H., Zhang, Y. H., Sugie, M.,
Sato, Y.
Rotational bands of ^{159}Dy
The 56th Annual Meeting of the Physical Society of Japan, Tokyo (Mar. 27, 2001)

Toh, Y., Oshima, M., Hayakawa, T., Hatsukawa, Y., Kusakari, H., Sugawara, M.,
Czosnyka, T., Matsuda, M.
The multiple Coulomb excitation experiments
"Science of low-energy unstable nuclei beam 2001" KEK, Tsukuba (Mar. 10, 2000)

Toh, Y., Czosnyka, T., Oshima, M., Hayakawa, T., Osa, A., Koizumi, K.,
Hatsukawa, Y., Shinohara, N., Kusakari, H., Sugawara, M.
Development of position-sensitive particle detector for Coulomb excitation experiment

The 55th Annual Meeting of the Physical Society of Japan, Niigata (Sept. 22, 2000)

NUCLEAR REACTIONS

Journal/Proceedings

Mitsuoka, S., Ikezoe, H., Nishio, K., Lu, J.

Sub-barrier fusion of deformed nuclei in $^{60}Ni+^{154}Sm$ and $^{32}S+^{182}W$ reactions

Phys. Rev. **C62** (2000) 054603.

Nishio, K., Ikezoe, H., Mitsuoka, S., Satou, K., Jeong, S. C.

Effects of nuclear deformation on fusion probability in the reactions of $^{82}Se + ^{nat}Ce$ and $^{76}Ge+^{150}Nd$ near the Coulomb barrier

Phys. Rev. **C63** (2001) 044610.

Nishio, K., Ikezoe, H., Mitsuoka, S., Lu, J., Satou, K.

Experimental study of synthesis of heavy nuclei at JAERI

Proc. of the 2000 Symposium on Nuclear Data,

JAERI Conf. 2001-006 (2001)p.269.

Shinohara, N., Tsukada, K., Ichikawa, S., Magara, M., Hatsukawa, Y.

Isomeric yield ratios of ^{134}I and ^{136}I in the proton-, ^{12}C-and ^{19}F-induced fission of ^{235}U, ^{237}Np and ^{238}U

Radochim. Acta. **88** (2000) 1.

Meetings

Fujita, H., Inotani, Y., Sugimitsu, T., Ikeda. N., Koga, M., Nakamura, F., Koto,S., Morinobu, S., Sugimitsu, T., Sugiyama, Y., Tomita, Y., Ikezoe, H., Yamanouchi, Y., Ideno, K., Hamada, S., Ikuta, T.

Intermediate resonances observed in $^{12}C(^{16}O,^{12}C[2^+])^{16}O$ at Ec.m.=22.6 MeV

The 56 Annual Meeting of the Physical Society of Japan, Tokyo (Mar. 27, 2001)

Mitsuoka, S.

Sub-barrier fusion between neutron rich projectile and deformed target

in the reactions of $^{60,64}Ni+^{154}Sm$

Science with Low Energy Radioactive Nuclear Beams 2001,

Tsukuba (Mar. 12-14, 2001)

Nishio, K., Ikezoe, H., Mitsuoka, S., Satou, K.

Fusion probability for $^{82}Se + ^{nat}Ce$ and $^{76}Ge+^{150}Nd$

The 56 Annual Meeting of the Physical Society of Japan, Niigata (Sept. 22, 2000)

Nishio, K., Ikezoe, H., Mitsuoka, S., Satou, K.

Fusion probability for $^{82}Se+^{nat}Ce$ and $^{76}Ge+^{150}Nd$

2001 Spring Meeting of Atomic Energy Society of Japan, Tokyo (Mar. 29, 2001)

Sugiyama, Y., Hamada, S., Yamazaki, A.

Nuclear Josephson effect observed in the $^{58}Ni+^{58}Ni$ reaction

The 56 Annual Meeting of the Physical Society of Japan, Niigata (Sept. 22, 2000)

Sugiyama, Y., Hamada, S., Yamazaki, A.

Strong enhancement of four-nucleon transfer in the $^{58}Ni+^{58}Ni$ reaction

Materials Science Symposium "Heavy ion Science in Tandem Energy Region",

Tokai (Jan. 9, 2001)

NUCLEAR CHEMISTRY

Journal/Proceedings

Akiyama, K., Zhao, Y. -L., Sueki, K., Tsukada, K., Haba, H., Nagame, Y., Kodama, T., Suzuki, S., Ohtsuki, T., Sakaguchi, M., Kikuchi, K., Katada, M., Nakahara, H.
Isolation and characterization of light actinide metallofullerenes
J. Am. Chem. Soc. **123** (2001) 181.

Haba, H., Tsukada, K., Nishinaka, I., Asai, M., Hirata, M., Ichikawa, S., Nagame, Y., Yokoyama, A., Toyosima, A., Shoji, Y., Shinohara, A., Goto, S., Kaneko, T., Kudo, H., Sakama, M., Oura, Y., Schadel, M.
Aqueous chemistry of Rf in JAERI
JAERI Review 2001-004 (2001)p.431.

Nagame, Y., Asai, M., Haba, H., Tsukada, K., Sakama, M., Goto, S., Nishinaka, I., Ichikawa, S.
Heavy element nuclear chemistry research in JAERI
Proceeding of the 2000 Symposium on Nuclear Data,
JAERI Conf. 2001-006 (2001)p.15.

Meetings

Akiyama, K., Sakaguchi, M., Zhao, Y. -L., Sueki, K., Tsukada, K., Kikuchi, K., Nagame, Y., Katada, M., Nakahara, H.
Attempts for synthesis of actinide metallofullerenes
The 78th Spring Meeting of the Chemical Society of Japan, Narashino, Chiba (Mar., 2000)

Akiyama, K., Zhao, Y. -L., Sueki, K., Kodama, T., Suzuki, S., Tsukada, K., Haba, H., Kikuchi, K., Ohtsuki, T., Nagame, Y., Nakahara, H., Katada, M.
Chemical properties of actinide fullreneas
The 44th Symposium on Radiochemistry, Kobe (Sept.12, 2000)

Haba, H., Tsukada, K., Nishinaka, I., Asai, M., Sakama, M., Goto, S., Hirata, M., Ichikawa, S., Nagame, Y., Kaneko, T., Kudo, H., Yokoyama, A., Toyosima, A., Shoji, Y., Shinohara, A., Oura, Y., Sueki, K., Schadel, M.

Startup of transactinide chemistry in JAERI

The 5th International Conference on Nuclear and Radiochemistry, Switzerland (Sept. 5, 2000)

Haba, H., Tsukada, K., Nishinaka, I., Asai, M., Sakama, M., Goto, S., Hirata, M., Ichikawa, S., Nagame, Y., Yokoyama, A., Toyosima, A., Shoji, Y., Shinohara, A., Kaneko, T., Kudo, H., Oura, Y., Schadel, M.

Aqueous chemistry of Rf in JAERI

The 44th Symposium on Radiochemistry, Kobe (Sept. 12, 2000)

Haba, H., Tsukada, K., Asai, M., Nishinaka, I., Hirata, M., Ichikawa, S., Nagame, Y., Yokoyama, A., Toyosima, A., Shoji, Y., Shinohara, A., Goto, S., Kaneko, T., Kudo, H., Sakama, M., Oura, Y., Suaki, K., Schadel, M.

Aqueous Chemistry of Rutherfordium (Rf) in JAERI

2001 The Chemical Society of Japan Spring Meeting, Kobe (Mar. 30, 2001)

Sueki, K., Akiyama, K., Zhao, Y, -L., Katada, M., Kikuchi, K., Nakahara, H., Tsukada, K., Nagame, Y.

Synthesis of actinide metallofullerenes

The 19th Fullerene General Symposium, Kiriyu, Gunma (Jur., 2000)

Toyoshima, A., Shoji, Y., Yokoyama, A., Shinohara, A., Haba, H., Tsukada, K., Nagame, Y.

Ion exchange behavior of Rf and the homologues -On the tracer experiments-

The 44th Symposium on Radiochemistry, Kobe (Sept. 14, 2000)

Tsukada, K., Haba, H., Asai, M., Nishinaka, I., Ichikawa, S., Nagame, Y., Sakama, M., Oura, Y., Goto, S., Kaneko, T., Kudo, H., Toyoshima, A., Shoji, Y., Yokoyama, A., Shinohara, A., Gaeggeler, H. W., Tuerler, A., Schaedel, M.

Synthesis of ^{261}Rf and ^{262}Db

The 44th Symposium on Radiochemistry, Kobe (Sept.12, 2000)

NUCLEAR THEORY

Journal/Proceedings

Chiba, S., Iwamoto, O., Sukhovitskij, E. S., Watanabe, Y., Fukahori, T.

Coupled-channels optical potential for interaction of nucleons with ^{12}C up to 150 MeV in the soft-rotator model

J. Nucl. Sci. Technol. **37** (2000) 498.

Chiba, S.

Proceedings of the second symposium on science of Hadrons under extreme conditions

ed. S. Chiba, JAERI Conf. 2000-011 (2000)

Chikazumi, S., Maruyama, T., Niita, K., Iwamoto, A.

QMD simulation of expanding nuclear matter

Phys. Lett. **B476** (2000) 273.

Fukushima, M., Suganuma, H.

Instanton properties in external color field

Dynamics of Gauge Field, Proc. of TMU-Yale Symposium, ed. A. Chodos et al,

Universal Academy Press (2000)p.213.

Chikazumi, S., Maruyama, T., Chiba, S., Niita, K., Iwamoto, A.

Quantum molecular dynamics simulation of expanding nuclear matter and nuclear multifragmentation

Phys. Rev. **C63** (2001) 024602.

Fujii, Y., Iwamoto, A., Fukahori, T., Ohnuki, T., Nakagawa, M., Hidaka, H., Oura , Y., Möller, P.

The nuclear interaction at Oklo 2 billion years ago

Nucl. Phys. **B573** (2000)377.

Chikazumi, S., Maruyama, T., Niita, K., Chiba, S. , Iwamoto, A.

Expanding nuclear matter by QMD
JAERI Conf.2000-011 (2000)p.13.

Hirata, Y., Ohnishi, A., Nara, Y., Ohtsuka, N., Niita, K., Chiba, S., Takada, H.
Fragment production in 12-GeV proton induced reactions
JAERI Conf 2000-011 (2000)p.48.

Iwamoto, A., Madland, D.G., Möller. P.
Systematic studies of fission saddle-point shapes and their reaction to the maxima of the fission-fragment mass and kinetic-energy distributions
Proc. second Int. Conf. on Fission and Properties of Neutron-Rich Nuclei (2000) p.371.

Kido, T., Maruyama, T., Niita, K., Chiba, S.
MD simulation study for nuclear matter
Nucl. Phys. **A663&664** (2000) 877c.

Kondratyev, V. N., Maruyama, T., Chiba, S.
Shell effects in nuclear magnetization
JAERI Conf. 2000-011 (2000)p.99.

Kondratyev, V. N., Maruyama, T., Chiba, S.
Magnetic field effect on masses of atomic nuclei
Astrophysical Journal **546** (2001) 1137.

Lee, J. Y., Sukhovitskij, E. S., Lee, Y. O., Chang, J., Chiba, S., Iwamoto, O.
Analysis of the nuclear lever structure and nucleon interaction data for ^{56}Fe based on the soft-rotator model
J. Korean Physics Society **38** (2001) 88.

Mao, G., Chiba, S., Greiner, W., Oyamatsu, K.
Vacuum discharge as a possible source of Gamma-ray bursts
Int. J. Mod. Phys. **E9** (2000) 185.

Mao, G., Chiba, S., Greiner, W., Oyamatsu, K.

Vacuum discharge as a possible source of gamma-ray bursts

JAERI Conf. 2000-011 (2000)p.93.

Maruyama, T., Chiba, S.

Isoscalar giant quadrupole resonance state in the relativistic approach with the momentum-dependent self-energies

Phys. Rev. **C61** (2000) 037301.

Maruyama, T., Hatsuda, T.

Color molecular dynamics for high density matter

Phys.Rev. **C61** (2000) 062201(R).

Maruyama, T., Hatsuda, T., Chiba, S.

Color molecular dynamics simulation of nuclei and dense matter

Nucl. Phys. **A681** (2001) 72c.

Maruyama, T., Hatsuda, T.

Color molecular dynamics for dense matter

JAERI Conf. 2000-011 (2000)p.118.

Möller. P., Madland D.G., Sierk , A.J., Iwamoto, A.

Nuclear fission modes and fragment mass asymmetries in a five-dimensional deformation space

Nature **409** (2001)785.

Möller. P., Madland D.G., Sierk , A.J., Iwamoto, A.

Five dimensional potential-energy surface and coexisting fission modes in heavy nuclei

Tours Symp. on Nuclear Physics IV, AIP Conf. Proc. **Vol.561** (2001)p.445.

Otsuka, T., Utsuno, Y., Mizusaki, T., Honma, M.

Shell model results for neutron-rich nuclei

Nucl. Phys. **A682** (2001) 155c.

Sukhovitskij, E. S., Lee, Y. O., Chang, J., Chiba, S., Iwamoto, O.

Nucleon interaction with ^{58}Ni up to 150 MeV studied in the coupled-channels approach based on the soft-rotator nuclear structure model

Phys. Rev. **C62** (2000) 044605.

Takemoto, H., Horiuchi, H., Ono, A.

Incident-energy dependence of the fragmentation mechanism reflecting the cluster structure of the ^{19}B nucleus

Phys. Rev. **C63** (2001) 034615.

Takemoto, H., Chiba, S., Horiuchi, H., Sugawa, N., Tohsaki, A.

Cluster formation in low-density condition

JAERI Conf. 2000-011 (2000)p.8.

Takemoto, H., Horiuchi, H., Ono, A.

Incident-energy dependence of the fragmentation mechanism reflecting the clustering structure of the ^{19}B nucleus

JAERI Research 2000-027 (2000)p.1.

Meetings

Chiba, S.

Molecular dynamics simulation and nuclear data

The 56 Annual Meeting of the Physics Society of Japan, Tokyo (Mar. 29, 2001)

Chikazumi, S., Maruyama, T., Chiba, S., Niita, K., Iwamoto, A.

Multifragmentation of expanding nuclear matter

Bologna 2000 - Structure of the Nucleus at the Dawn of the Century -,

Bologna, Itary (May 29 - Jun. 3, 2000)

Chikazumi, S., Maruyama, T., Chiba, S., Niita, K., Iwamoto, A.

Simulation of expanding nuclear matter

Seventh International Conference on Nucleus-Nucleus Collisions,

Strasbourg, France (Jul. 3-7, 2000)

Chikazumi, S., Maruyama, T., Chiba, S., Niita, K., Iwamoto, A.

Molecular dynamics simulation of expanding infinite matter

The Third Symposium on Science of Hadrons under Extreme Conditions,

Toaki (Jan. 29 - 31, 2001)

Fukushima, M.

Topological objects in QCD

The Third Symposium on Science of Hadrons under Extreme Conditions,

Tokai (Jan. 29 - 31, 2001)

Hirata, Y., Ohnishi, A., Nara, Y., Otuka, N., Niita, K., Chiba, S., Takada, H.

Fragment production in 12-GeV proton induced reactions

The 55th Annual Meeting of the Physics Society of Japan, Niigata (Sept. 22, 2000)

Hirata, Y., Ohnishi, A., Nara, Y., Otuka, N., Niita, K., Chiba, S., Takada, H.

Multifragmentation in the 12 GeV proton induced reaction

The Third Symposium on Science of Hadrons under Extreme Conditions,

Tokai (Jan. 29 - 31, 2001)

Kondratyev, V. N., Chiba, S.

Magnetic noise in crusty nuclear matter

The 55th Annual Meeting of the Physics Society of Japan, Niigata (Sept. 24, 2000)

Kondratyev, V. N., Maruyama, T., Chiba, S.

Nuclear magics in crusts of magnetars

The YITP workshop on Prospects of High Energy Astrophysics,

Kyoto (Nov. 23-25, 2000)

Kondratyev, V. N., Maruyama, T., Chiba, S.

Magnetization of crusty nuclear matter

Workshop on Quarks, Hadron Matter and Neutron Stars,

Tokyo (Nov. 29 - Dec.1, 2000)

Kondratyev, V. N.

Magnetodynamics of crusty nuclear matter

The Third Symposium on Science of Hadrons under Extreme Conditions,

Tokai (Jan. 29 - 31, 2001)

Lee, Y. O., Chang, J., Fukahori, T., Chiba, S.

Optical model potential search for neutron- and proton-induced reactions of ^{12}C, ^{16}O,

^{27}Al, ^{56}Fe, ^{90}Zr and ^{208}Pb up to 250 MeV

PHYSOR 2000 (Advances in Reactor Physics and Mathematics and Computation into

the Next Millennium), Pittsburgh, USA (May 7-11, 2000)

Takemoto, H., Ono, A. , Horiuchi, H.

Clustering effect of ^{19}B and its fragmentation

The 9th Inter. Conf. on Nuclear Reaction Mechanisum, Varenna, Italy (Jun. 5-9, 2000)

Takemoto, H.

Clustering effect of ^{19}B in its fragmentation

The Third Symposium on Science of Hadrons under Extreme Conditions,

Tokai (Jan. 29 - 31, 2001)

Utsuno, Y., Otsuka, T., Mizusaki, T., Honma, M.

Effective interaction and the structure of unstacle nuclei in the sd-pf region

Workshop on "Physics of Cluster - Tensor Interaction and Nuclear Structure -",

Wako, Saitama (Aug. 22, 2000)

Utsuno, Y., Otsuka, T., Mizusaki, T., Honma, M.

Structure of unstable nuclei around N=20

CNS/RIKEN Workshop on "Physics of Low-energy RIB",

Wako, Saitama (Aug. 23, 2000)

Utsuno, Y., Otsuka, T., Mizusaki, T., Honma, M.

Deformed band in Ar isotopes

The 55th Annual Meeting of the Physical Society of Japan, Niigata (Sept. 25, 2000)

Utsuno, Y., Otsuka, T., Mizusaki, T., Honma, M.

Vanishing of the N=20 magic number and its mechanism

JAERI Workshop on "Heavy Ion in the Tandem Region", Tokai (Jan. 9, 2001)

Utsuno, Y., Otsuka, T., Mizusaki, T., Honma, M.

Structure of unstable nuclei around N=20 studied by the monte carlo

shell model calculation

The 3rd Symposium on "Hadron Science in the Extreme Condition",

Tokai (Jan. 29, 2001)

Utsuno, Y.

Shell structure in unstable and stable nuclei

Workshop on "Recent Progress and Perspectives in the Nuclear Physics",

Tsukuba (Mar. 15, 2001)

Utsuno, Y., Otsuka, T., Mizusaki, T., Honma, M.

Electromagnetic moment and deformation in Na isotopes

The 56th Annual Meeting of the Physical Society of Japan, Tokyo (Mar. 27, 2001)

ATOMIC PHYSICS AND SOLID STATE PHYSICS

Journal/Proceedings

Ishikawa, N., Iwase, A., Chimi, Y., Michikami, O., Wakana, H., Kambara, T.

Defect production induced by primary ionization in ion-irradiated oxide super-conductors

J. Phys. Soc. Jpn. **69** (2000) 3563.

Ishikawa, N., Chimi, Y., Iwase, A., Michikami, O., Wakana, H., Kambara, T.

Scaling of irradiation effects by primary ionization rate in ion-irradiated oxide super-conductors

RIKEN Accel. Prog. Rep. **34** (2001) 93.

Iwase, A.

Lattice relaxation process in GeV-ion irradiated materials

Proc. 11th Symp. on Beam Engineering of Advanced Material Syntheses,

Tokyo (2000)p.123.

Meetings

Imai, M., Sataka, M., Kitazawa, S., Kawatsura K., Komaki, K., Shibata, H. Tawara, H., Azuma, T., Kanai, Y., Yamazaki, Y.

Angular momentum distribution of sulfur Rydberg states produced through foil penetration

The 55th Annual Meeting of the Physical Society of Japan, Niigata (Sept. 23, 2000)

Imai, M., Sataka, M., Kitazawa, S., Kawatsura K., Komaki, K., Shibata, H. Tawara, H., Azuma, T., Kanai, Y., Yamazaki, Y.

Angular momentum distribution of dulfur Rydberg sates produced through foil penetration (II)

The 56th Annual Meeting of the Physical Society of Japan, Tokyo (Mar. 27, 2001)

Ishikawa, N., Chimi, Y., Iwase, A., Michikami, O., Wakana, H., Kambara, T.

Electronic excitation and defect production in oxide superconductors irradiated with ions

Symposium on Effects of High Density Electronic Excitation, Saitama (Oct. 6, 2000)

Ishikawa, N., Chimi, Y., Iwase, A., Michikami, O., Wakana, H., Kambara, T.

Electronic excitation effects in oxide superconductors irradiated with high energy ions

Symposium on Particle Beam Science by Tandem Accelerator, Tsukuba (Dec. 13, 2000)

Ishikawa, N., Chimi, Y., Iwase, A., Michikami, O., Wakana, H.,

Hashimoto, T., Neumann, R., Kambara, T.

Defect production process in oxide superconductors irradiated with high energy ions

Fall Meeting of the Physical Society of Japan, Hachioji, Tokyo (Mar. 27, 2001)

Ishikawa, N., Sueyoshi, T., Iwase,A., Chimi, Y., Fujiyoshi, T., Miyahara, K., Kiss, T.

Critical current density of $YBa_2Cu_3O_y$ containing inclined columnar defects

The 13th International Symposium on Superconductivity, Tokyo (Oct. 15, 2000)

Iwase, A.

Study on lattice defects and high energy beam irradiation

Lattice Defects Forum 2000, Niigata (Sept. 26, 2000)

Iwase, A.

Electronic excitation and atomic displacements in materials irradiated with high-energy particles

GSI-Institut Materalforschung-Seminar, Darmstat, Germany (Nov. 7, 2000)

Iwase, A.

Lattice relaxation process in GeV-ion irradiated materials

The 11th Symp. on Beam Engineering of Advanced Material Syntheses,

Tokyo (Nov. 21, 2000)

Iwase, A.

Electronic excitation and atomic displacements in materials irradiated with swift heavy ions

Okayama University of Science Seminar, Okayama (Dec. 14, 2000)

RADIATION EFFECTS IN MATERIALS

Journal/Proceedings

Aruga, T., Katano, Y., Ohmichi, T., Okayasu, S., Kazumata, Y.

Amorphization behaviors in polycrystalline alumina irradiated with energetic iodine ions

Nucl. Instr. Meth. in Phys. Res. **B166-167** (2000) 913.

Chimi, Y., Iwase, A., Ishikawa, N., Kuroda, N., Kambara, T.

Radiation annealing induced by electronic excitation in iron

Nucl. Instr. Meth. in Phys. Res. **B164-165** (2000) 408.

Chimi, Y., Iwase, A., Ishikawa, N., Kuroda, N., Kambara, T.

Radiation annealing induced by electronic excitation in iron

RIKEN Accel. Prog. Rep. **33** (2000) 89.

Iwase, A., Ishino, S.

Comparison between radiation effects in some FCC and BCC metals irradiated with energetic heavy ions – A Review

J. Nucl. Mater. **276** (2000) 178.

Kurumada, A., Imamura, Y., Oku, T.

Evaluation of properties and development of plasma facing materials with radiation resistance (3)

RIAM Collaboration Research Report, RIAM,

Kyushu, Vol.4 (2001)p.138.

Ogikubo, K., Terai, T., Yamaguchi, K., Yamawaki, M., Okayasu, S., Hojou, K.

Pinning property change of high-energy heavy-ion irradiated Bi-2212 single crystals due to thermal annealing after irradiation

Physica **C 341-348** (2000) 1149.

Oku, T., Kurumada, A., McEnaney, B., Burchell, T. D., Ishihara, M., Hayashi, K., Baba, S., Aihara, J.

Ion irradiation effect on different carbon fibers

Eurocarbon 2000, 1ˢᵗ World Conference on Carbon,

Berlin, Germany (Jul. 9-13, 2000), Abstracts and Programme Vol.II, p.947.

Meetings

Chimi, Y., Iwase, A., Ishikawa, N., Kobiyama, M., Inami, T., Okuda, S.

Defect production and recovery in nanocrystalline gold irradiated with high energy ions

Fifth International Conference on Nanostructured Materials,

Sendai (Aug. 22, 2000)

Chimi, Y., Adachi, K., Iwase, A., Ishikawa, N., Yamakawa, K.

Disordering of hydrogen atoms in Pd-H system induced by high-energy particle irradiation

International Symposium on Metal-Hydrogen Systems, Noosa, Australia (Oct. 4, 2000)

Chimi, Y., Iwase, A., Ishikawa, N., Kobiyama, M., Inami, T., Okuda, S.

Effects of high-energy ion irradiation in nanocrystalline gold

The 55th Annual Meeting of the Physical Society of Japan, Niigata (Sept. 23, 2000)

Chimi, Y., Adachi, K., Iwase, A., Ishikawa, N., Yamakawa, K.

Effects of energetic charged particle irradiation on Pd-H system

The 55th Annual Meeting of the Physical Society of Japan, Niigata (Sept. 23, 2000)

Hasegawa, T., Ishino, S., Tobita, T., Suzuki, M., Chimi, Y., Ishikawa, N ., Iwase, A.

"In- Situ" electrical resistivity measurement of Fe-Cu Alloys

Spring Meeting of Atomic Energy Society of Japan, Tokyo (Mar. 26-28, 2001)

Hasegawa, T., Ishino, S., Chimi, Y., Ishikawa, N., Iwase, A., Tobita, T., Suzuki, M.

Heavy ion irradiation effects on Fe-Cu alloys

Kyoto University KUR Symposium "Irradiation Embrittlement Mechanism of Reactor

Pressure Vessel Steels" Kumatori, Kyoto (Jan. 19-20, 2001)

Ishino, S., Morita, K., Hasegawa, T., Iwase, A., Chimi, Y., Ishikawa, N., Tobita, T.
Use of high energy ions for the mechanistic study of radiation embrittlement in pressure vessel steels
The 20th Symposium on Effects of Radiation on Materials ASTM,
Williamsburg, USA (Jun. 6-8, 2000)

Ishino, S., Hasegawa, T., Ikusawa, Y., Iwase, A., Chimi, Y., Ishikawa, N.,
Tobita, T., Suzuki, M.
Study of mechanism of irradiation embrittlement in pressure vessel steels with high energy ions
The 9th meeting of Int. Group on Radiation Damage Mechanism in pressure vessel steels (IGRDM), Leuven, Belgium (Sept. 18-22, 2000)

Kurumada, A., Imamura, Y., Oku, T.
Ion irradiation effect on mechanical properties of carbon fibers
PSI Research Meeting, H12-No.3, RIAM, Kyushu (Feb. 15-16, 2001)

Matsunami, N., Sataka, M., Iwase, A.,
Sputtering of nano-crystalline Au by high energy heavy ions
Fifth International Conference on Nanostructured Materials
Sendai (Aug.23, 2000)

Matsunami, N., Sataka, M., Iwase, A.,
Sputtering of high Tc superconductor $YBa_2Cu_3O_{7-\delta}$ by high energy heavy ions
XIIth International Conference on the Ion Beam Modification of Materials
Rio Grande, Brazil (Sep.8, 2000)

Matsunami, N., Sataka, M., Iwase, A.,
Electronic excitation effects in perovskite Oxides by high energy heavy ions
The 55th Annual Meeting of the Physical Society of Japan, Niigata, (Sept.25, 2000)

Matsunami, N., Sataka, M., Iwase, A.,

Electronic excitation effects in Oxides by high energy heavy irradiation

The 56th Annual Meeting of the Physical Society of Japan, Tokyo (Mar. 27, 2000)

Ogikubo, K., Nakano, M., Terai, T., Yamaguchi, K., Yamawaki, M.

Pinning property change of high-energy heavy-ion irradiated $Bi_2Sr_2CaCu_{28+x}$ single crystals due to thermal annealing

The 13th International Symposium on Superconductivity, Tokyo (Oct.14-16, 2000)

Ohtsuka, H., Hojo, K,. Maeta, H,. Otsu, H., Sugai, H., Yamamoto, H.

Radiation defects in nano-structured materials

ISSPIC10, Atlanta, USA (Oct. 11, 2000)

Oku, T., Kurumada, A., Imamura, Yoshida, N., Watanabe, H., Tokunaga, K.

Evaluation of properties and development of plasma facing materials with radiation resistance

RIAM Forum 2000, RIAM, Kyushu (Jun. 1-2, 2000)

Sasase, M., Satou, T., Okayasu, S., Kurata, H., Hojou, K.

Defect Structure of high-T_c Superconductor by high-energy heavy ion irradiation

Meeting of the Japan Electron Microscopy, Tokyo (May 18, 2000)

Sasase, M., Okayasu, S., Kurata, H., Hojou, K.

Columnar defects of high-T_c huperconductor by high-Energy heavy ion irradiation

Fall Meeting of the Japan Society of Applied Physics, Hokkaido (Sept. 5, 2000)

Sasase, M., Satou, T., Okayasu, S., Kurata, H., Hojou, K.

Irradiated damage in high-T_c superconductor

International Symposium on superconductivity (ISS'00), Tokyo (Oct. 15, 2000)

Sasase, M., Okayasu, S., Kurata, H., Hojou, K.

Defect structure of high-T_c superconductor by high-energy heavy ion irradiation

The 8th Conference on Frontiers of Electron Microscopy in Materials Science,

Matsue (Nov. 15, 2000)

Sasase, M., Okayasu, S., Yamamoto, H., Kurata, H., Hojou, K.
Effect of high-energy heavy ion irradiation in Bi-2212
Spring Meeting of the Japan Society of Applied Physics, Tokyo (Mar. 31, 2001)

— 135 —

9. Personnel and Committees

This is a blank page.

(1) Personnel (FY 2000)

Department of Materials Science

Akira	Iwamoto	Director
Katsuichi	Tachimori	Deputy Director
Tohoru	Ogawa	Deputy Director
Sigeru	Mori	Administrative Manager

Tandem Accelerator Group

Scientific Staff

Tadashi	Yoshida*
Suehiro	Takeuchi
Susumu	Hanashima
Makoto	Matsuda

Technical Staff

Susumu	Kanda
Isao	Ohuchi
Katsuzo	Horie
Yoshihiro	Tsukihashi
Shinichi	Abe
Nobuhiro	Ishizaki
Hidekazu	Tayama

Research Group for Innovative Nuclear Science

Masumi	Oshima*	
Akihiro	Iwase	
Nobuo	Shinohara	
Hideki	Iimura	
Youichi	Hatsukawa	
Norito	Ishikawa	
Yasuhiro	Chimi	
Akihiko	Osa	
Yutaka	Utsuno	
Yosuke	Toh	
Tadayuki	Hasegawa	(Student)

Research Group for Solid State Phyics under Extreme Conditions

Kiichi	Hojou*
Masao	Sataka

Hideo	Ohtsuka
Satoru	Okayasu
Masato	Sasase

Research Group for Radiation Effects and Analyses

Shiro	Jitsukawa*
Takeo	Aruga
Tetsuya	Nakazawa
Daijyu	Yamaki

Advanced Science Research Center

Research Group for fusion of Heavy Deformed Nuclei

Hiroshi	Ikezoe*
Tetsuro	Ishii
Yasuharu	Sugiyama
Shin-ichi	Mitsuoka
Katsuhisa	Nishio

Research Group for Hadron Science

Satoshi	Chiba*	
Toshiki	Maruyama	
Hiroki	Takemoto	
Masahiro	Fukusima	
V. N. Kondratyev		(Research Fellow)
Shinpei	Chikazumi	(Student)

Research Group for Nuclear Chemistry of Heavy Elements

Yuichiro	Nagame*
Shin-ichi	Ichikawa
Kazuaki	Tsukada
Ichiro	Nishinaka
Hiromitsu	Haba
Masato	Asai

Department of Health Physics

Radiation Control Division

Yukihiro	Miyamoto
Hitoshi	Ogose
Kouichi	Sato

Advanced Photon Research Center

Free Electron Laser Research Group

Takehito   Hayakawa

Toshiyuki   Shizuma

Takasaki Radiation Chemistry Research Establishment

Radiation Engineering Division

Toshio   Hirao

Oarai Research Establishment

High Temerature Irradiation Laboratory

Kimio   Hayashi*

Masahiro   Ishihara

Shinchi   Baba

Jun   Aihara

* : Head

(2)Tandem Consultative Committee

(Chairman)	Toru	Nomura	(Professor, Prime Scientist, High Energy Accelerator Research Organization (KEK))
(Vice Chairman)	Akira	Iwamoto	(Director, Department of Materials Science)
	Hiroyasu	Ejiri	(Professor Emeritus of Osaka University)
	Kohei	Furuno	(Professor, Tsukuba University)
	Jun	Imasato	(Professor, High Energy Accelerator Research Organization (KEK))
	Kenji	Katori	(Professor Emeritus of Osaka University)
	Ken-ichiro	Komaki	(Professor, The University of Tokyo)
	Shigeru	Kubono	(Associate professor, The University of Tokyo)
	Hisaaki	Kudo	(Associate professor, Niigata University)
	Hiroshi	Kudo	(Professor, Tsukuba university)
	Shunpei	Morinobu	(Professor, Kyushu University)
	Kenji	Morita	(Professor, Nagoya University)
	Seiichi	Shibata	(Professor, Kyoto University)
	Hiromi	Shibata	(Associate professor, The University of Tokyo)
(Secretary)	Masao	Sataka	(Research Group for Solid State Physics under Extreme Conditions)
(Secretary)	Suehiro	Takeuchi	(Tandem Accelerator Group)
(Secretary)	Tadashi	Yoshida	(Head, Tandem Accelerator Group)
(Secretary)	Sigeru	Mori	(Administrative Manager, Department of Materials Science)

(3)Research Planning and Assessment Committee

(a) Sub-committee for Nuclear Physics and Nuclear Chemistry

(Head)	Shunpei	Morinobu	(Professor, Kyushu University)
	Shigeru	Kubono	(Associate professor, The University of Tokyo)
	Seiichi	Shibata	(Professor, Kyoto University)
	Kouhei	Furuno	(Professor, Tsukuba University)
	Hiroshi	Ikezoe	(Head, Research Group for Fusion of

			Heavy Deformed Nuclei)
	Toshiaki	Sekine	(Research Group for Innovative Nuclear Science)
	Suehiro	Takeuchi	(Tandem Accelerator Group)
(Secretary)	Susumu	Hanashima	(Tandem Accelerator Group)
(Secretary)	Tadashi	Yoshida	(Head, Tandem Accelerator Group)

(b) Sub-committee for Materials and Radiation Damage

(Head)	Kenji	Morita	(Professor, Nagoya University)
	Ken-ichiro	Komaki	(Professor, The University of Tokyo)
	Hiromi	Shibata	(Associate professor, The University of Tokyo)
	Hiroshi	Kudo	(Professor, Tsukuba University)
	Kiichi	Hojou	(Head, Research Group for Solid State Physics under Extreme Conditions)
	Akihiro	Iwase	(Research Group for Innovative Nuclear Science)
	Suehiro	Takeuchi	(Tandem Accelerator Group)
(Secretary)	Susumu	Hanashima	(Tandem Accelerator Group)
(Secretary)	Tadashi	Yoshida	(Head, Tandem Accelerator Group)

This is a blank page.

10. Cooperative Researches

This is a blank page.

	Title	Contact person Organization
1.	Systematic Investigation on Magnetic Rotation in Atomic Nucleus	Masahiko SUGAWARA Department of Natural Science, Chiba Institute of Technology
2.	Study of Electromagnetic Properties of Nuclear High-spin State through Crystal Ball (II)	Tetsuro KOMATSUBARA Tandem Accelerator Center, Tsukuba University
3.	Investigation on Anomalous Phenomena of Electromagnetic Transitions between Multipole Deformed State	Hideshige KUSAKARI Faculty of Education, Chiba University
4.	Correlation between Fission Modes and Mass-number of Fissioning Nucleus	Hisaaki KUDO Department of Chemistry, Niigata University
5.	Direct Measurement of the Astro-Physical Reaction Rate with Radio-active Nuclear Beams	Hiroari MIYATAKE Institute of Particle and Nuclear Studies, High Energy Accelerator Research Organization
6.	Precise Measurement of Gamma-ray Emission Probability for Proton-rich Nuclides	Hiroshi MIYAHARA Department of Radiological Technology, School of Health Science, Nagoya University
7.	Study of Nuclear Astrophysics through Exotic Nuclear Reaction	Shigeru KUBONO Center for Nuclear Study, Graduate School of Science, The University of Tokyo

8.   Electronic Excitation Effects in Oxides   Noriaki MATSUNAMI
     by High Energy Heavy Ion   School of Engineering,
                                                    Nagoya University

9.   Study of Single-events Induced by   Sumio MATSUDA
     High Energy Ions   NASDA, Tsukuba

10. High-Energy Ion Beam Irradiation of   Takayuki TERAI
     Functional Electronic Materials   Engineering Research Institute,
                                                    School of Engineering,
                                                    The University of Tokyo

11. Electron Excitation Effect on Sputter-   Mititaka TERASAWA
     ing Induced by Heavy Ion Bombard-   Faculty of Engineering,
     ment   Himeji Institute of Technology

12. Electron Spectra Induced by the Colli-   Ken-ichiro KOMAKI
     sion of Highly Charged Ions with Matter   Graduate School of Arts and Science,
                                                    The University of Tokyo

13. Study of Property and Microstructure   Yukichi SASAKI
     on the Oxide Superconductors Irradiat-   Japan Fine Ceramics Center,
     ed with High Energy Ions   Nagoya

14, Observation of Dynamical Interaction   Akira TONOMURA
     between Vortices and Columnar Defects   Advanced Research Laboratory,
     by Lorentz Microscpopy (II)   Hitachi Ltd.

15. Study on Damage Production Mecha-   Shiori ISHINO
     nism in Steel Materials Irradiated with   Faculty of Engineering,
     High Energy Ions   Tokai University

16. Effect of Ion Irradiation for New   Tatsuo OKU
     Carbon Composite Materials and Fibers   Faculty of Engineering,
     with High Thermal Conductivity   Ibaraki University

17. Study on Transport Property Change in High-Tc Superconductors by Introducing Columnar Defects

Takanobu KISS

Department of Electrical and Electronic Systems Engineering,

Kyushu University

This is a blank page.

国際単位系 (SI) と換算表

表1 SI基本単位および補助単位

量	名称	記号
長さ	メートル	m
質量	キログラム	kg
時間	秒	s
電流	アンペア	A
熱力学温度	ケルビン	K
物質量	モル	mol
光度	カンデラ	cd
平面角	ラジアン	rad
立体角	ステラジアン	sr

表3 固有の名称をもつSI組立単位

量	名称	記号	他のSI単位による表現
周波数	ヘルツ	Hz	s^{-1}
力	ニュートン	N	$m \cdot kg/s^2$
圧力，応力	パスカル	Pa	N/m^2
エネルギー，仕事，熱量	ジュール	J	$N \cdot m$
工率，放射束	ワット	W	J/s
電気量，電荷	クーロン	C	$A \cdot s$
電位，電圧，起電力	ボルト	V	W/A
静電容量	ファラド	F	C/V
電気抵抗	オーム	Ω	V/A
コンダクタンス	ジーメンス	S	A/V
磁束	ウェーバ	Wb	$V \cdot s$
磁束密度	テスラ	T	Wb/m^2
インダクタンス	ヘンリー	H	Wb/A
セルシウス温度	セルシウス度	℃	
光束	ルーメン	lm	$cd \cdot sr$
照度	ルクス	lx	lm/m^2
放射能	ベクレル	Bq	s^{-1}
吸収線量	グレイ	Gy	J/kg
線量当量	シーベルト	Sv	J/kg

表2 SIと併用される単位

名称	記号
分，時，日	min, h, d
度，分，秒	°, ′, ″
リットル	l, L
トン	t
電子ボルト	eV
原子質量単位	u

$1 \text{ eV} = 1.60218 \times 10^{-19} \text{ J}$

$1 \text{ u} = 1.66054 \times 10^{-27} \text{ kg}$

表4 SIと共に暫定的に維持される単位

名称	記号
オングストローム	Å
バーン	b
バール	bar
ガル	Gal
キュリー	Ci
レントゲン	R
ラド	rad
レム	rem

$1 \text{ Å} = 0.1 \text{ nm} = 10^{-10} \text{ m}$

$1 \text{ b} = 100 \text{ fm}^2 = 10^{-28} \text{ m}^2$

$1 \text{ bar} = 0.1 \text{ MPa} = 10^5 \text{ Pa}$

$1 \text{ Gal} = 1 \text{ cm/s}^2 = 10^{-2} \text{ m/s}^2$

$1 \text{ Ci} = 3.7 \times 10^{10} \text{ Bq}$

$1 \text{ R} = 2.58 \times 10^{-4} \text{ C/kg}$

$1 \text{ rad} = 1 \text{ cGy} = 10^{-2} \text{ Gy}$

$1 \text{ rem} = 1 \text{ cSv} = 10^{-2} \text{ Sv}$

表5 SI接頭語

倍数	接頭語	記号
10^{18}	エクサ	E
10^{15}	ペタ	P
10^{12}	テラ	T
10^9	ギガ	G
10^6	メガ	M
10^3	キロ	k
10^2	ヘクト	h
10^1	デカ	da
10^{-1}	デシ	d
10^{-2}	センチ	c
10^{-3}	ミリ	m
10^{-6}	マイクロ	μ
10^{-9}	ナノ	n
10^{-12}	ピコ	p
10^{-15}	フェムト	f
10^{-18}	アト	a

（注）

1. 表1－5は「国際単位系」第5版，国際度量衡局 1985年刊行による。ただし，1 eV および 1 u の値は CODATA の1986年推奨値によった。

2. 表4には海里，ノット，アール，ヘクタールも含まれているが日常の単位なのでここでは省略した。

3. bar は，JISでは流体の圧力を表わす場合に限り表2のカテゴリーに分類されている。

4. EC閣僚理事会指令では bar，barn および「血圧の単位」mmHg を表2のカテゴリーに入れている。

換算表

力	N(=10^5dyn)	kgf	lbf
	1	0.101972	0.224809
	9.80665	1	2.20462
	4.44822	0.453592	1

粘度 $1 \text{ Pa} \cdot s(N \cdot s/m^2) = 10 \text{ P}(ポアズ)(g/(cm \cdot s))$

動粘度 $1 \text{ m}^2/s = 10^4 \text{ St}(ストークス)(cm^2/s)$

圧力	MPa(=10 bar)	kgf/cm²	atm	mmHg(Torr)	lbf/in²(psi)
	1	10.1972	9.86923	7.50062×10^3	145.038
	0.0980665	1	0.967841	735.559	14.2233
	0.101325	1.03323	1	760	14.6959
	1.33322×10^{-4}	1.35951×10^{-3}	1.31579×10^{-3}	1	1.93368×10^{-2}
	6.89476×10^{-3}	7.03070×10^{-2}	6.80460×10^{-2}	51.7149	1

エネルギー・仕事・熱量	J(=10^7erg)	kgf·m	kW·h	cal(計量法)	Btu	ft·lbf	eV
	1	0.101972	2.77778×10^{-7}	0.238889	9.47813×10^{-4}	0.737562	6.24150×10^{18}
	9.80665	1	2.72407×10^{-6}	2.34270	9.29487×10^{-3}	7.23301	6.12082×10^{19}
	3.6×10^6	3.67098×10^5	1	8.59999×10^5	3412.13	2.65522×10^6	2.24694×10^{25}
	4.18605	0.426858	1.16279×10^{-6}	1	3.96759×10^{-3}	3.08747	2.61272×10^{19}
	1055.06	107.586	2.93072×10^{-4}	252.042	1	778.172	6.58515×10^{21}
	1.35582	0.138255	3.76616×10^{-7}	0.323890	1.28506×10^{-3}	1	8.46233×10^{18}
	1.60218×10^{-19}	1.63377×10^{-20}	4.45050×10^{-26}	3.82743×10^{-20}	1.51857×10^{-22}	1.18171×10^{-19}	1

1 cal = 4.18605 J（計量法）

= 4.184 J （熱化学）

= 4.1855 J （15 ℃）

= 4.1868 J（国際蒸気表）

仕事率 1 PS（仏馬力）

= 75 kgf·m/s

= 735.499 W

放射能	Bq	Ci
	1	2.70270×10^{-11}
	3.7×10^{10}	1

吸収線量	Gy	rad
	1	100
	0.01	1

照射線量	C/kg	R
	1	3876
	2.58×10^{-4}	1

線量当量	Sv	rem
	1	100
	0.01	1

（86年12月26日現在）

JAERI TANDEM Annual Report 2000 April 1, 2000 - March 31, 2001